Durham E-Theses

Mechanistic studies of plasma polymerization

Ryan, Martin Edward

How to cite:

Ryan, Martin Edward (1995) *Mechanistic studies of plasma polymerization*, Durham theses, Durham University. Available at Durham E-Theses Online: http://etheses.dur.ac.uk/5455/

Use policy

The full-text may be used and/or reproduced, and given to third parties in any format or medium, without prior permission or charge, for personal research or study, educational, or not-for-profit purposes provided that:

- a full bibliographic reference is made to the original source
- a link is made to the metadata record in Durham E-Theses
- the full-text is not changed in any way

The full-text must not be sold in any format or medium without the formal permission of the copyright holders.

Please consult the full Durham E-Theses policy for further details.

Academic Support Office, The Palatine Centre, Durham University, Stockton Road, Durham, DH1 3LE
e-mail: e-theses.admin@durham.ac.uk Tel: +44 0191 334 6107
http://etheses.dur.ac.uk

MECHANISTIC STUDIES OF PLASMA POLYMERIZATION

Martin Edward Ryan

Ph.D Thesis

Department of Chemistry
University of Durham

September 1995

The copyright of this thesis rests with the author.
No quotation from it should be published without
his prior written consent and information derived
from it should be acknowledged.

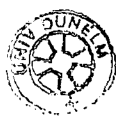

18 MAR 1996

For My Parents

DECLARATION

STATEMENT OF COPYRIGHT

The copyright of this thesis rests with the author. No quotation from it should be published without his written consent and information derived from it should be acknowledged.

The work described in this thesis was carried out in the Department of Chemistry at the University of Durham and Daresbury Laboratory, Warrington between October 1992 and September 1995. It is the original work of the author except where otherwise acknowledged or where specific reference is may to other sources.

Atomic force microscopy analysis (chapter 2) was performed by Dr. J. P. S. Badyal. The ion beam experiments (chapter 3) were carried out by Dr. R. K. Mitford. X-ray absorption analysis (chapter 6) was done collaboratively with Dr. R. M. Ormerod (University of Keele) and Dr. C. Hardacre (Queens University, Belfast).

Work in this thesis has formed all or part of the following publications:-

'Modeling of Non-Isothermal Glow Discharge Modification of PTFE Using Low-Energy Ion Beams'; R. K. Wells, M. E. Ryan, J. P. S. Badyal *Journal of Physical Chemistry*, **1993**, *97*, 12879.

'Surface Texturing of PTFE Film Using Non-Equilibrium Plasmas'; M. E. Ryan, J. P. S. Badyal *Macromolecules*, **1995**, *28*, 1377.

'Plasma Polymerization of Sputtered Poly(tetrafluoroethylene)'; M. E. Ryan, J. L. C. Fonseca, S. Tasker, J. P. S. Badyal *Journal of Physical Chemistry*, **1995**, *99*, 7060.

'Pulsed Plasma Polymerization of Maleic Anhydride'; M. E. Ryan, A. M. Hynes, J. P. S. Badyal submitted for publication.

'Plasma Polymerization of 2-iodothiophene'; M. E. Ryan, A. M. Hynes, S. H. Wheale, J. P. S. Badyal, C. Hardacre, R. M. Ormerod submitted for publication.

ACKNOWLEDGEMENTS

I would like to express my sincere thanks to my supervisor, Dr. J. P. S Badyal, for his help, support and enthusiasm during my Ph.D.

Thanks to everyone in Lab 98, past and present, for the good times over the last three years. A special thank you must go to Alan Hynes for all his time spent at Daresbury and his effort on the data analysis of the XANES experiments.

I would like to acknowledge the technical assistance of Gordon and Ray the glassblowers, Jim, Mel, and Neil in the mechanical workshop, and Barry and Kelvin from the electronics workshop.

Finally, I express my gratitude to George Rowe who at times seemed more like a magician than an electrician in managing to keep 'Gramps' (ES 200 spectrometer) running.

ABSTRACT

Plasma polymerization is a solventless method for depositing polymeric layers onto any substrate at room temperature. This technique comprises excitation, fragmentation, and polymerization of precursor molecules by an electrical discharge. Although widely used, the fundamental molecular processes associated with plasma polymerization are not fully understood.

Basic plasma / polymer interactions were studied by investigating the surface treatment of polytetrafluoroethylene (PTFE) using inert and reactive gas discharges. Depending upon the feed gas employed, chemical, UV, or ion beam modification of the PTFE surface were found to be important. Argon glow discharge treatment was found to result in similar physicochemical phenomena at the PTFE surface to that observed during argon ion beam studies, thereby supporting the relative importance of ion bombardment during noble gas plasma modification. In high power discharges it has been shown that extensive ion bombardment of PTFE can lead to the simultaneous sputtering and plasma polymerization of ejected species onto an adjacent substrate. The chemical nature of the resultant fluorocarbon deposits for various gases was found to correlate to the earlier surface treatment studies.

Another way of carrying out plasma polymerization is to use pulsed plasmas; these offer the advantage of greater retention of monomer structure within the plasma polymer matrix. In the case of maleic anhydride less fragmentation of the precursor, reduced beam damage of the polymer, and radically initiated polymerization was observed by increasing the off-period of the pulse. Similarly the structural characteristics of 2-iodothiophene plasma polymers were found to be influenced by the electrical discharge power and pulsing parameters leading to a gradual destruction of the aromatic ring structure.

CONTENTS

CHAPTER 1 1

AN INTRODUCTION TO GLOW DISCHARGE PROSESSES AND ANALYTICAL TECHNIQUES

1.1 INTRODUCTION 2

1.2 PLASMAS 2

1.2.1 Types of Plasma 3

1.2.2 Plasma Generation 4

1.2.2.1 Electron Energy Distribution Function 5

1.2.2.2 Plasma Potential 6

1.2.2.3 Floating Potential 7

1.2.2.4 Plasma Sheaths 7

1.2.3 Methods of Plasma Generation 7

1.2.3.1 DC Glow Discharges 7

1.2.3.2 Radio Frequency Plasmas 8

1.2.3.3 Microwave Discharges 8

1.2.4 Non-Equilibrium Plasma Chemistry 9

1.2.4.1 Plasma Reactions 9

1.2.4.2 Plasma Surface Interactions 12

1.2.5 Plasma Modification of Polymer Surfaces 12

1.2.6 Plasma Polymerization 14

1.2.6.1 Mechanism of Plasma Polymerization 17

1.2.6.2 Polymerization Parameters 20

1.2.7 Aims of Current Work 20

1.3 ANALYTICAL TECHNIQUES 21

1.3.1 Introduction 21

1.3.2 X-ray Photoelectron Spectroscopy 21

1.3.2.1 The Photoionization Process 22

1.3.2.2 Spectral Interpretation 24

1.3.2.2.1 X-ray Satellites 25

1.3.2.2.2 Shake-up and Shake-off Satellites 26

1.3.2.2.3 Multiplet Splitting 27

1.3.3 Atomic Force Microscopy 27

1.3.4 Infrared Spectroscopy 28

1.3.5 X-ray Absorption Spectroscopy 32

1.3.6 Optical Emission Spectroscopy 35

1.4 REFERENCES 37

CHAPTER 2 43

SURFACE TEXTURING AND CHEMICAL MODIFICATION OF PTFE USING NON-EQUILIBRIUM PLASMAS

2.1 INTRODUCTION 44

2.1.1 Wet Chemical Modification of PTFE 44

2.1.2 Plasma Modification of PTFE Surfaces 45

2.1.2.1 Oxygen Plasma Treatment 45

2.1.2.2 Hydrogen Plasma Treatment 46

2.1.2.3 Nitrogen Plasma Treatment 46

2.1.2.4 Carbon Tetrafluoride Plasma Treatment 46

2.1.2.5 Inert Gas Plasma Treatment 47

2.1.2.6 Miscellaneous Plasma Treatments 47

2.1.3 Summary 48

2.2 EXPERIMENTAL 48

2.2.1 Analysis 50

2.2.2 Calculation of Leak and Flow Rates 51

2.3 RESULTS 53

2.3.1 Clean PTFE 53

2.3.2 Oxygen Plasma Treatment 63
2.3.3 Hydrogen Plasma Treatment 63
2.3.4 Nitrogen Plasma Treatment 63
2.3.5 Inert Gas Plasma Treatment (Helium, Neon, and Argon) 64
2.3.6 CF_4 Plasma Treatment 65
2.4 DISCUSSION 65
2.5 CONCLUSIONS 72
2.6 REFERENCES 74

CHAPTER 3 79
MODELLING OF NON-ISOTHERMAL ARGON GLOW DISCHARGE MODIFICATION OF PTFE USING LOW ENERGY ARGON ION BEAMS

3.1 INTRODUCTION 80
3.1.1 Ion Beam Modification of Polymers 80
3.1.1.1 Fundamentals of Ion-Polymer Interactions 80
3.1.1.2 Ion Beam Modification of PTFE 82
3.1.2 Ion Source 84
3.2 EXPERIMENTAL 85
3.2.1 Plasma Modification 85
3.2.2 Ion Beam Modification 85
3.3 RESULTS 86
3.3.1 Argon Plasma Modification 86
3.3.2 Argon Ion Beam Modification 89
3.4 DISCUSSION 92
3.5 CONCLUSIONS 93
3.6 REFERENCES 94

CHAPTER 4 97

PLASMA POLYMERIZATION OF SPUTTERED PTFE

4.1 INTRODUCTION 98

4.1.1 Plasma Sputter Deposition 98

4.1.2 Sputter Deposited PTFE 99

4.2 EXPERIMENTAL 100

4.2.1 Glow Discharge Experiments 100

4.2.2 Analysis 101

4.3 RESULTS 102

4.3.1 X-ray Photoelectron Spectroscopy 102

4.3.2 Infrared Spectroscopy 106

4.3.3 UV Emission Spectroscopy 106

4.4 DISCUSSION 114

4.5 CONCLUSIONS 116

4.6 REFERENCES 117

CHAPTER 5 121

PULSED PLASMA POLYMERIZATION OF MALEIC ANHYDRIDE

5.1 INTRODUCTION 122

5.1.1 Pulsed Plasma Polymerization 123

5.2 EXPERIMENTAL 124

5.3 RESULTS 126

5.3.1 Continuous Wave Plasma Polymerization 126

5.3.2 Pulsed Plasma Polymerization 129

5.4 DISCUSSION 140

5.5 CONCLUSIONS 143

5.6 REFERENCES 144

CHAPTER 6 147

CONTINUOUS WAVE AND PULSED PLASMA POLYMERIZATION OF 2-IODOTHIOPHENE

6.1 INTRODUCTION 148

6.1.1 Polymerization of Thiophene 149

6.2 EXPERIMENTAL 150

6.3 RESULTS 152

6.3.1 Continuous Wave Plasma Polymers 152

6.3.1.1 X-ray Photoelectron Spectroscopy 152

6.3.1.2 X-ray Absorption Near Edge Structure 153

6.3.1.3 Infrared Spectroscopy 164

6.3.2 Pulsed Plasma Polymers 166

6.4 DISCUSSION 169

6.5 CONCLUSIONS 170

6.6 REFERENCES 171

CHAPTER 7 174

CONCLUSIONS

7.1 CONCLUSIONS 175

APPENDIX 178

SEMINARS, CONFERENCES AND COURSES ATTENDED

CHAPTER 1

AN INTRODUCTION TO GLOW DISCHARGE PROCESSES AND ANALYTICAL TECHNIQUES

UNIV DUNELM

1.1 INTRODUCTION

Plasma processing of materials has been investigated for over 25 years. During this time progress has been made in the utilization of these methods but understanding of reaction pathways is still at a very basic level. This thesis is aimed at elucidating the important mechanisms occurring in plasma / polymer interactions and during plasma polymerization. This chapter introduces the plasmas, plasma processes and analytical techniques used during the course of this work.

1.2 PLASMAS

The term 'plasma' was first used in 1929 by Langmuir[1] to describe the ionized gases he studied during the development of vacuum tubes. These partially ionized gases, composed of ions, electrons and neutral species, are often termed the fourth state of matter[2]. This is illustrated in figure 1.1[3].

For the discharge to be classified a plasma the number of positive and negative charge carriers must be approximately equal, leading to electrical quasi-neutrality[3,4]. This criterion is fulfilled when the dimensions of the gas discharge are larger than the Debye length, λ_D, the distance over which a charge imbalance can exist. λ_D is defined in equation 1.1.

$$\lambda_D = (\varepsilon_o k T_e / n_e e^2)^{1/2} \qquad (1.1)$$

where ε_o = permittivity of free space, k = Boltzmann constant, T_e = electron temperature, n_e = electron density and e = charge on the electron.

Figure 1.1

Schematic diagram showing the states of matter versus temperature and particle energy (where the temperature range is of the gas neutrals).

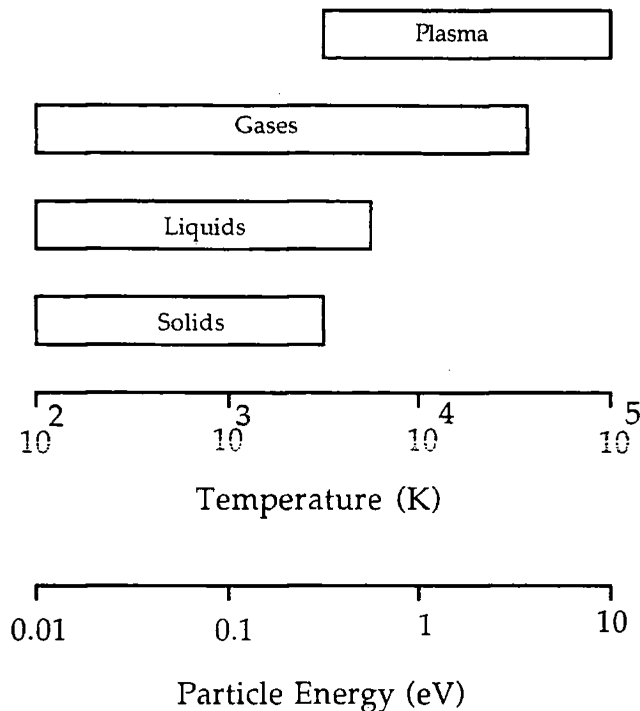

1.2.1 Types of Plasma

There are two main categories of plasma, equilibrium and non-equilibrium plasmas. The equilibrium or 'thermal' discharges occur when the electron and gas temperatures in the plasma are approximately equal[5]. Their production and properties lead to uses in the deposition of coatings by plasma spraying, the reduction and smelting of ores, and even in attempts to create controlled thermonuclear fusion[3]. The high temperatures obtained make processing of polymers impossible, so this type of plasma will not be considered further.

Non-equilibrium or 'cold' plasmas are characterised by a lack of thermodynamic equilibrium between the electrons and the ions, atoms and molecules in the discharge. The electron temperature is much higher than

that of other plasma particles allowing electron initiated physical and chemical reactions to occur while the gas is at a relatively low temperature[6].

1.2.2 Plasma Generation

A plasma is created by applying an electric field across a volume of gas. Small numbers of free electrons are always present in the gas as a result of ionization by naturally occurring radioactivity or cosmic rays[3]. The electric field applied to the discharge accelerates these electrons and they collide with gas atoms or molecules. If the electrons have gained enough kinetic energy they will collide inelastically with the gas molecules causing ionization or dissociation. A cascade effect of free electron production quickly spreads through the entire gas, generating the plasma. Not every free electron participates in inelastic collisions. Many are lost by diffusion or drift to the boundaries surrounding the plasma. Others are lost by recombination with positive ions and attachment to neutrals to form negative ions. The plasma attains steady state when electron generation and loss are equal.

The minimal threshold voltage required to produce the glow discharge is called the breakdown voltage[7]. Radiative energy decay of many of the electronically excited states of molecules and atoms account for the luminous glow of the gaseous discharge. The electron temperature (T_e) in the bulk of a non-equilibrium plasma is much greater than that of the ion temperature (T_i), typical values being T_e = 3-30 eV and T_i = 0.5 eV[3]. This occurs because of the vast difference in mass between ions and electrons. Electrons, being much lighter, obtain more kinetic energy from the applied field illustrated by equation 1.2[4].

$$\text{Work done by field} = Eex = (Eet)^2/2m \qquad (1.2)$$

where E = applied electric field, e = charge on an electron, x = distance travelled, t = time and m = mass of particle being considered.

1.2.2.1 Electron Energy Distribution Function

The electron velocity relationship is central in defining the physical properties of a plasma as it leads to the electron energy distribution, the average electron energy and electron transport properties[3]. The energy of electrons is governed by their interactions with other particles and the total field they are subjected to. The distribution of electron energies, known as the electron energy distribution function[8,9] (EEDF), in a plasma is approximately described by a Maxwellian distribution, shown in figure 1.2.

Figure 1.2

Examples of Maxwellian and Druyvesteyn distributions for an average electron energy of 1 eV.

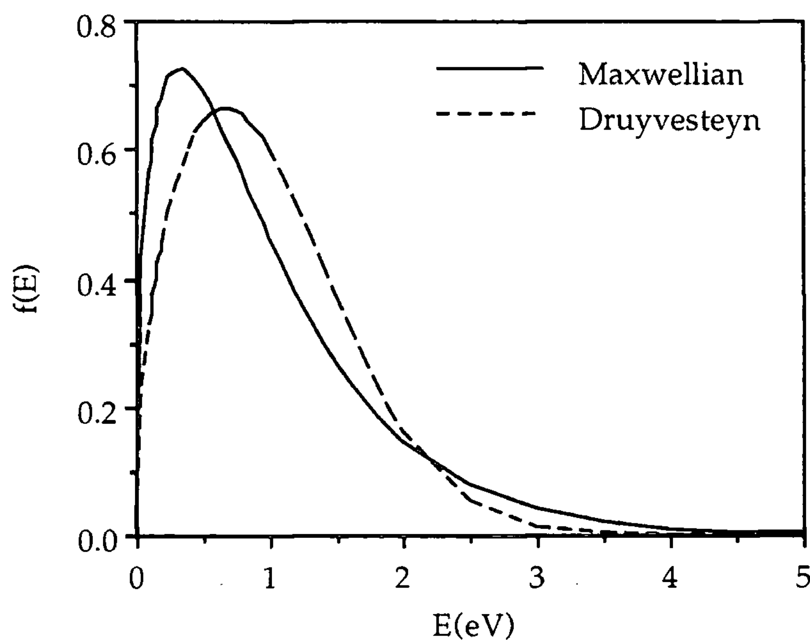

However, this only provides a first approximation of the electron energy (or velocity) distribution in a cold plasma as it assumes that $T_e = T_i$. For non-equilibrium plasmas a Druyvesteyn distribution is found to give a better aprroximation[3,5] as it accounts for $T_e >> T_i$. This is also displayed in figure 1.2. The Druyvesteyn distribution is characterised by a shift toward higher average electron energies. Both distributions indicate the presence of a high energy tail of electrons which are significant as these sustain the plasma.

1.2.2.2 Plasma Potential

The electron density and ion density are, on average, equal within the plasma[3]. This number, which is lower in magnitude than the density of neutrals is often known as the plasma density[4]. As discussed above, the average speed of the electrons is very large compared with that of the ions and neutrals. This leads to electrons reaching the surrounding surfaces at a faster rate than the ions[10] and the plasma slowly becomes positively charged with respect to the surrounding surfaces. As the net charge increases on these surfaces, it becomes less energetically favourable for the electrons to escape because the walls of the chamber are more negative than the plasma. Eventually, a steady state arises when the plasma potential is high enough so that the rate of loss of electrons is reduced to the same level as the rate of loss of ions. This bulk 'plasma potential' is on average several volts more positive than surfaces in contact with the plasma[3] and ions leaving the plasma are accelerated by this voltage to the reactor walls.

1.2.2.3 Floating Potential

When an electrically isolated substrate is placed in a plasma it becomes negatively charged due to the greater flux of electrons compared to the flux of ions[10]. After a short period of time the surface becomes sufficiently negative, with respect to the plasma bulk, that enough electrons are repelled to cause an equal flux of ions and electrons. The substrate has now reached its floating potential, which is typically negative of the plasma potential[10].

1.2.2.4 Plasma Sheaths

Isolated substrates placed in plasmas are observed to have associated dark regions immediately adjacent to them. These are known as space charge regions or sheaths[4]. As the substrate begins to repel electrons a net positive charge builds up close to its surface. The low electron density in the 'sheath' region leads to a low amount of gas excitation and therefore no visible emission occurs in this region, hence it is often called a dark space.

1.2.3 Methods of Plasma Generation

1.2.3.1 DC Glow Discharges

The simplest means of forming a plasma is by using a DC discharge[10]. This is produced by applying DC voltage between two conductive electrodes inserted into a gas at low pressure. As the electrodes are in direct contact with the plasma, if the discharge is used for depositing dielectric films the electrodes become covered with an insulator. Consequently, although a DC discharge may be initiated, it will quickly be extinguished as the electrons accumulate on the insulator and recombine with the available ions[3]. It is

therefore often preferred to have the electrodes outside the reactor which can be achieved by alternating the polarity of the discharge, i.e. AC discharges.

1.2.3.2 Radio Frequency Plasmas

In RF plasmas (>1MHz) the electrodes can be remote from the reactor[5]. A frequency of 13.56 MHz has been adopted as the standard because it complies with government communication regulations. The energy is supplied to the discharge by either capacitive or inductive coupling via a matching unit. The unit is required to match the impedance of the partially ionized gas to the output impedance of the power supply[3]. RF plasmas are quite homogeneous because the electrical field wavelength is much larger than the reactor dimensions. This discharge can be operated at low pressures (as low as 1 mTorr) and has become the popular type of laboratory plasma.

1.2.3.3 Microwave Discharges

Microwave plasmas are sustained by power supplies operating at a frequency of 2.45 GHz[3]. The optimum operating pressure for efficient microwave absorption (0.5 - 10 Torr), is higher than that of RF discharges. The microwave plasma has its greatest glow intensity at the coupling microwave cavity. This diminishes rapidly outside the cavity because of the much smaller wavelength of the microwave compared to that of the RF wavelength[3]. The magnitude of the electric field can vary within the reactor and active species can be found persisting in the afterglow region[3]. Microwave plasmas have greater electron and ion densities than RF plasmas, and they have a higher population of high energy electrons[11,12].

1.2.4 Non-Equilibrium Plasma Chemistry

The complex nature of glow discharges has now been illustrated. They are composed of many different reactive species such as ions, electrons, radicals, metastables and neutrals, all of which can undergo different sets of reactions simultaneously.

1.2.4.1 Plasma Reactions

Chemical reactions in a plasma reactor, shown in figure 1.3, can be classified into homogeneous and heterogeneous reactions. The gas phase homogeneous reactions result from inelastic collisions between electrons and heavy species, and between heavy species themselves. Some examples of the homogeneous reactions are given below (A, B and C denote atoms and M is a third body)[3,13].

a) Excitation - the impact of electrons with heavy targets leading to excited states of atoms and molecules,

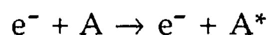

$$e^- + A \rightarrow e^- + A^*$$

b) Dissociative attachment - low energy electrons attach to gas molecules, which dissociate producing a negative ion,

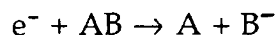

$$e^- + AB \rightarrow A + B^-$$

c) Dissociative ionization - leading to ion pair formation,

$$e^- + AB \rightarrow A^+ + B^- + e^-$$

d) Dissociation - inelastic collision of an electron with a molecule without ion formation,

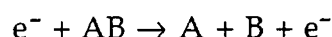

$$e^- + AB \rightarrow A + B + e^-$$

e) Ionization - electron impact induced ionization,

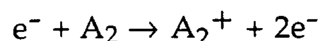

$$e^- + A_2 \rightarrow A_2^+ + 2e^-$$

Figure 1.3

Schematic diagram of reactions in a plasma reactor.

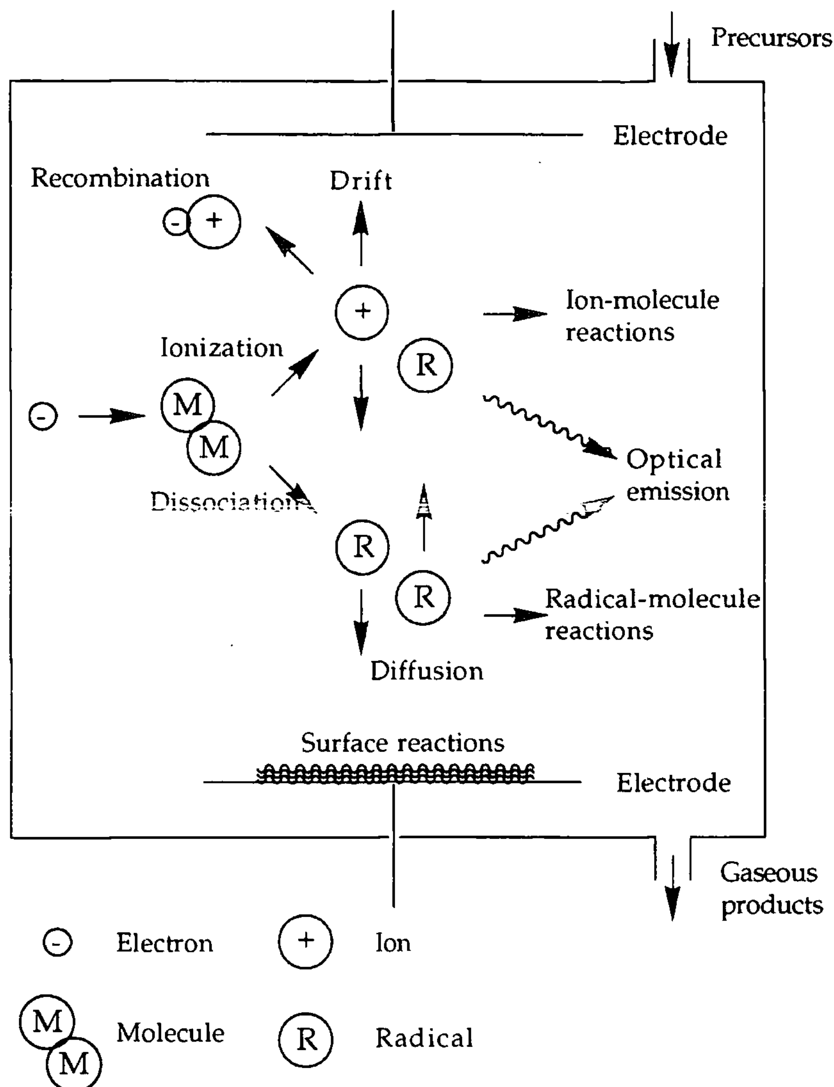

f) Recombination - charged particles are lost from the plasma through recombination (the excess energy is dissipated by radiative de-excitation),

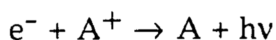

$$e^- + A^+ \rightarrow A + h\nu$$

g) Recombination of ions,

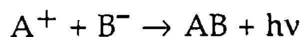

$$A^+ + B^- \rightarrow AB + h\nu$$

h) Charge transfer,

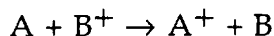

$$A + B^+ \rightarrow A^+ + B$$

i) Associative detachment - collisions between negative ions and radicals leading to electron release and a new compound,

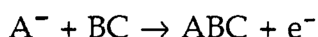

$$A^- + BC \rightarrow ABC + e^-$$

j) Penning ionization - the reaction of energetic metastables, involving the transfer of energy to the target,

$$A + B^* \rightarrow A^+ + B + e^-$$

k) Attachment of atoms,

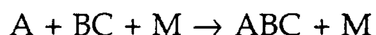

$$A + BC + M \rightarrow ABC + M$$

l) Disproportionation,

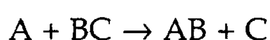

$$A + BC \rightarrow AB + C$$

Heterogeneous reactions occur at surfaces (S) in contact with the plasma or plasma species which may be atoms (A or B), monomer (M), radicals (R) or polymer formed in the plasma phase (P). Examples of this type of reaction include[3,13]:-

m) Adsorption - plasma species adsorbed onto the surface,

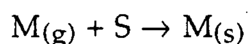

$$M_{(g)} + S \rightarrow M_{(s)}$$

(g) and (s) represent species in the gas and solid phases respectively.

n) Recombination - atoms or radicals react with species already adsorbed to form compounds,

$$S\text{-}A + A \rightarrow S + A_2$$

o) Metastable de-excitation,

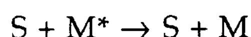

$$S + M^* \rightarrow S + M$$

p) Sputtering - accelerated ions with sufficient energy remove atoms from the surface,

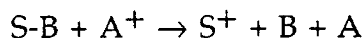

$$S\text{-}B + A^+ \rightarrow S^+ + B + A$$

q) Polymerization - radicals in the plasma react with radicals adsorbed on surfaces,

$$R_{(g)} + R_{(s)} \rightarrow P_{(s)}$$

1.2.4.2 Plasma Surface Interactions

The various particles which can impinge on a surface in contact with a plasma are ions, atoms, radicals, metastables, electrons and photons[14]. Unreactive particles only transmit small amounts of energy to a surface, usually resulting in substrate heating. Electron impact can lead to desorption and/or dissociation of adsorbed molecules and electron induced reactions. Positive ions, accelerated by the plasma sheath to energies of up to 100 eV[15], collide with surfaces imparting this energy to them. The photons, which have energies up to about 10 eV depending on the type of plasma, are able to break chemical bonds and induce cross-linking in surfaces and activate surface molecules.

1.2.5 Plasma Modification of Polymer Surfaces

The ability of non-equilibrium plasmas to modify polymer surfaces has been known for over 25 years[16]. Many polymers are difficult to adhere to other materials. For instance fluoropolymers, characterized by high chemical inertness, thermal stability and electrical insulating properties also have very low surface tension, which causes difficulty in bonding to other materials. Plasma treatments allow modification of the surface characteristics of polymers without affecting bulk properties[15,17-34]. Other advantages of plasma methods are the speed and uniformity of modification, the chemical selectivity attained, and their positive environmental impact i.e. no solvent waste. These processes may be categorised into two major types of reaction, plasma modification (the focus of this section) and plasma polymerization (discussed in the next section).

Surface modification of a polymer by plasma treatment refers to chemical and physical changes incurred by exposure to non-polymer

forming plasmas[35]. These changes can produce more reactive surfaces and affect wetting properties, cross-linking and molecular weight[3,5,17,36].

Changes in the wettablity of a polymer are produced by adding functional groups to the polymer surface[5]. The bombardment of the polymeric network breaks covalent bonds in the surface region and leads to surface radical formation. These radicals are able to react with other species from the plasma to form new functional groups. For example, most types of polymer can be made hydrophilic by oxygen or nitrogen plasma treatment where the active species in the discharge attack the surface and cause incorporation of functionalities such as carbonyl, carboxyl, hydroxyl and amino groups[36,37]. It is believed that radical species rather than ions or electrons play the important role in this type of modification[3].

Molecular weight changes are a second property that may be altered by a plasma. Variations in molecular weight affects a number of physical properties of the polymer such as permeability, solubility, melt temperature and cohesive strength[5]. The principle processes by which the molecular weight of the surface layer is changed are bond scission, branching and cross-linking[38]. In general, for noble gas, nitrogen and hydrogen plasmas the molecular weight increases due to cross-linking, while for an oxygen plasma the molecular weight decreases due to bond breaking. The cross-linking effect of noble gas plasmas has been suggested to occur via the excited metastable states[39]. The energy transfer mechanism for this process, known as CASING (cross-linking by activated species of inert gases)[39], is shown in reactions (1.1a) to (1.1c).

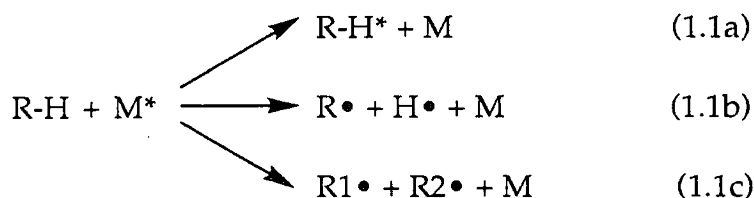

Oxygen plasmas produce polymer free radicals which can cross-link, but competitive oxidation prevents rebonding and produces a decrease in the molecular weight by loss of volatile compounds which ablate from the surface[5]. The removal of volatile compounds illustrates another facet of polymer surface modification by plasmas, known as etching[40].

Plasma etching generally refers to material removal performed with low ion bombardment and is caused mainly by chemical reaction with plasma species. It is carried out under conditions where physical effects are negligible and is usually an isotropic etching process, proceeding through the following steps[3]:-

1. active species are formed in the plasma from non-reactive gases,
2. the active species adsorb onto the surface of the substrate and react with the surface to form volatile products,
3. the volatile products leave the treated surface and are pumped out with plasma effluent.

Reactive ion etching (RIE) is the most popular dry-etching technique and is particularly important in the electronics industry[41]. RIE is based on the combined action of the reactive species generated in the plasma together with the physical effects caused by ion bombardment. The RIE arrangement generally causes the substrate to be exposed to higher energy ion bombardment than in the plasma etching mode. This is achieved by positioning the substrate on a powered electrode, where a larger negative potential relative to the plasma bulk is established, compared with the grounded electrode used in plasma etching.

1.2.6 Plasma Polymerization

The discussion so far in this chapter has centred on glow discharges ignited in atomic or molecular gases. However, almost all organic compounds that have a sufficient vapour pressure are polymerizable in a

plasma[42]. At this stage it should be made clear that plasma polymerization, which is an atomic process, results in the preparation of new kinds of material and is not a type of conventional polymerization, which is molecular in nature[43]. Plasma polymerization is strongly system dependent and in most cases the polymers formed are highly branched, cross-linked and amorphous[44]. These materials often have high thermal stability, high melting point and low solubility. Plasma polymerization is characterized by several important features[3]:-

1. plasma polymers have no discernible repeat unit, unlike conventional polymers,
2. the properties of plasma polymers are determined by the process parameters and not the original monomer structure,
3. monomers used do not have to contain a double bond for the polymerization to proceed.

The mechanism of polymerization, which will be discussed in detail shortly, consists of three major steps all of which can occur heterogeneously or homogenously[3]. Initiation involves formation of free radicals or atoms of monomer by the plasma. Addition of radical atoms to other radicals or molecules leaving a growing radical chain is the propagation step of the polymerization. Termination takes place by processes similar to propagation but ends in the final product or a closed polymer chain.

While in conventional polymerization termination finishes the process, in plasma polymerization neutral products formed in the termination step can undergo reinitiation and propagation reactions. Chain fragments are reconverted into radicals by collision with electrons in the gas phase or by impact of energetic particles on the surface of the polymer film. The homogeneous and heterogeneous nature of plasma polymer growth is shown in a scheme proposed by Poll[45], figure 1.4. Reaction k_1 where the monomer is directly polymerized into the growing film, is termed 'plasma

induced polymerization'[46]. Film formation through reactions k_2 and k_3 is called 'plasma polymerization'[43].

Figure 1.4

Schematic diagram showing the different types of reaction involved in formation of plasma polymers[45].

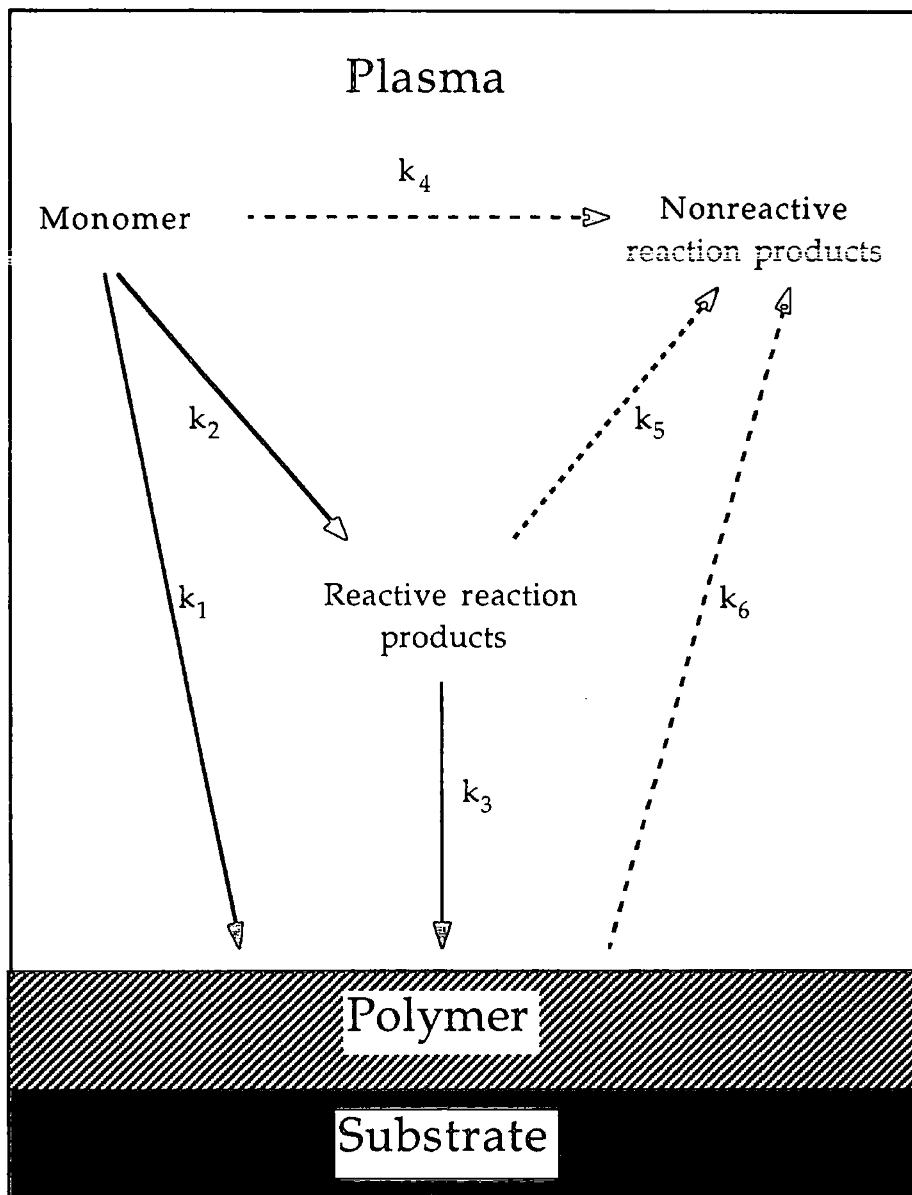

Propagation of the reaction scheme through plasma activation of the growing polymer is believed to be very important. Fluoropolymer film

deposition has been explained in terms of an activated growth model (AGM)[47] which is represented by the following scheme:-

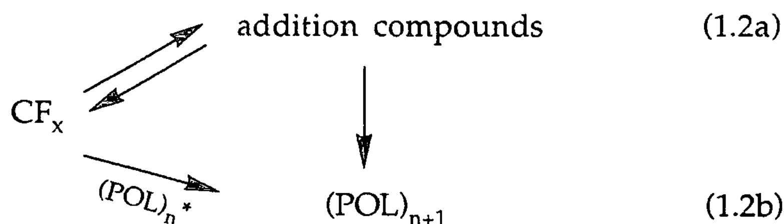

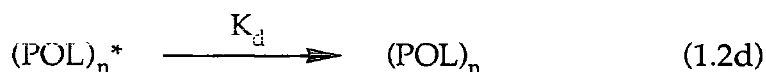

CF_x radicals originating from the monomer may react with other gas phase radicals to form addition compounds, or with the activated polymer. K_a is the activation step of the polymer film by both electrons and positive ions depending on the substrate potential. K_d is the deactivation step.

1.2.6.1 Mechanism of Plasma Polymerization

Conventional polymerization falls into two general groups of reaction, step-growth polymerization and chain-growth polymerization[48]. The former involves slow step-wise repetition of the same reaction, the product of which retains functional groups to react further. The latter mechanism is a series of consecutive steps completed quickly leading to final polymer, intermediates cannot be isolated as in step-growth polymerization.

Yasuda[43,44,46] has proposed that plasma polymerization proceeds according to a rapid step growth polymerization mechanism (RSGP) described by reaction (1.3).

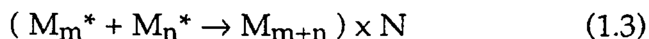

$$(M_m^* + M_n^* \rightarrow M_{m+n}) \times N \qquad (1.3)$$

where N = number of repeat reactions and M* = reactive species produced from the monomer by the plasma. If M* is a monofunctional species (e.g. a free radical), reaction (1.3) is essentially a termination reaction and growth may only proceed by reinitiation of the product. The RSGP model is shown in figure 1.5

Figure 1.5

The rapid step growth polymerization scheme (RSGP)[43].

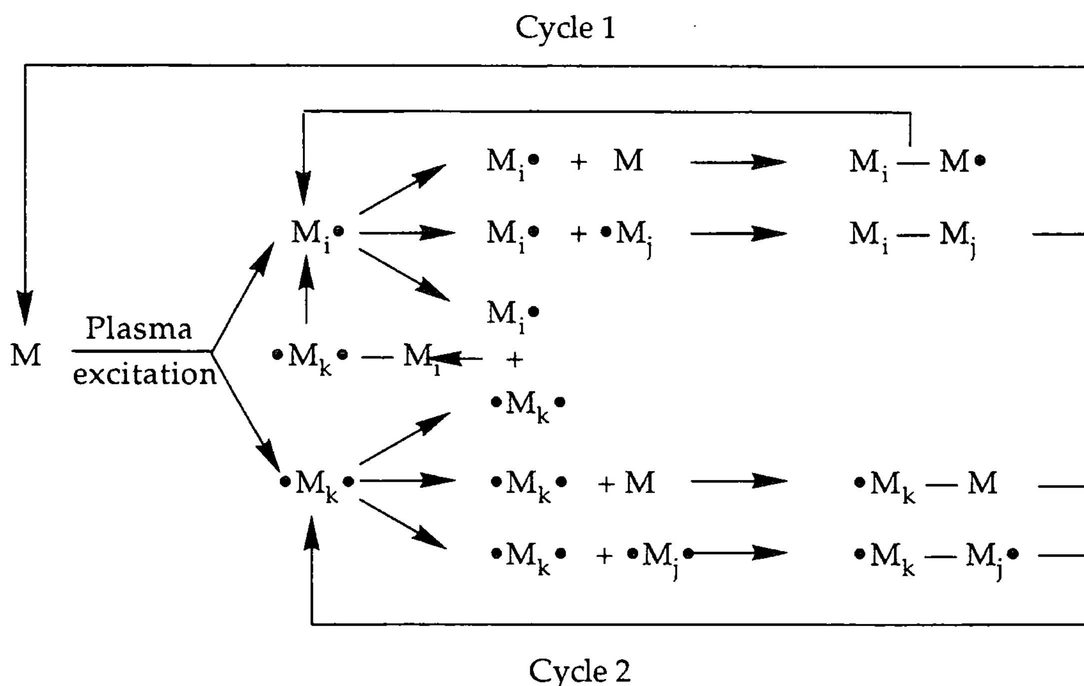

As can be seen, the RSGP proceeds through two parallel cycles. Cycle 1 takes place through repeated activation of the reaction products from monofunctional species. Cycle 2 occurs through difunctional or multifunctional species. The RSGP model illustrates the complex nature of the plasma polymerization process.

Ionic species can contribute to the polymerization through ion-molecule reactions or the interaction of positive and negative ions[3]. However, it appears that free radicals are the dominating species controlling

the polymerization by radical-molecule or radical-radical reactions[49,50]. The reason for this may be explained by considering the ionization energy of organic molecules and the bond energies of primary bonds, some of which are given in table 1.1[51].

Table 1.1

Examples of the energy of some common bonds.

Bond	Energy/eV	Bond	Energy/eV
C-H	4.3	C=O	8.0
C-N	2.9	C-C	3.4
C-Cl	3.4	C=C	6.1
C-F	4.4	C≡C	8.4

The energies required to disrupt such bonds are more easily attained by species in the plasma than the energies (i.e. > 10 eV) needed for ionization. Residual free radicals involved in the RSGP mechanism remain trapped in the polymer. Monomers with triple bonds yield the greatest number of trapped free radicals followed by monomer with double bonds[43].

To allow greater control over plasma polymer structure attempts have been made to limit the degree of dissociation during deposition, so that functional groups within monomers, such as oxygen or nitrogen containing groups, are preserved and incorporated in to the film. Among the methods investigated are pulsed RF discharges[52,53] and remote plasma deposition[54]. Pulsed plasma polymerization is the subject of studies in chapters 5 and 6 of this thesis. Minimization of precursor fragmentation can also be achieved by lowering the substrate temperature during deposition causing increased precursor adsorption which consequently increases the fraction of unfragmented monomer in the film[3].

1.2.6.2 Polymerization Parameters

A distinguishing feature of plasma polymerization mentioned earlier is that the chemical structure of the resultant material is dependent on the process parameters and not the original monomer. The most important factor that governs structure under conditions of constant pressure, plasma excitation source, and monomer is the power (W) to flow-rate (F) ratio, W/F[55].

Taking into consideration the molecular weight of the monomer (M) a modified parameter[43,56] W/FM is obtained. As the dissociation of a monomer into reactive fragments in the plasma should be related to the energy received per unit molecule the dependence of chemical structure on this parameter is well rationalized[3].

The parameter W/FM does not account for the effects of reactor geometry so straightforward comparison of specific W/FM values between different reactors is difficult[57]. Attempts have been made to include a reactor volume factor, but work in this area is far from complete[43]. The major drawback is that plasma polymerization occurs in the glow discharge volume which for different reactor configurations is not always the same as the reactor volume.

1.2.7 Aims of Current Work

The aims of this thesis are two-fold. The first aim is to provide a greater understanding of the basic processes that occur within glow discharges. Both the chemical and physical nature of the plasmas will be studied. The second aim is to explore the mechanisms that occur in plasma polymerization, and find ways of controlling the chemistry of the plasma polymer formed.

1.3 ANALYTICAL TECHNIQUES

1.3.1 Introduction

The analytical tools used in this work fall into three categories; surface characterization, bulk characterization, and plasma diagnostics. Surface analysis has been carried out using both X-ray photoelectron spectroscopy, to study the chemistry of the systems, and atomic force microscopy used to assess physical modifications. Bulk analysis was performed using infrared spectroscopy and the relatively new technique of X-ray absorption spectroscopy. Finally, optical emission spectroscopy has been used to probe the plasma phase.

1.3.2 X-ray Photoelectron Spectroscopy

Surface analysis by X-ray photoelectron spectroscopy (XPS) involves irradiating a solid under vacuum with monoenergetic soft X-rays and analysing the energy spectrum of emitted electrons[58]. Each element has a unique spectrum. As the inelastic mean free path of electrons in a solid is small, the detected electrons originate from only the top few atomic layers, making XPS an extremely surface sensitive technique. Quantitative compositional data can be obtained from peak areas and chemical states can be identified from exact measurement of peak positions and separations, as well as from certain spectral features[58].

Emitted photoelectrons studied in XPS lie in the energy range of 0 eV up to the energy of the X-ray source These electrons have inelastic mean free paths of 2-3 nm which corresponds to about 10 atomic layers in most materials[6]. Measurement of inelastic mean free paths is difficult so a parameter known as attenuation length, which also includes the effect of

elastic scattering, is determined. The variation of attenuation length with the kinetic energy of escaping electrons[59] is shown in figure 1.6.

Inelastic energy loss processes for electrons in solids include excitation of lattice vibrations (phonons), collective oscillations of the electron gas (plasmons) and electron interband transitions or ionization[60]. At very low kinetic energy electrons are unable to excite any of the above quantized transitions and their mean free paths are long. At high kinetic energies the cross-section of exciting these transitions is low and escape depths are again large[60]. At the intermediate energies (those studied in XPS) the photoelectrons lose a large proportion of their energy to these processes and so the mean free paths are very short.

Figure 1.6

An illustration of how attenuation length varies with increasing kinetic energy of the escaping photoelectron.

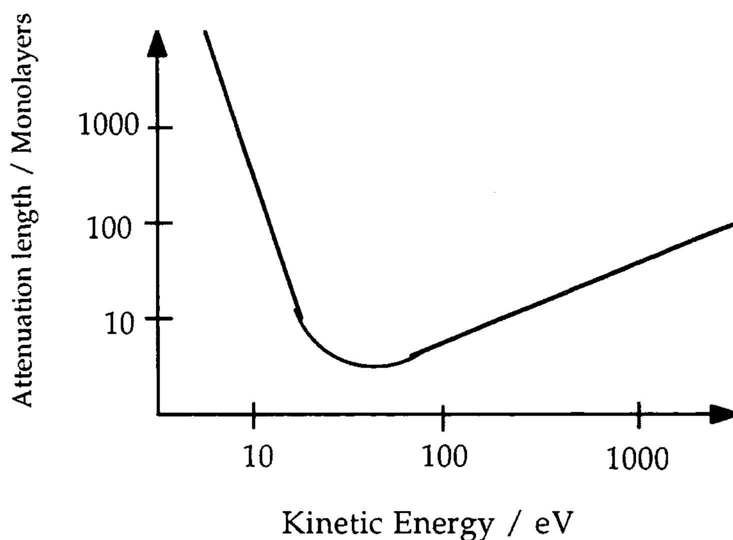

1.3.2.1 The Photoionization Process

Photoelectron spectroscopy is based on the photoelectric effect[61] which describes the ejection of electrons from atoms or molecules upon

exposure to electromagnetic radiation. Each atom present at a surface has valence electrons involved in bonding and, except for hydrogen, core electrons not directly involved in bonding[62]. The binding energy (E_b) of these core electrons is characteristic of the individual atom to which it is bound. Information on the binding energy of electrons within a sample allows qualitative elemental analysis. In the XPS experiment, the sample is irradiated by low-energy X-rays under ultra high vacuum (UHV) conditions (better than 10^{-6} Torr). Photoionization occurs in the sample surface and the resultant photoelectrons are ejected (provided they overcome the work function of the solid, ϕ, and they are not inelastically scattered) with kinetic energy (E_k) which is related to the incident photon ($h\upsilon$) energy and binding energy by the Einstein relation[62], equation 1.3.

$$E_k = h\upsilon - E_b - \phi \qquad (1.3)$$

Two other competing processes can occur simultaneously after photoionization[63], all three are shown in figure 1.7.

Figure 1.7
The processes of photoionization, X-ray fluorescence and Auger electron emission.

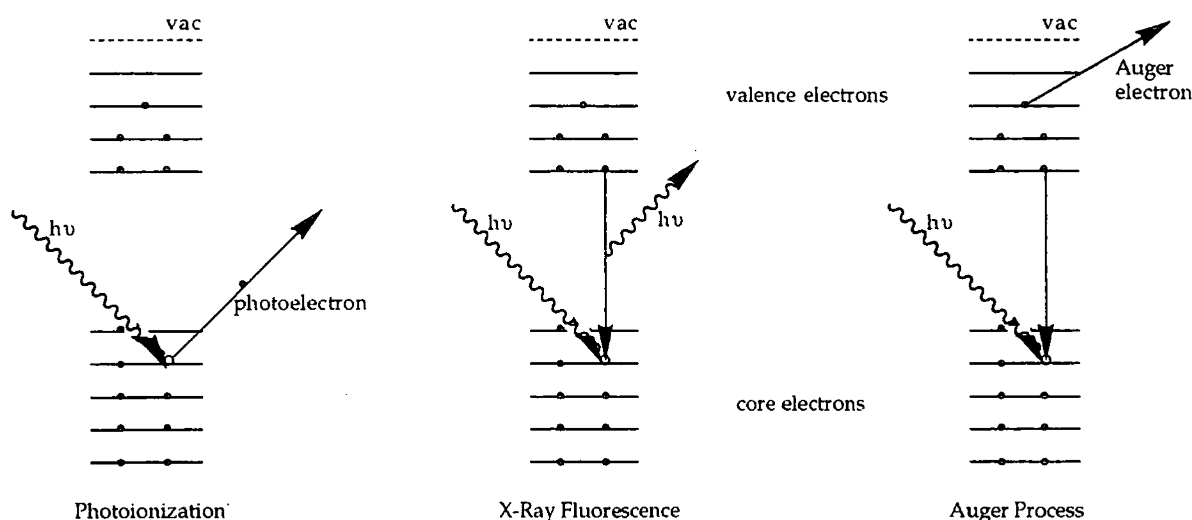

During X-ray fluorescence the hole created by ionization is filled by an outer shell electron. A photon (usually in the X-ray region) is emitted with energy equal to the difference in energy between the hole and electron. This process can lead to information about the energy levels within the sample. The Auger process occurs when a secondary electron is ejected after the outer shell electron fills the hole. The ionization potential of the secondary electron must be lower than the available energy from the relaxation processes. Auger electron spectroscopy (AES) also gives information about energy levels and elemental composition of materials[58,63,64]. X-ray fluorescence is the dominant de-excitation process in small atoms and Auger electron emission dominates in larger atoms.

Since X-ray fluorescence and Auger processes are independent of the primary ionization mechanism, they can be initiated by electron impact ionization as well as by photon impact. The kinetic energy of electrons emitted from photoionization increases with increasing photon energy but the energy of an Auger electron is not affected due to the indirect mechanism of electron release. This provides a useful way of distinguishing between photoelectrons and Auger electrons in an XP spectrum[63].

The probability that photoionization will occur is called the photoionization cross-section, σ. This is defined[65] as the transition probability per unit time of a core level electron with a unit incident photon flux of 1 cm^{-1} s^{-1}. Photoionization cross sections are a function of photon energy, core level binding energy, atomic number and the relative directions of photon incidence and electron emission[65].

1.3.2.2 Spectral Interpretation

The XP spectrum is displayed as a plot of electrons counted per second versus electron binding energy. The number of photoelectrons collected

from a particular atom's core level, per unit time, is a measure of the abundance of that element. The most intense photoelectron lines are relatively symmetrical and typically the narrowest lines observed in the spectrum. Peak width is a combination of natural line width, X-ray line width and instrumental contributions[58]. When comparing XPS lines from the same element in different chemical environments, shifts in the peak are observed[65]. Chemical shifts can be understood by examining the basic physics involved with the change in binding energy. The attractive potential of a nucleus and the repulsive Coulomb interaction with other electrons determines the energy of an electron in a tightly bound core state. When the chemical environment of the atom changes, a spatial rearrangement of the average charge distribution occurs because of the creation of a different potential by the nuclear and electronic charges of the other atoms in the compound. The magnitude of the shift is determined by the type and strength of the bond[65].

1.3.2.2.1 X-ray Satellites

Standard X-ray sources consist of a heated filament (cathode) and a target anode (usually Mg or Al) with a large (kV) potential applied between them. Electron bombardment of the anode causes characteristic X-ray emission together with a continuous background of bremsstrahlung radiation which results from the electrons decelerated by impact with the target. A magnesium anode produces an X-ray spectrum dominated by a very intense, unresolved, $K\alpha_1$ - $K\alpha_2$ doublet resulting from transitions $2p_{3/2} \rightarrow 1s$ and $2p_{1/2} \rightarrow 1s$ respectively.

Most laboratory X-ray sources are non-monochromatic, and contain not only the characteristic X-ray energy, but also some minor components at higher photon energies (e.g. Mg $K\alpha_3$, $K\alpha_4$, $K\alpha_5$, $K\alpha_6$ and K_β)[66]. Each of these can give rise to a family of peaks in the XP spectrum at binding energies

below the peak position expected from the most intense X-ray line. These less intense peaks are called X-ray satellites[65,66].

1.3.2.2.2 Shake-up and Shake-off Satellites

Due to rearrangement of charge around the core hole the photoionization event may be accompanied by excitation or emission of a valence electron. These processes are termed shake-up and shake-off respectively and are shown in figure 1.8.

Figure 1.8

The processes of photoionization, shake-up and shake-off.

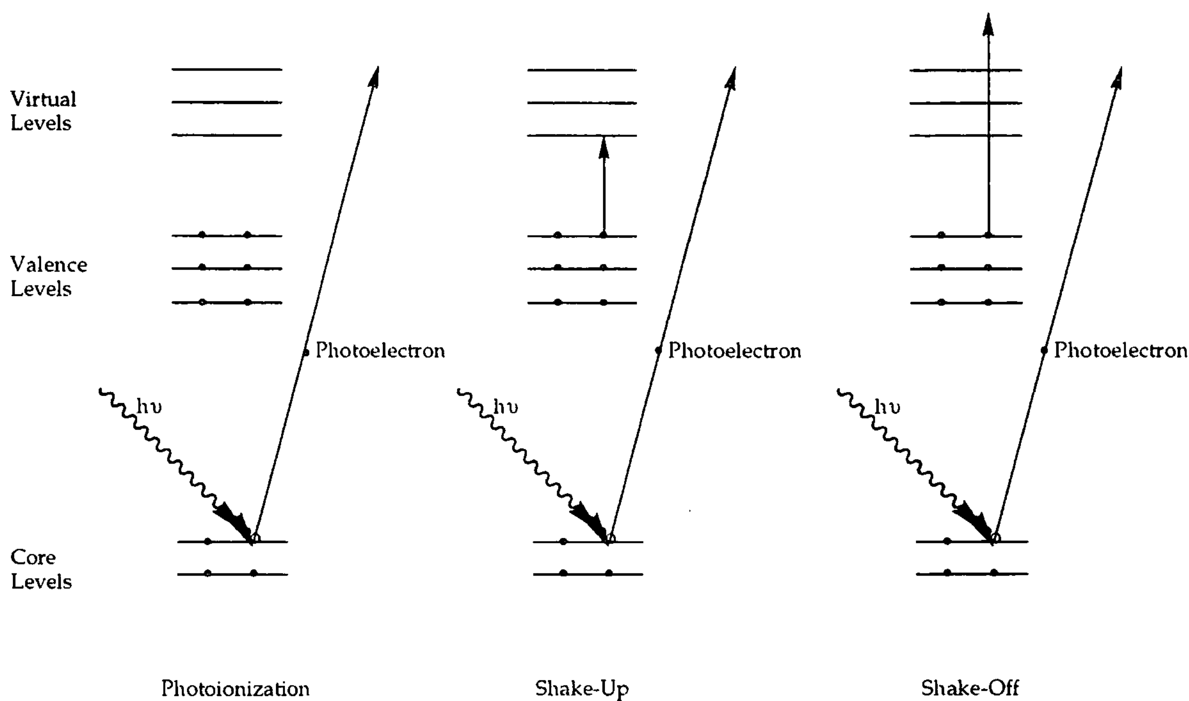

When this occurs the kinetic energy of the emitted photoelectron is reduced by an amount corresponding to the energy difference between the ground state and the excited state of the atom. This results in the formation of satellite peaks a few eV higher in binding energy (lower in kinetic energy)

than the main photoelectron peak. In organic compounds the presence of shake-up satellites is indicative of aromatic species ($\pi \rightarrow \pi^*$ transitions)[67].

1.3.2.2.3 Multiplet Splitting

Multiplet splitting arises when the system being studied has unpaired electrons in the valence levels[66]. After photoionization an unpaired electron is left behind. If, for example, the system has unpaired electrons with parallel spins and the unpaired electron generated on photoionization is parallel to these, then interactions can occur, resulting in a lower energy than for the case of anti-parallel spin.

1.3.3 Atomic Force Microscopy

Atomic force microscopy (AFM) is an exciting technique available for imaging surface morphology. The AFM can be operated under atmospheric conditions and requires no special sample preparation. The method was developed by Binnig[68] to examine non-conducting solids on the atomic scale[69]. It belongs to the family of scanning force microscopies and is closely related to the scanning tunnelling microscope (STM).

In the AFM experiment a sharp tip, mounted on the end of a cantilever, is brought close enough to a sample such that it interacts with the atoms on the surface, figure 1.9. The AFM monitors the atomic force interaction between the tip and the surface. The deflection of the tip is measured via a laser configuration as the surface is rastered under the tip using a piezoelectric scanner. The AFM can be operated in either contact mode or Tapping® mode. The sample and tip are kept in close contact throughout the entire scan during contact mode. A feedback system is used to adjust the vertical position of the AFM tip above the sample surface to keep the deflection of the tip, and therefore the force, constant. In Tapping®

mode the cantilever vibrates and small shifts in the vibration amplitude can be detected[70] hence the force imparted on the surface is very small. This mode is particularly useful for imaging soft samples.

Figure 1.9

A schematic diagram of the AFM experimental set-up.

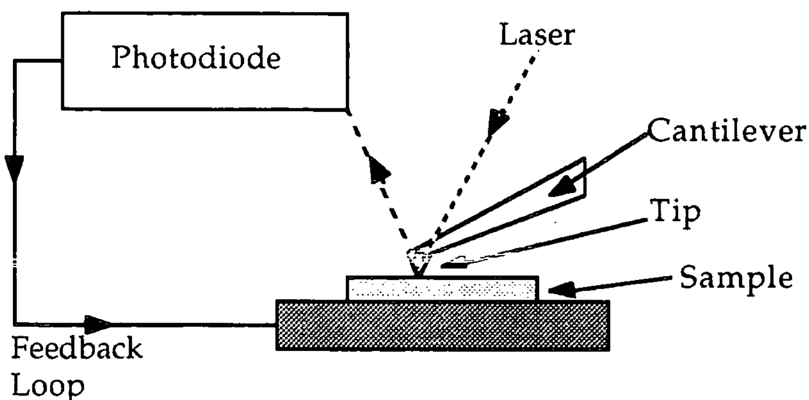

AFM explores the interaction of potential functions between the tip and the sample with no transfer of electrons, whereas STM requires a conducting sample. The technique is therefore gaining immense popularity in the imaging of polymers[71-75].

1.3.4 Infrared Spectroscopy

Surface analysis of plasma modified and deposited polymers is very important in order to elucidate their surface chemistry. Bulk analysis can also prove very useful especially in the case of plasma polymers and this section deals with the method of transmission infrared (IR) spectroscopy.

When a molecule absorbs electromagnetic radiation it's energy increases in proportion to the energy of the photon[76] as expressed by equation 1.4.

$$\Delta E = hc/\lambda \qquad (1.4)$$

where h = Plancks constant, c = speed of light, λ = wavelength of the photon. The increase in energy may be in the electronic, vibrational, or rotational energy of the molecule. If a molecule absorbs radiation in the microwave region only its rotational energy will change. If the radiation absorbed is in the infrared region both vibrational and rotational energies of the molecule will change. If the energy is much greater, i.e. UV light, there will be increases in the electronic, vibrational, and rotational energies of the molecule[77].

According to classical theory, absorption of electromagnetic radiation is possible only when there is a change in the dipole moment of the molecule during the normal vibration. This is the selection rule for infrared absorption, defining allowed transitions. When there is no change in the dipole moment of a molecule during normal vibration, it will be infrared inactive and the transition is said to be forbidden. It is for this reason that a lower number of vibrational frequencies are sometimes observed than would be expected for certain molecules[77], especially molecules with a high degree of symmetry.

The vibrations associated with covalently linked atoms may be classified into stretching vibrations, involving periodic extension and contraction of the bonds, and bending or deformation vibrations involving periodic bending of bonds. Force constants for the bending mode are generally about an order of magnitude smaller than for stretching modes and are more sensitive to their chemical bonding environment. Complex types of vibrations involving both stretching and bending of several bonds attached to the same atom are also possible. Some examples of different stretching and bending vibrations of XY_2 and XY_3 groups are shown in figure 1.10.

Figure 1.10

Molecular vibrations seen in the IR (a) XY_2 symmetrical stretching, (b) XY_2 asymmetric stretching, (c) XY_3 symmetrical stretching, (d) XY_3 asymmetric stretching, (e) XY_2 in-plane deformation (scissoring), (f) XY_2 out-of-plane deformation (twisting), (g) XY_2 out-of-plane deformation (wagging), (h) XY_2 rocking, (i) XY_3 symmetrical deformation, (j) XY_3 asymmetrical deformation. (Note that + and - indicate above and below the plane of paper respectively).

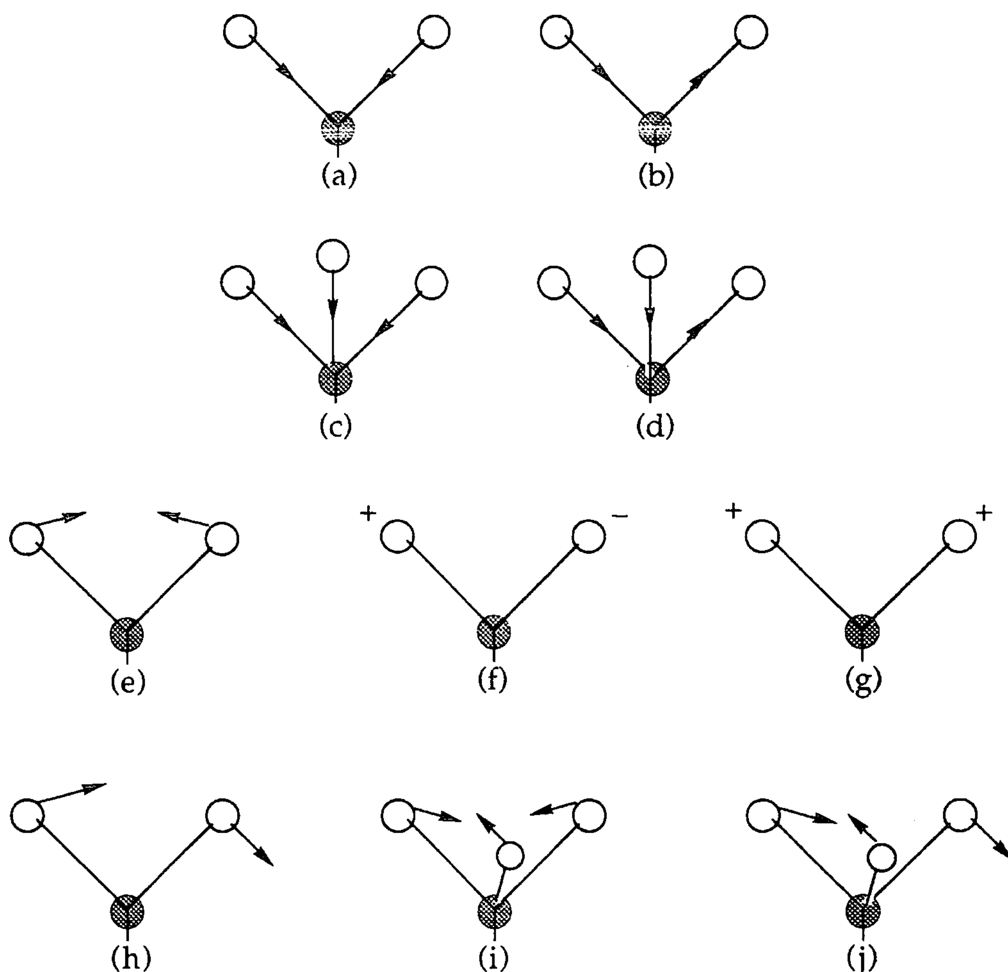

Bending vibrations occur at lower frequencies in the spectrum than stretching vibrations due to their smaller force constants. The infrared spectrum of a solid may differ significantly from that of the free molecule due to intermolecular interactions restricting some bond movements. IR spectra of plasma polymers often bear some relationship to the spectrum of

the monomer or a conventional polymer of the monomer. Peaks in the spectra of plasma polymers tend to be broader and less well defined than in the monomer. This indicates the formation of a large variety of slightly different chemical environments for each functional group within the plasma polymer[78].

Attenuated total reflectance (ATR) spectroscopy is a method often used to study the surface of materials[79]. A trapezoidal block of transparent material (e.g. thallium bromide/thallium iodide known as KRS-5)[80], as shown in figure 1.11, is used in this method[81].

Figure 1.11

A diagram of the ATR-IR cell set up.

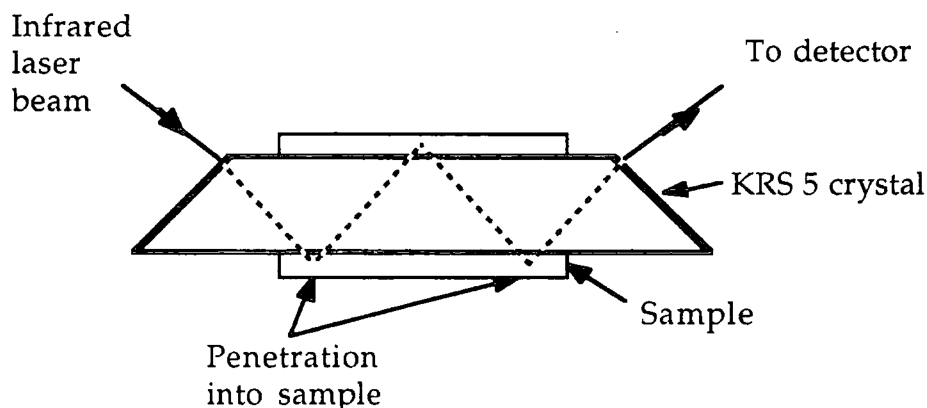

The incident angle is chosen so that the radiation will strike the flat surfaces at less than the critical angle and will undergo total internal reflection to emerge, only slightly diminished in intensity. Although the internal reflection is conventionally called 'total', the radiation penetrates slightly beyond the surface of the crystal during each reflection. If a sample is pressed closely to the outside of the crystal the beam will travel a small distance through the sample at each reflection and beam intensity is lost at wavelengths absorbed by the sample surface. The amount of penetration into the sample depends on the wavelength of the radiation, the angle of

incidence and the refractive index of both the crystal and sample, but is in the order of 10^{-4} to 10^{-3} cm for infra-red. During its passage through the crystal the beam may undergo some 10-20 reflections, so the total path length is 10^{-3} - 10^{-2} cm which is adequate for the production of a reasonable spectrum.

1.3.5 X-ray Absorption Spectroscopy

Over the past twenty years X-ray absorption spectroscopy (XAS) has developed into a standard bulk technique for the determination of structure in condensed matter systems[82]. This is a consequence of the increased availability of synchrotron radiation sources. The strength of the technique arises from its ability to probe the local structure around a specific element within the material[83-86]. Since it has no requirement for long range order unlike X-ray diffraction, it is ideal for studying amorphous, disordered and biological systems.

The basic physical processes involved in X-ray absorption are depicted in figure 1.12. The energies of the core electron levels are determined uniquely by the atom and its bonding environment, therefore, tuning the photon energy to a particular core level immediately gives an atom-specific probe. When the photon energy is greater than the binding energy of the core level, a photon may be absorbed resulting in the ejection of a photoelectron[87].

If the X-ray absorption cross-section of a particular element in the solid state is measured as a function of increasing photon energy, a characteristic absorption 'edge' is observed which corresponds to the onset of electron transitions from core states on the atom to unoccupied states of higher energy, figure 1.13. These cross-sections then typically reduce in magnitude over a range of thousands of electron volts beyond the edge.

Superimposed on this gradual decay are modulations in the cross-section which appear as peaks in the XA spectrum.

Figure 1.12

Photon absorption by an atom followed by (a) photoelectron emission and (b) backscattering by neighbouring atoms.

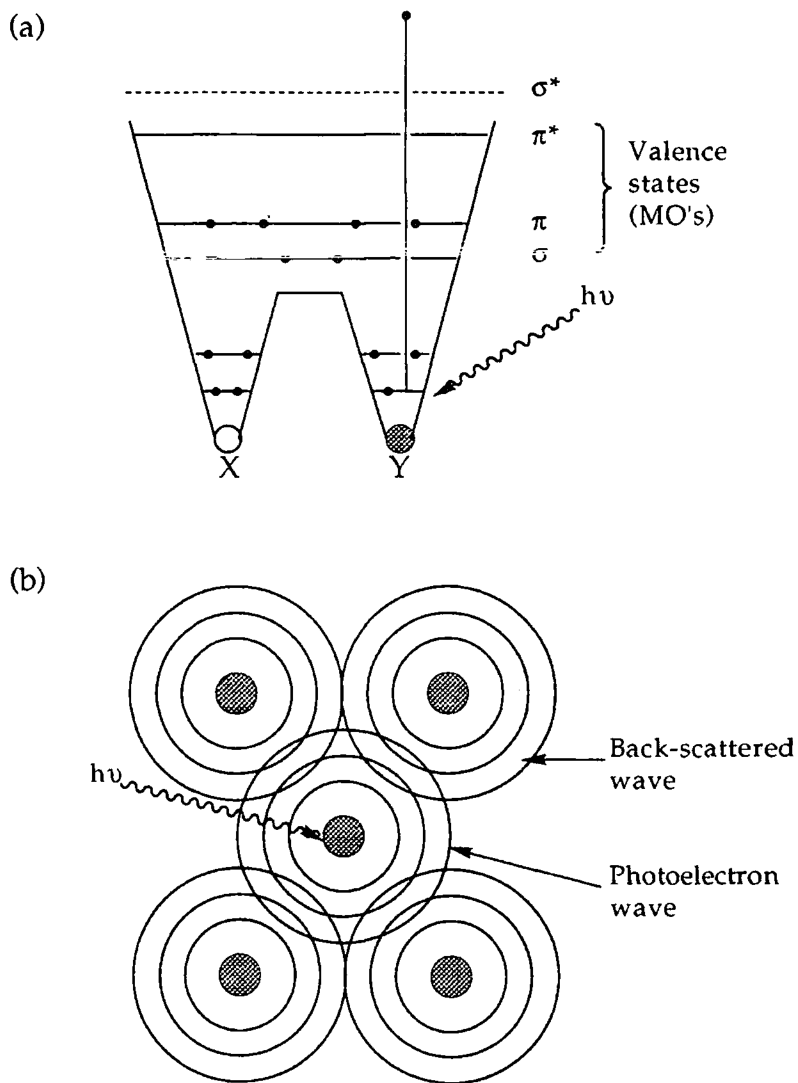

Figure 1.13

The S K edge X-ray absorption spectrum of a sulfur standard, the important features are labelled.

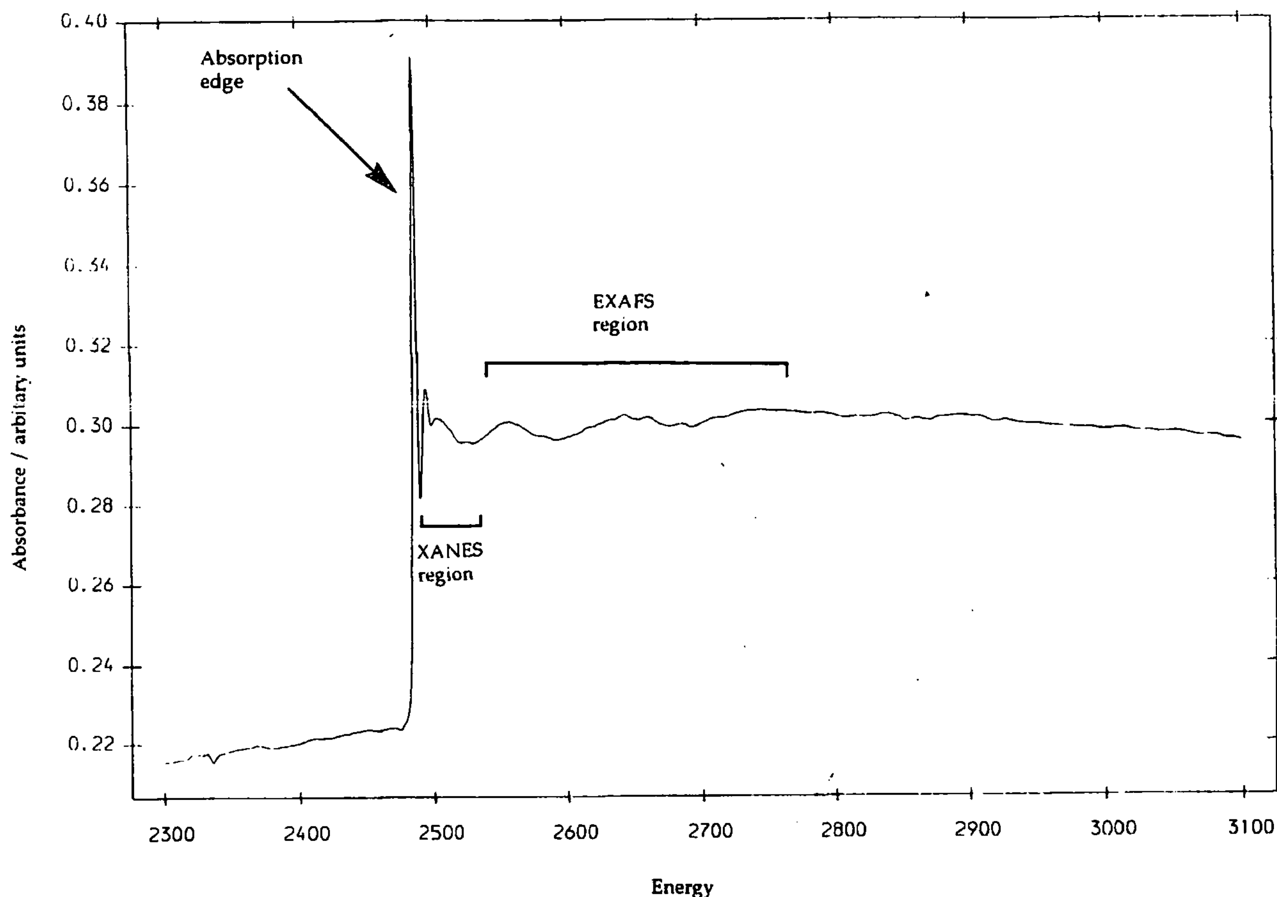

For photon energies immediately after (up to ≈ 50 eV) the absorption edge, the photoelectron interacts with the molecular orbital and so the absorption cross-section is strongly affected by the electronic structure of the material, figure 1.12(a). Two types of features may be observed in this region. Strong, narrow peaks at the absorption edge generally correspond to excitation to bound π^* unoccupied molecular orbitals. Broader, less intense peaks at slightly higher photon energies are usually σ^* shape resonances from transitions to quasibound σ^* states. The modulations in this region are commonly referred to as X-ray absorption near edge structure (XANES) or near edge X-ray absorption fine structure (NEXAFS), figure 1.13. At

higher photon energies (more than 50 eV pass the edge), the photoelectron has a much higher kinetic energy and so behaves more like a free electron. The modulations in this region are due to scattering of the photoelectron wavefunction by neighbouring atoms, which modifies the amplitude of the wavefunction by interference. Thus the oscillations in this energy region are sensitive to the structure of the material and using rigorous mathematical analysis the short range order may be determined. These modulations can extend hundreds of electron volts above the edge and so are known as extended X-ray absorption fine structure (EXAFS)[82], figure 1.13.

1.3.6 Optical Emission Spectroscopy

Analysis of the surface and bulk of materials resulting from plasma processes have been described. Diagnostic techniques are also available allowing the active plasma to be probed during deposition. One of the most commonly used diagnostic tools is optical emission spectroscopy (OES) which operates by spectral analysis of the light emitting from the plasma. It has the advantage of being external and non-intrusive to the plasma[88].

Optical emission can be produced in a plasma as a result of electron impact excitation or dissociation:-

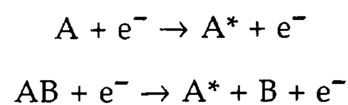

$$A + e^- \rightarrow A^* + e^-$$
$$AB + e^- \rightarrow A^* + B + e^-$$

or by ion impact process:-

$$A^+ + X \rightarrow A^*(+M)$$

which creates an excited species A^*, followed by release of this energy

$$A^* \rightarrow A^{**} + h\upsilon$$

In the above reactions A^* = an excited emitting species, X = a neutral, a negative ion, an electron plus a third body or a surface in contact with the plasma, A^{**} = a ground state or excited state in an energy level lower than A^*.

Usually, the most intense radiation emitted from the plasma originates in the transition from the first excited state W_1, to the ground state W_0 of the particle[3]. As every particle has precisely quantized levels, each emits a characteristic spectral line of frequency:-

$$\nu_{1,0} = W_1 - W_0/h$$

and wavelength:-

$$\lambda_{1,0} = hc/W_1 - W_0$$

where c is the velocity of light.

The apparatus for OES comprises a monochromator to disperse the light emitted from the plasma , optics to image the light and a photodetector to measure the dispersed light. Although the emissions from the plasma span a very large range of frequencies , from the infrared to the soft X-ray, the spectra most widely used in OES span the range 200 to 900 nm[3].

For ion identification the detector must be able to monitor lines with wavelength $\lambda < 200$ nm because ion transitions occur at shorter wavelengths and the monochromator must be under vacuum to avoid absorption of these shorter wavelengths. Emission spectra from plasmas are often very complicated. Atomic or diatomic species have simpler, narrower spectra than polyatomic species which have broad spectra due to their vibrational and rotational transitions.

1.4 REFERENCES

1. Langmuir, I. *Phys. Rev.* **1929**, *33*, 954.
2. Watson, C. J. H. In *Plasma Physics*; Keen, B. E. Ed.; The Institute of Physics: London, 1974; chapter 1.
3. Grill, A. *Cold Plasma in Materials Fabrication*; IEEE Press: Piscataway NJ, 1993.
4. Chapman, B. *Glow Discharge Processes*; Wiley: New York, 1980.
5. Hollahan, J. R.; Bell, A. T. *Techniques and Applications of Plasma Chemistry*; Wiley: New York, 1974.
6. Graves, D. B.; Jensen, K. F. *IEEE Trans. Plasma Sci.* **1986**, *PS 14*, 78.
7. Fang, D.; Marcus, R. K. In *Glow Discharge Spectroscopies*; Marcus, R. K. Ed.; Plenum: New York, 1993; chapter 2.
8. Braithwaite, N. St. *J Pure Appl. Chem.* **1990**, *62*, 1721.
9. Okuno, Y.; Ohtsu, Y.; Komatsu, C.; Fujita, H. *J. Appl. Phys.* **1993**, *73*, 1612.
10. Rossnagel, S. M. In *Thin Film Processes II*; Vossen, J. L.; Kern, W. Eds.; Academic: London, 1991; chapter II-I.
11. Wertheimer, M. R.; Moisan, M. *J. Vac. Sci. Technol.* **1985**, *A3*, 2643.
12. Moisan, M; Barbeau, C.; Claude, R.; Ferreria, C. M.; Margot, J.; Paraszczak, J.; Sa, A. B.; Sauve, G.; Wertheimer, M. R. *J. Vac. Sci. Technol.* **1991**, *B9*, 8.
13. McTaggart, F. K. *Plasma Chemistry in Electrical Discharges*; Elsevier: Amsterdam, 1967.
14. Winters, H. F. In *Topics in Current Chemistry, Plasma Chemistry III*; Veprek, S.; Venugopalan, M. Eds.; Springer-Verlag: Berlin, 1980; page 69.
15. Morra, M.; Occhiello, E.; Garbassi, F. *Sur. Int. Anal.* **1990**, *16*, 412.
16. Beachamp, J. L.; Buttrill, S. E. *J. Chem. Phys.* **1968**, *48*, 1783.

17. Chan, C-M. *Polymer Surface Modification and Characterization*; Hanser: New York, 1993.

18. Morra, M.; Occhiello, E.; Garbassi, F. *Langmuir* **1989**, *5*, 872.

19. Golub, M. A.; Wydeven, T.; Cormaia, R. D. *Langmuir* **1991**, *7*, 1026.

20. Clark, D. T.; Hutton, D. R. *J. Polym. Sci., Polym. Chem. Ed.* **1987**, *15*, 2643.

21. Yasuda, H.; Marsh, H. C.; Brandt, S.; Reilley, C. N. *J. Polym. Sci., Polym. Chem. Ed.* **1977**, *15*, 991.

22. Kusabriaki, M. *Japn. J. Appl. Phys.* **1990**, *29*, 2809.

23. Golub, M. A.; Lopata, E. S.; Finney, L. S. *Langmuir* **1993**, *9*, 2240.

24. Hoshino, S.; Yumoto, M.; Sakai, T. *Proc. 11th Internat. Symp. Plasma Chem.* Loughborough, England, 1993, 1253.

25. Egitto, F. D.; Matienizo, L. J.; Schreyer, H. B. *J. Vac. Sci. Technol.* **1992**, *A10*, 3060.

26. Klausner, M.; Loh, I. H.; Baddour, R. F.; Cohen, R. E. *Proc. ACS Div. Polymeric Mater. Sci. Eng.* **1987**, *56*, 227.

27. Momose, Y.; Tamura, Y.; Ogino, M.; Okazaki, S.; Hirayama, M. *J. Vac. Sci. Technol.* **1992**, *A10*, 229.

28. Wheeler, D. R.; Pepper, S. V. *J. Vac. Sci. Technol.* **1982**, *20*, 226 and 442.

29. Clark, D. T.; Dilks, A. *J. Polym. Sci., Polym. Chem. Ed.* **1977**, *15*, 2321.

30. LeMoe, A.; Duraud, J. P.; Le Gressus, C.; Okuzumi, H. *Scanning Electron Microscopy* **1986**, 1319.

31. Hansen, R. H.; Schonhorn, H. *J. Polym. Sci. Polym. Lett.* **1966**, *4*, 203.

32. Gilman, A. B.; Goldshtein, D. V.; Potapov, V. K.; Shifrina, R. R. *High Energy Chemistry* **1988**, *22*, 393.

33. Tran, C. N. B.; Walt, D. R. *J. Colloid. Interface. Sci.* **1989**, *132*, 373.

34. Hollahan, R.; Stafford, B. B.; Falb, R. D.; Payne, S. T. *J. Appl. Polym. Sci.* **1969**, *13*, 807.

35. Kramer, P. W.; Yeh, Y. S.; Yasuda, H. *J. Membr. Sci.* **1989**, *46*, 1.

36. Garbassi, F.; Morra, M.; Occhiello, E. *Polymer Surfaces*; Wiley: Chichester, 1994.

37. Gerenser, L. J. *J. Adhes. Sci. Tech.* **1987**, *1*, 303.

38. Flory, P. J. *Principles of Polymer Chemistry*; Cornell Univ. Press: Ithaca NY, 1967.

39. Hansen, R. H.; Schonhorn, H. *J. Polym. Sci.* **1966**, *B4*, 203.

40. Flamm, D. L. In *Plasma Etching*; Manos, D. M.; Flamm, D. L. Eds.; Academic: London, 1989; chapter 2.

41. Moisan, M.; Barbeau, C.; Claude, R.; Ferreria, C. M.; Margot, J.; Paraszczak, J.; Sa, A. B.; Sauve, G.; Wertheimer, M. R. *J. Vac. Sci. Tech.* **1991**, *B9*, 8.

42. Bell, A. T In *Topics in Current Chemistry, Plasma Chemistry III*; Veprek, S.; Venugopalan, M. Eds.; Springer-Verlag: Berlin, 1980; page 43.

43. Yasuda, H. *Plasma Polymerization*; Academic: London, 1985.

44. Yasuda, H. *J. Polym. Sci.: Macro. Rev.* **1981**, *16*, 199.

45. Poll, H. U.; Artz, M.; Wickleder, K. H. *Eur. Polym. J.* **1970**, *12*, 505.

46. Yasuda, H.; Iriyama, Y. In *Comprehensive Polymer Science Vol. 4*; Allen, G.; Bevinton, J. C. Eds.; Pergamon: Oxford, 1989; chapter 21.

47. d'Agostino, R.; Cramarosa, F.; Fracassi, F.; Illuzzi, F. In *Plasma Deposition, Treatment, and Etching of Polymers*; d'Agostino, R. Ed.; Academic: London, 1990; chapter 2.

48. Stevens, M. P. *Polymer Chemistry 2nd Ed.*; Oxford Uni. Press: New York, 1990.

49. Kobayashi, H.; Shen M.; Bell, A. T. *J. Macromol. Sci. Chem.* **1974**, *8*, 1345.

50. Morita, S.; Migutani, T.; Ieda, M. *Jpn. J. Appl. Phys.* **1971**, *10*, 1275.

51. Morosoff, N. In *Plasma Deposition, Treatment, and Etching of Polymers*; d'Agostino, R. Ed.; Academic: London, 1990; chapter 1.

52. Pedrow, P. D.; Nasiruddin, A. M.; Mahalingam, R. *IEEE Trans. Plasma Sci.* **1990**, *18*, 945.

53. Savage, C. R.; Timmons, R. B. *Chem. Mat.* **1991**, *3*, 575.

54. Kushner, M. J. *J. Appl. Phys.* **1993**, *73*, 4098.

55. Morosoff, N.; Yasuda, H. Brandt, E. S.; Reilley, C. N. *J. Appl. Polym. Sci.* **1979**, *23*, 3449.

56. Yasuda, H.; Hirotsu, T. *J. Polym. Sci.: Polym. Chem. Ed.* **1978**, *16*, 743.

57. Yeh, Y. S.; Shyy, I. N.; Yasuda, H. *J. Appl. Polym. Sci.: Appl. Polym. Sym.* **1988**, *42*, 1.

58. Chastain, J. *Handbook of X-Ray Photoelectron Spectroscopy*; Perkin Elmer Corporation: Eden Prairie Mn, 1992; chapter 1.

59. Smith, G. C. *Surface Analysis by Electron Spectroscopy*; Plenum: New York, 1994; chapter 1.

60. Prutton, M. *Surface Physics*; Oxford Uni. Press: Oxford, 1983.

61. Sherwood, P. M. A. In *Spectroscopy*; Straughan, B. P.; Walker, S. Eds.; Chapman and Hall: London, 1976, chapter 7.

62. Christie, A. B. In *Methods of Surface Analysis*; Walls, J. M. Ed.; Cambridge Uni. Press: Cambridge, 1989, chapter 5.

63. Ghosh, P. K. *Introduction to Photoelectron Spectroscopy*; Wiley: New York, 1983.

64. Alvarez, J.; Asensio, M. C. In *Spectroscopic Characterization of Heterogeneous Catalysis*; Fierro, J. L. G. Ed.; Elsevier: Amsterdam, 1990, chapter 2.

65. Nelson, A. J. In *Microanalysis of Solids*; Yacobi, B. G.; Holt, D. B.; Kazmerski, L. L. Eds.; Plenum: New York, 1994, chapter 9.

66. Briggs, D.; Seah, M. P. *Practical Surface Analysis*; Wiley: Chichester, 1990.

67. Clark, D. T.; Dilks, A. *J. Polym. Sci., Polym. Chem, Ed.* **1976**, *14*, 533.

68. Binnig, G.; Quate, C. F.; Gerber, C. *Phys. Rev. Lett.* **1986**, *56*, 930.

69. Reneker, D. H. In *New Characterization Techniques for Thin Polymer Films*; Tong, H-M, Nguyen, L. T. Eds.; Wiley: New York, 1990, chapter 12.

70. *NanoScope Optical Viewing System Manual;* Digital Instruments Inc: Santa Barbara Ca.

71. Dietz, P.; Hansma, P. K.; Ihn, K. J.; Motamedi, F.; Smith, P. *J. Mater. Sci.* **1993**, *28*, 1372.

72. Albrecht, T. R.; Dovek, M. M.; Lang, C. A.; Grutter, P.; Quate, C. F.; Kuan, S. W. J.; Frank, C. W.; Pease, R. F. W. *J. Appl. Phys.* **1988**, *64*, 1178.

73. Aime, J. P.; Elkaakour, Z.; Odin, C.; Bouhacina, T.; Michel, D.; Curely, J.; Dautant, A. *J. Appl. Phys.* **1994**, *76*, 754.

74. Kasper, K.; Herrmann, K-H, Dietz, P.; Hansma, P. K.; Inacker, O.; Lehmann, H-D. *Ultramicroscopy* **1992**, *42-44*, 1181.

75. Yang, J.; Laurion, T.; Jao, T-C.; Fendler, J. H. *J. Phys. Chem.* **1994**, *98*, 9391.

76. Atkins, P. W. *Physical Chemistry 4th Ed.*; Oxford Uni. Press: Oxford, 1990.

77. Rao, C. N. R. *Chemical Applications of Infrared Spectroscopy;* Academic: New York, 1963.

78. Shard, A. *Ph.D. Thesis*; 1992, University of Durham.

79. Johnston, S. F. *Fourier Transform Infrared;* Ellis Horwood: London, 1991.

80. Hollas, J. M. *Modern Spectroscopy*; Wiley: Chichester, 1987.

81. Banwell, C. N. *Fundamentals of Modern Spectroscopy*; McGraw-Hill: New York, 1983.

82. Crapper, M. D. *Vacuum*, **1994**, 45, 691.

83. Stohr, J. *NEXAFS Spectrocopy;* Springer-Verlag: Berlin, 1992.

84. Margaritondo, G. *Introduction to Synchrotron Radiation;* Oxford Uni. Press: New York, 1988.

85. Stern, E. A. In *EXAFS Spectroscopy*; Teo, B. K.; Joy, D. C. Eds.; Plenum: New York, 1981, chapter 1.

86. Hodgson, K. O.; Hedman, B.; Penner-Hahn, J. E. *EXAFS and Near Edge Structure III*; Springer-Verlag: Berlin, 1984.

87. Norman, D. J. *Phys. C* **1986**, *19*, 3273.

88. Donnelly, V. M. In *Plasma Diagnostics*; Auciello, O.; Flamm, D. L. Eds.; Academic: London, 1989, chapter 1.

CHAPTER 2

SURFACE TEXTURING AND CHEMICAL MODIFICATION OF PTFE USING NON-EQUILIBRIUM PLASMAS

2.1 INTRODUCTION

The surface of polytetrafluoroethylene (PTFE) can be modified by a vast range of methods which are discussed shortly. For environmental reasons, the recent trend has been to move away from the traditional wet chemical techniques towards cleaner, dryer processes. Plasmas have provided a major alternative route in recent years when modifying the bonding characteristics of polymers. In this chapter, surface treatment of PTFE by O_2, H_2, N_2, He, Ne, Ar, and CF_4 non-isothermal glow discharges is investigated. X-ray photoelectron spectroscopy and atomic force microscopy, are used to evaluate how the chemical and topographical modification of the polymer surface is influenced by the type of feed gas employed.

2.1.1 Wet Chemical Modification of PTFE

The solution most commonly used for PTFE modification is sodium in liquid ammonia. It is believed that the sodium is solvated or coordinated into a complex with several molecules of ammonia[1]. This complex still has an unshared electron, and the group of atoms may be considered as a free radical. The complex can act as a Lewis base by donating its lone electron to the acidic fluorine atoms in PTFE leaving the surface fluorine deficient. The lone electrons then combine to form crosslinked carbon leading to a modified polymer surface[1].

A sodium-naphthalene complex in tetrahydrofuran (THF) has been found to attack the surface of Teflon[2]. The electrical properties remained identical to those of untreated Teflon, however the surface became much more wettable[2]. Another method of modifying the PTFE surface uses alkali metal amalgams (e.g. Li in Hg)[3]. It is believed that the reaction is electrochemical with both active materials forming a typical galvanic cell[4].

It is possible to reduce PTFE using the benzoin dianion to give a surface which has a reflective metallic lustre as opposed to the black colour that arises when using alkali metal solutions. Costello[5] has reported that exposure of PTFE film to the potassium salt of benzoin dianion (in DMSO solvent) produces changes consistent with reduction of PTFE to polymeric carbon, scheme 2.1.

Scheme 2.1

Benzoin dianion reduction of PTFE.

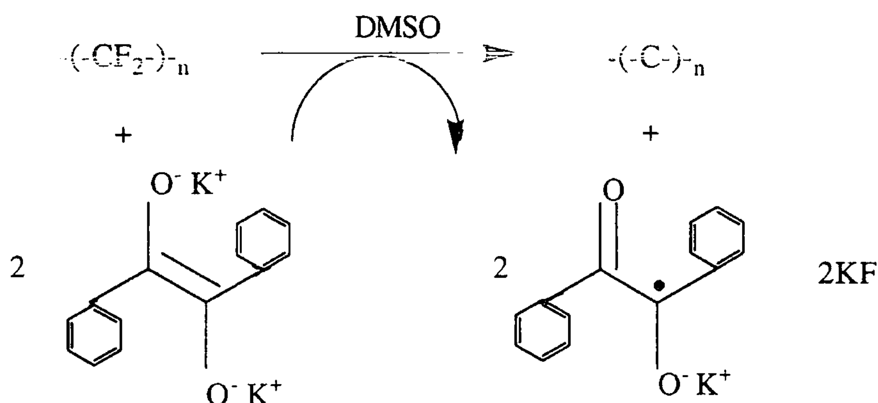

2.1.2 Plasma Modification of PTFE Surfaces

2.1.2.1 Oxygen Plasma Treatment

Morra [6,7] has previously carried out an examination of oxygen plasma treated PTFE. From XPS and scanning electron microscopy (SEM) results he concludes two kinds of reaction are competing. The first is chemical modification leading to fluorine depletion and some oxygen introduction, the second is etching leading to a chemically 'PTFE-like' but morphologically 'spongy-like' surface. Chemical modification is dominant at first, but is then overwhelmed by etching. Golub[8] has also shown that an

'equilibrium' oxygen uptake, soon after initial exposure, results from the dynamic competition between oxidation and etching (surface regeneration).

2.1.2.2 Hydrogen Plasma Treatment

Hydrogen plasmas have been used to modify the surface of PTFE[9]. Hydrogen atoms are considered to be one of the main constituents of a hydrogen plasma[9], and can be used to defluorinate PTFE. Clark[9] has shown a hydrogen plasma may react chemically and combine with the polymer surface to form stable products.

2.1.2.3 Nitrogen Plasma Treatment

Plasma treatment of PTFE by nitrogen has been studied by many workers[10-13]. The surface was found by Yasuda[10] to be modified with the removal of fluorine, and incorporation of nitrogen and oxygen. Kusabiraki[10] reported similar effects and also noted a change in morphology using SEM. Similarly to oxygen plasma treatment, Golub[12] has shown steady state chemical composition of the PTFE surface is soon attained.

2.1.2.4 Carbon Tetrafluoride Plasma Treatment

In general, CF_4 plasma treatment of polymers is similar to that of oxygen plasmas, as it can be used for etching. However, Egitto[14] has suggested that different etching mechanisms apply as the SEM of CF_4 treated PTFE is very smooth compared to the rough surface observed after O_2 exposure. The contact angle of water is increased by CF_4 treatment as reported by Klausner[15]. This was not attributed to morphological changes but to a chemical contribution, since the C(1s) XP spectrum shows the development of a small CF_3 shoulder.

2.1.2.5 Inert Gas Plasma Treatment

Inert gas plasma (particularly argon) treatment of PTFE is a very popular method of surface modification[7,10,16-20]. Momose[16] recently studied argon plasma treatment of PTFE followed by exposure to the atmosphere. He concluded that the oxygen was captured at the surface mainly in the form of the peroxy radical bonded to carbon in the crosslinked structure. It was also suggested that the chain scission peroxy radical is generated in the bulk by the effect of the UV radiation in the plasma.

Morra[7] has studied the argon plasma treatment over a range of times. A large oxygen incorporation was initially observed which was reduced on further exposure. SEM indicated that Ar plasma does not alter the morphology of the PTFE.

2.1.2.6 Miscellaneous Plasma Treatments

PTFE has been treated in an AC glow discharge in air[21] and analysed for changes in wettability (contact angles), surface functionalities (IR) and morphology (SEM). The contact angle of water decreased to a limiting value after about 2 minutes treatment time, while ATR-IR showed -C(F)=O groups (1800-1900cm^{-1}), and SEM indicated topographical changes. Gilman[21] concluded the difference in wettability may be related to the morphological changes, but did not rule out a role for the oxygen bearing groups, which may contribute to the phenomenon.

Tran[22] treated PTFE grafts with an argon plasma followed by a hexane plasma and then an ammonia plasma. Collagen was successfully bound to the graft and the treatment was confined to the surface so the bulk properties of the graft were preserved. Hollahan[23] also used ammonia plasma and nitrogen/hydrogen plasmas in the attachment of amino groups to PTFE surfaces. The mechanism of NH_2 groups entering the surface was

believed to involve plasma bombardment, forming CF_2-$CF\bullet$- radicals which subsequently combined with $\bullet NH_2$ radicals in the plasma.

2.1.3 Summary

The good dielectric properties, high thermal stability, low surface energy and chemical inertness of PTFE makes bonding virtually impossible without some form of surface pretreatment. Activation methods include electrochemical reduction[4], sodium solution etching[1] and plasma modification[6-23].

Non-isothermal glow discharge treatment of polymer surfaces can give rise to desirable adhesive and wettability characteristics[24,25]. The active plasma medium consists of atomic and molecular species, as well as ions, electrons, and a broad electromagnetic spectrum[26]. This highly reactive and complex mixture can offer a low cost and attractive route for altering the surface properties of a polymer at ambient temperatures[27].

This study examines the chemical and topographical changes encountered during the glow discharge treatment of PTFE using a variety of non-polymerizable gases.

2.2 EXPERIMENTAL

Small strips of polytetrafluoroethylene (Goodfellows) were ultrasonically washed in an isopropyl alcohol (BDH)/ hexane (BDH) mixture for 30 seconds and dried in air. High purity oxygen (BOC 99.6%), hydrogen (BOC 99.99%), nitrogen (BOC 99.995%), helium (BOC 99.995%), neon (BOC 99.999%), argon (BOC 99.999%), and carbon tetrafluoride (Air Products 99.7%) gases were used in the different types of electrical discharge treatments.

Electrical, inductively coupled plasmas were ignited in a cylindrical glass reactor (4.5 cm diameter, 460 cm^3 volume, base pressure of 1.0×10^{-3} Torr, and with a leak rate better than 4.0×10^{-3} cm^3 min^{-1}) enclosed in a Faraday cage[28]. This was fitted with an externally wound copper coil (4 mm diameter, 9 turns, spanning 8 - 15 cm from the gas inlet), an Edwards LV 10 needle valve gas inlet, an Edwards PR-10K Pirani pressure gauge, and a Leybolds 27 L min^{-1} two-stage rotary pump attached to a liquid nitrogen cold trap. A home built L-C matching network was used to match the output impedance of the RF (13.56 MHz) generator to that of the partially ionized gas load, this was achieved by minimising the standing wave ratio (SWR). A schematic diagram of the set up used is shown in figure 2.1. All joints were grease-free. Gas flow and leak rates were calculated by assuming ideal gas behaviour[29] as described in section 2.2.2. A typical experimental run comprised initially scrubbing the reactor with detergent, rinsing with isopropyl alcohol, and oven drying, this was followed by a 30 min high power (50 W) air plasma cleaning treatment. Next, the reactor was opened up to atmosphere, a strip of polymer was inserted into the centre of the RF coils, the system was evacuated back down to its original base pressure and the leak rate determined. Subsequently, if the leak rate was acceptable (typically better than 4×10^{-3} cm^3 min^{-1}) the gas of interest was introduced into the reaction chamber at a pressure of 0.2 Torr, and a flow rate of approximately 1.0 cm^3 min^{-1}. After allowing 5 min for purging, the glow discharge was ignited at 20 W for 5 min. Upon termination of treatment, the RF generator was switched off, and the system flushed with feed gas for 5 min prior to venting up to atmospheric pressure. Each sample was characterized immediately after electrical discharge treatment.

Figure 2.1

A schematic of the reactor set up.

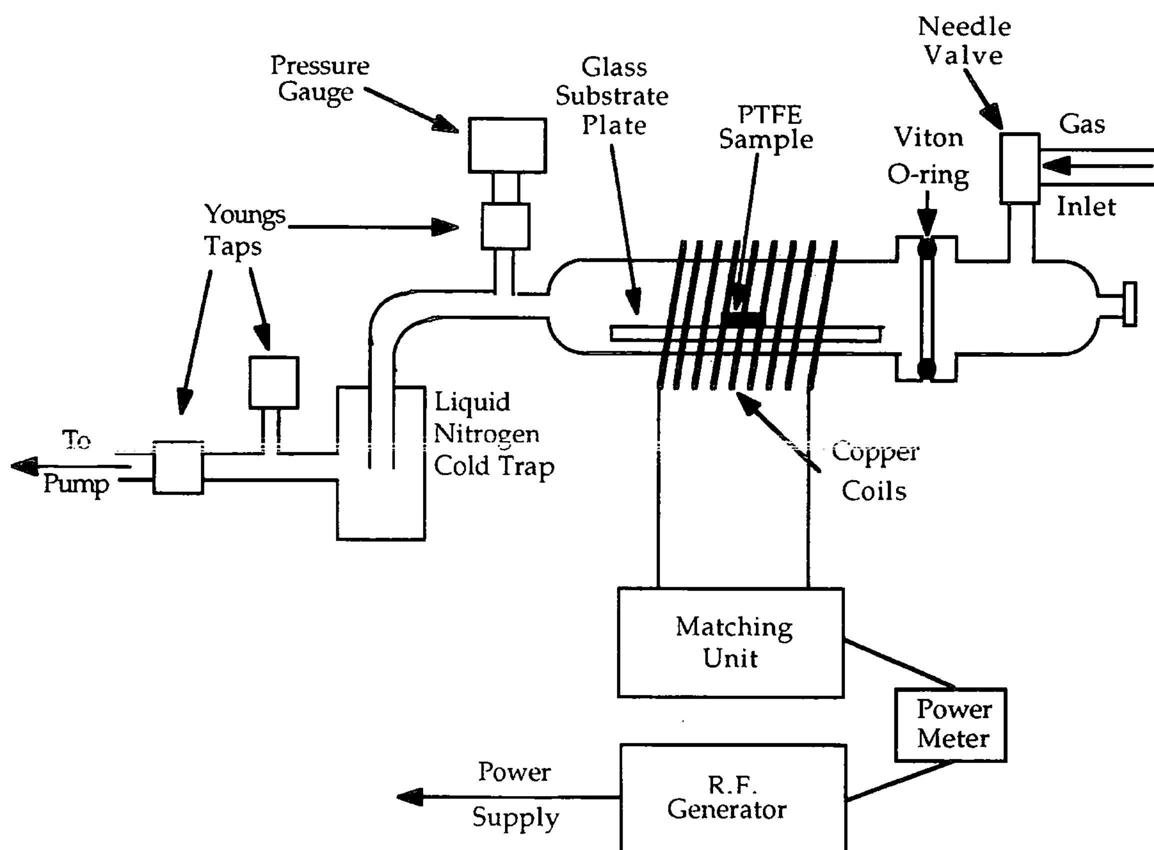

2.2.1 Analysis

A Kratos ES200 photoelectron spectrometer equipped with an unmonochromatized Mg Kα X-ray source (1253.6 eV) and a hemispherical analyser was used for XPS surface analysis. Photo-emitted core level electrons were collected at a take-off angle of 30° from the substrate normal, with electron detection in the fixed retarding ratio (FRR, 22:1) mode. Instrument performance was calibrated with respect to the gold $4f_{7/2}$ peak at 83.8 eV with a full width at half-maximum (FWHM) of 1.2 eV. XP spectra were accumulated on an interfaced PC computer. Instrumentally determined sensitivity factors for unit stoichiometry were taken as being C(1s) : O(1s) : N(1s) : F(1s) equals 1.00 : 0.55 : 0.74 : 0.53. XPS was used to check

cleanliness of the PTFE substrate and for the absence of any surface-active inorganic additives. Gross and experimental errors were calculated for each surface treatment.

A Digital Instruments Nanoscope III atomic force microscope was used to examine the topographical nature of the PTFE surface prior to and after electrical discharge exposure. All of the AFM images were acquired in air using the Tapping® mode[30], and are presented as unfiltered data. This technique employs a stiff silicon cantilever oscillating at a large amplitude near its resonance frequency (several hundred kHz). The root mean square (RMS) amplitude is detected by an optical beam system. A large RMS amplitude is used to overcome the capillary attraction of the surface layer, whilst the high oscillation frequency allows the cantilever to strike the surface many times before being displaced laterally by one tip diameter. These features offer the advantage of low contact forces and no shear forces.

2.2.2 Calculation of Leak and Flow Rates

At the pressures used in glow discharges the gases and vapours can be regarded as ideal and behave according to equation (2.1)[31]:-

$$PV = nRT \qquad (2.1)$$

where P = pressure, V = volume, n = number of moles of gas, R = universal gas constant, and T = absolute temperature. Rearrangement gives equation (2.2):-

$$n = \frac{PV}{RT} \qquad (2.2)$$

In a reactor continually fed by gas, if the pump is sealed off at t=0, F_v (volumetric flow rate) is related to the pressure increase as follows:-

$$F_v = \frac{dn}{dt} = \frac{V}{RT} \times \frac{dP}{dt}\Big|_{t=0}^{t=t}$$

if the value of $\frac{dP}{dt}\Big|_{t=0}^{t=t}$ is approximated as $\frac{\Delta P}{\Delta t}$:-

$$F_v \approx \frac{V}{RT} \times \frac{\Delta P}{\Delta t}$$

At STP one mole of gas occupies 22414 cm^3, and with V in cm^3, R = 82.06 atm cm^3 K^{-1} mol^{-1}, T in Kelvin, P in atm, and t in min :-

$$F_v \approx \frac{V}{RT} \times \frac{\Delta P}{\Delta t} \times 22414 \qquad cm^3\ min^{-1}$$

For mass flow rates, F_m, which are used in later chapters, a similar argument outlined as above leads to:-

$$F_m \approx \frac{MV}{RT} \times \frac{\Delta P}{\Delta t} \qquad kg\ min^{-1}$$

where M = relative molecular weight of monomer.

2.3 RESULTS

2.3.1 Clean PTFE

The C : F ratio for untreated PTFE film obtained from XPS is in good agreement with the theoretically expected value of 1 : 2, table 2.1. C(1s) XP spectra were fitted with Gaussian peaks of equal full FWHM[32], using a Marquardt minimisation computer program, and showed only a main >$\underline{C}F_2$ peak at 291.2 eV, and the corresponding Mg $K\alpha_{3,4}$ satellite at lower binding energy[33], figure 2.2(a). Throughout this thesis errors stated for elemental percentages are purely experimental, while those from peak fitted data also include an error of between 1-2% due to the Marquardt minimization program.

A common method for making PTFE film is by compaction and sintering of PTFE granules[34]. The constituent particles and surface voids are clearly discernible in the AFM micrograph of untreated PTFE, figure 2.3. Furthermore, uniaxial alignment of the surface texture is indicative of the substrate having undergone tribological deformation during manufacture[35].

Table 2.1

Elemental surface composition following plasma modification of PTFE (20 W, 5 min).

Gas	% C	% F	% O	% N
PTFE	33.3 ± 0.6	66.8 ± 0.6	---	---
CF_4	32.8 ± 0.6	67.2 ± 0.6	---	---
O_2	33.0 ± 0.2	65.4 ± 0.2	1.7 ± 0.4	---
N_2	33.2 ± 0.0	64.0 ± 0.6	1.6 ± 0.3	1.3 ± 0.4
Ne	34.6 ± 1.3	62.0 ± 1.0	2.6 ± 0.4	0.9 ± 0.0
Ar	37.2 ± 0.5	56.8 ± 0.8	4.3 ± 0.2	1.8 ± 0.1
He	38.7 ± 0.4	55.8 ± 2.0	4.1 ± 1.4	1.5 ± 1.0
H_2	56.1 ± 1.1	37.7 ± 0.4	4.7 ± 0.7	1.5 ± 0.1

Figure 2.2

C(1s) XP spectra of PTFE: (a) clean, (b) CF_4 plasma treated, (c) O_2 plasma treated, (d) N_2 plasma treated, (e) Ne plasma treated, (f) Ar plasma treated, (g) He plasma treated, and (h) H_2 plasma treated.

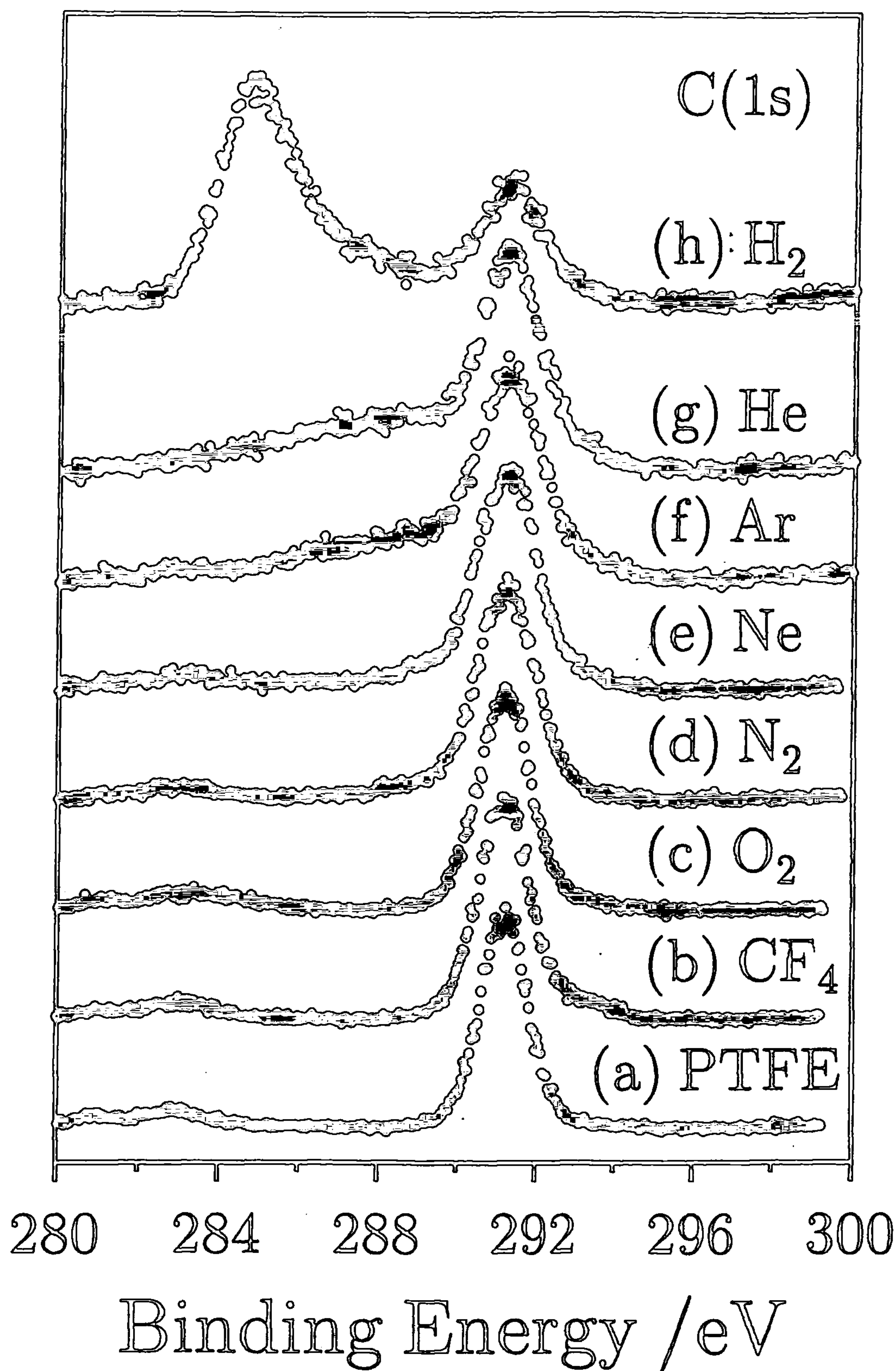

Figure 2.3

Atomic force micrograph of clean PTFE.

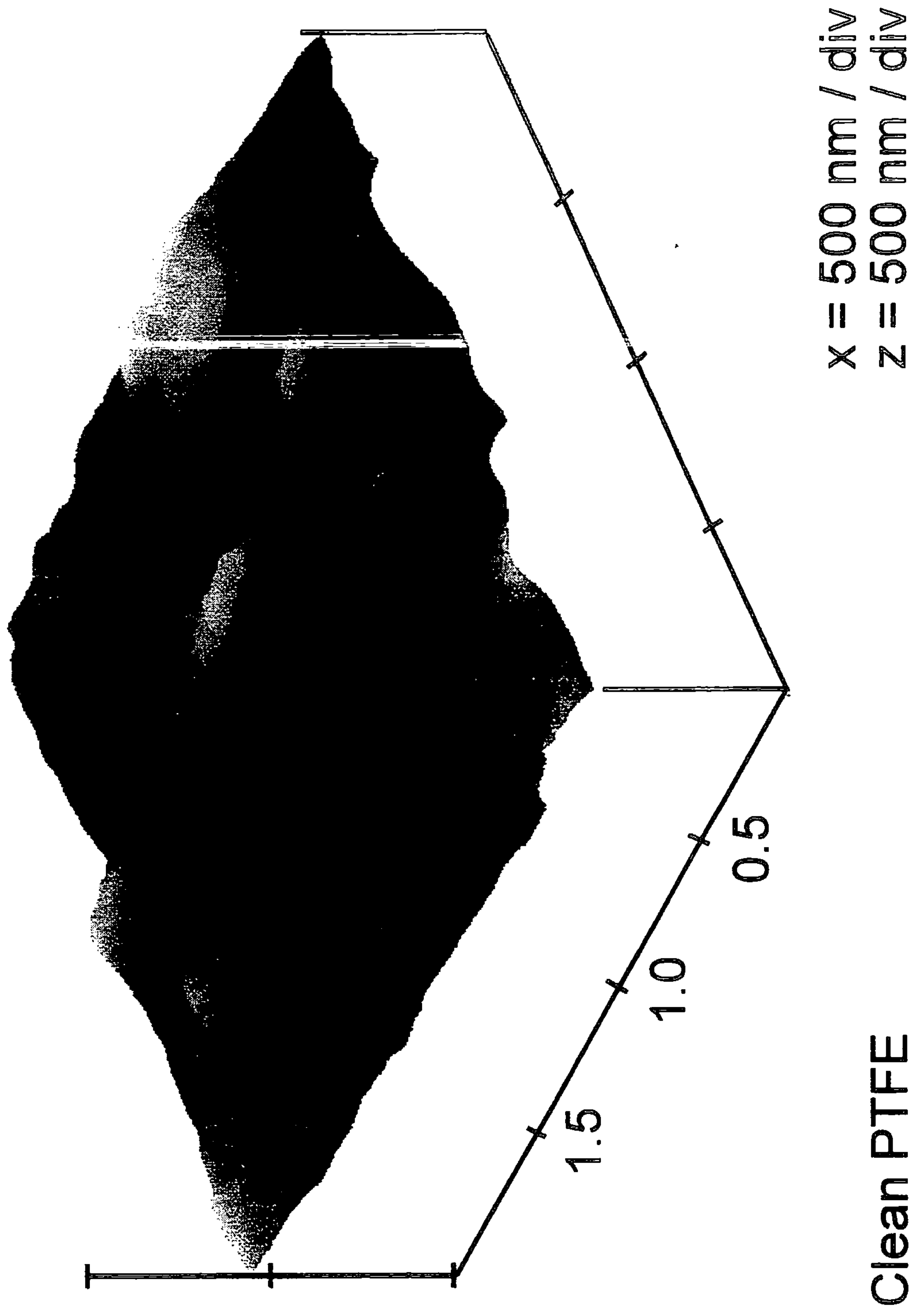

Figure 2.4

Atomic force micrograph of O_2 plasma treated PTFE.

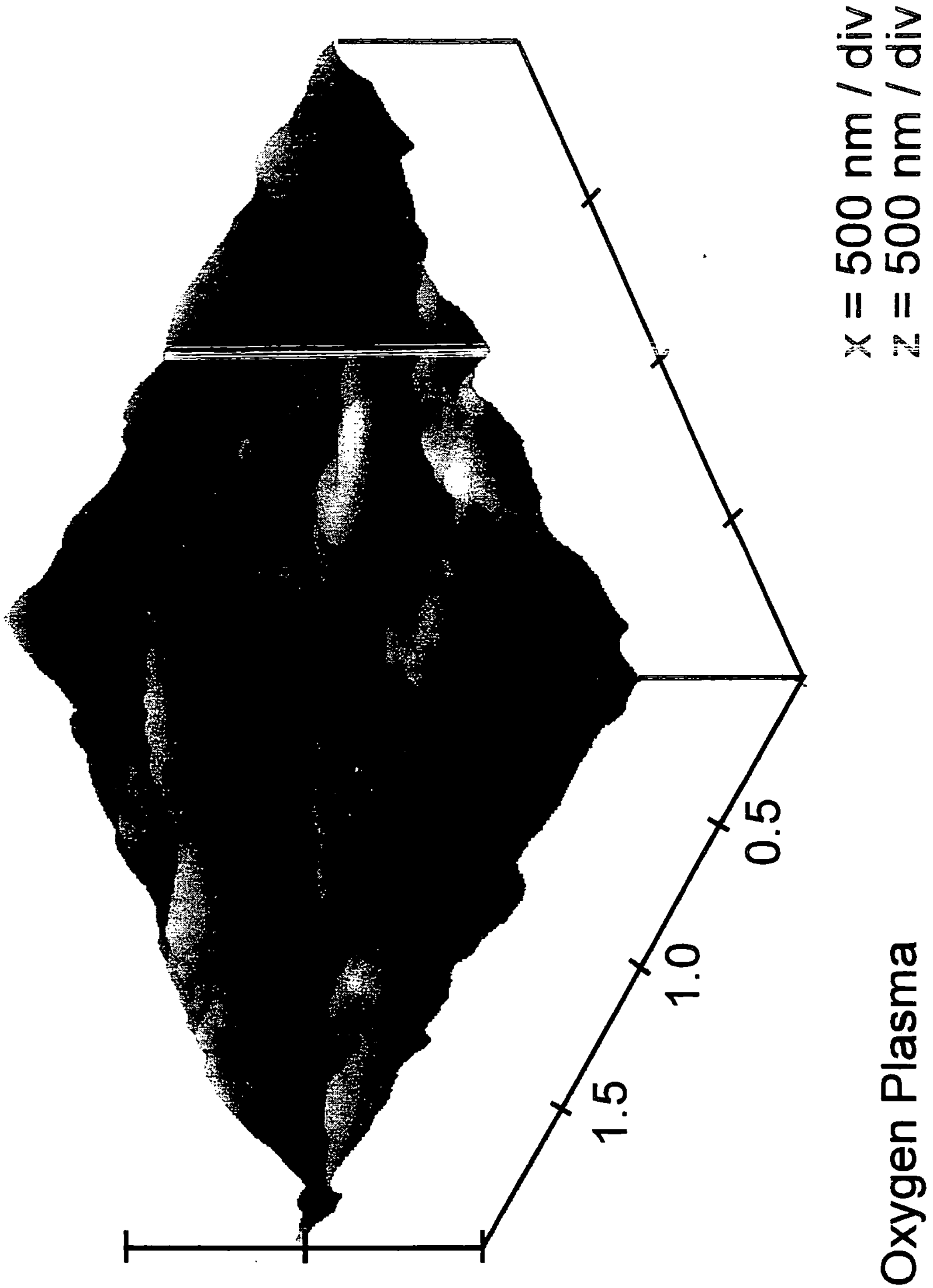

Figure 2.5

Atomic force micrograph of H_2 plasma treated PTFE.

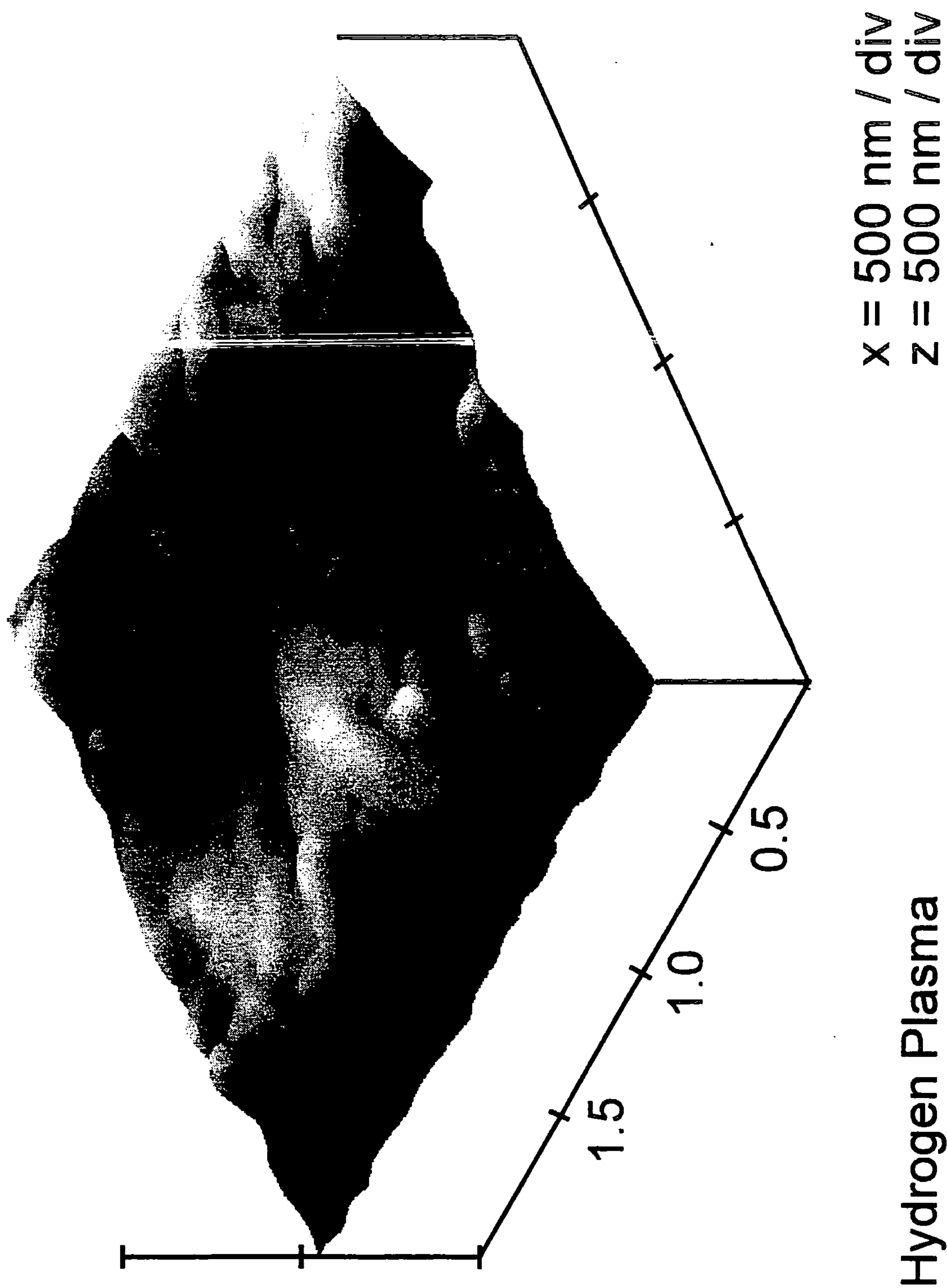

Figure 2.6

Atomic force micrograph of N_2 plasma treated PTFE.

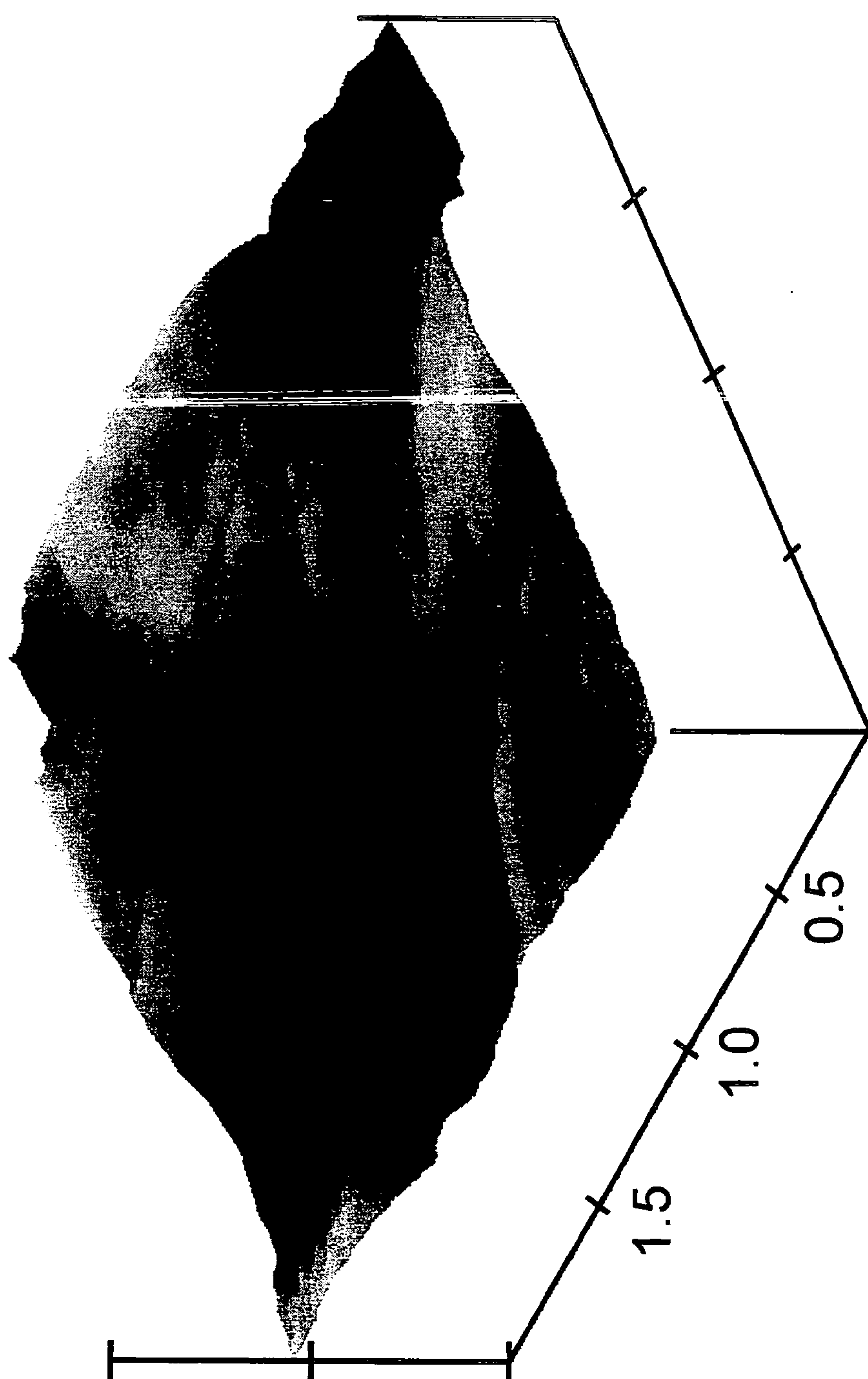

Figure 2.7

Atomic force micrograph of He plasma treated PTFE.

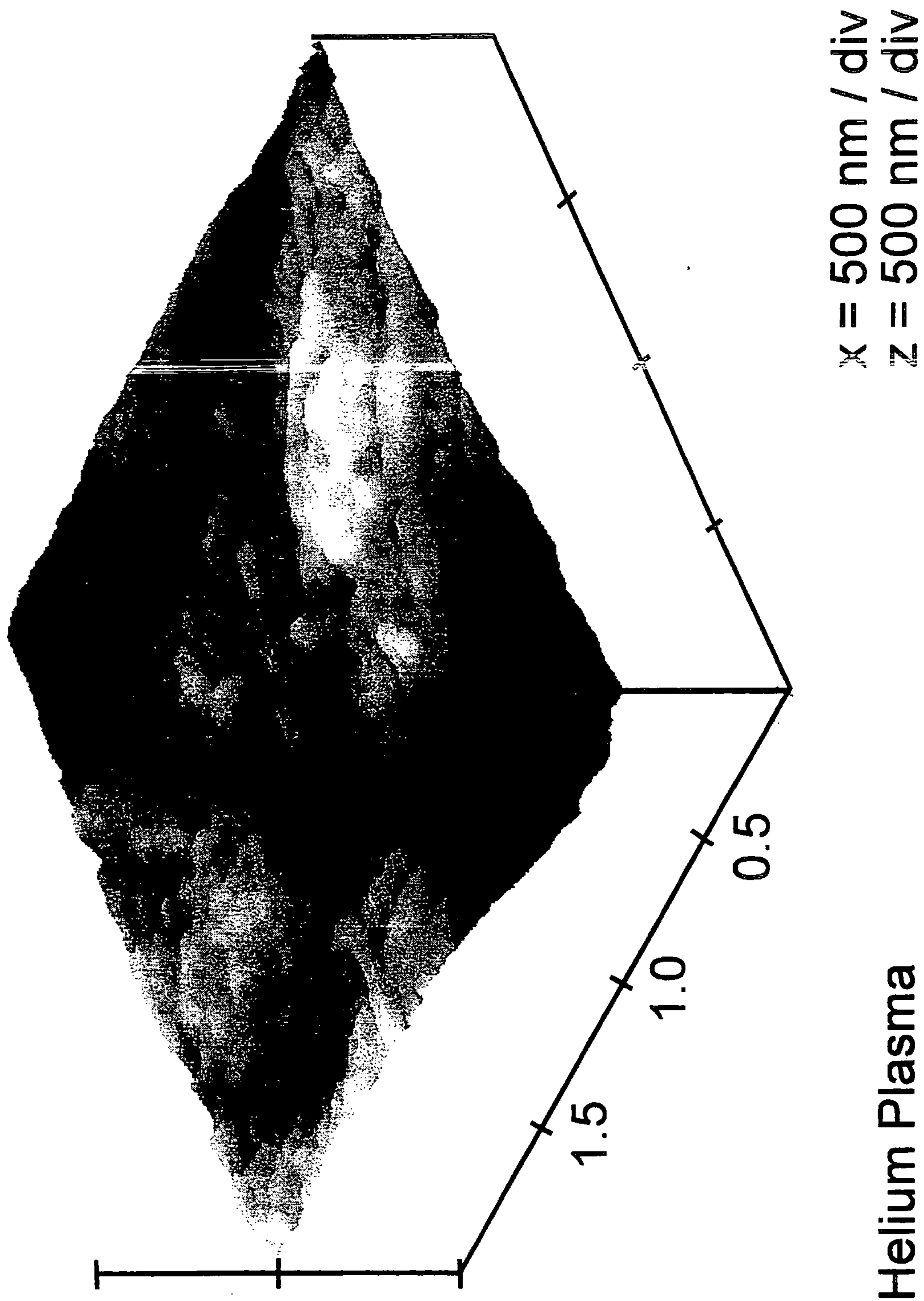

Figure 2.8

Atomic force micrograph of Ne plasma treated PTFE.

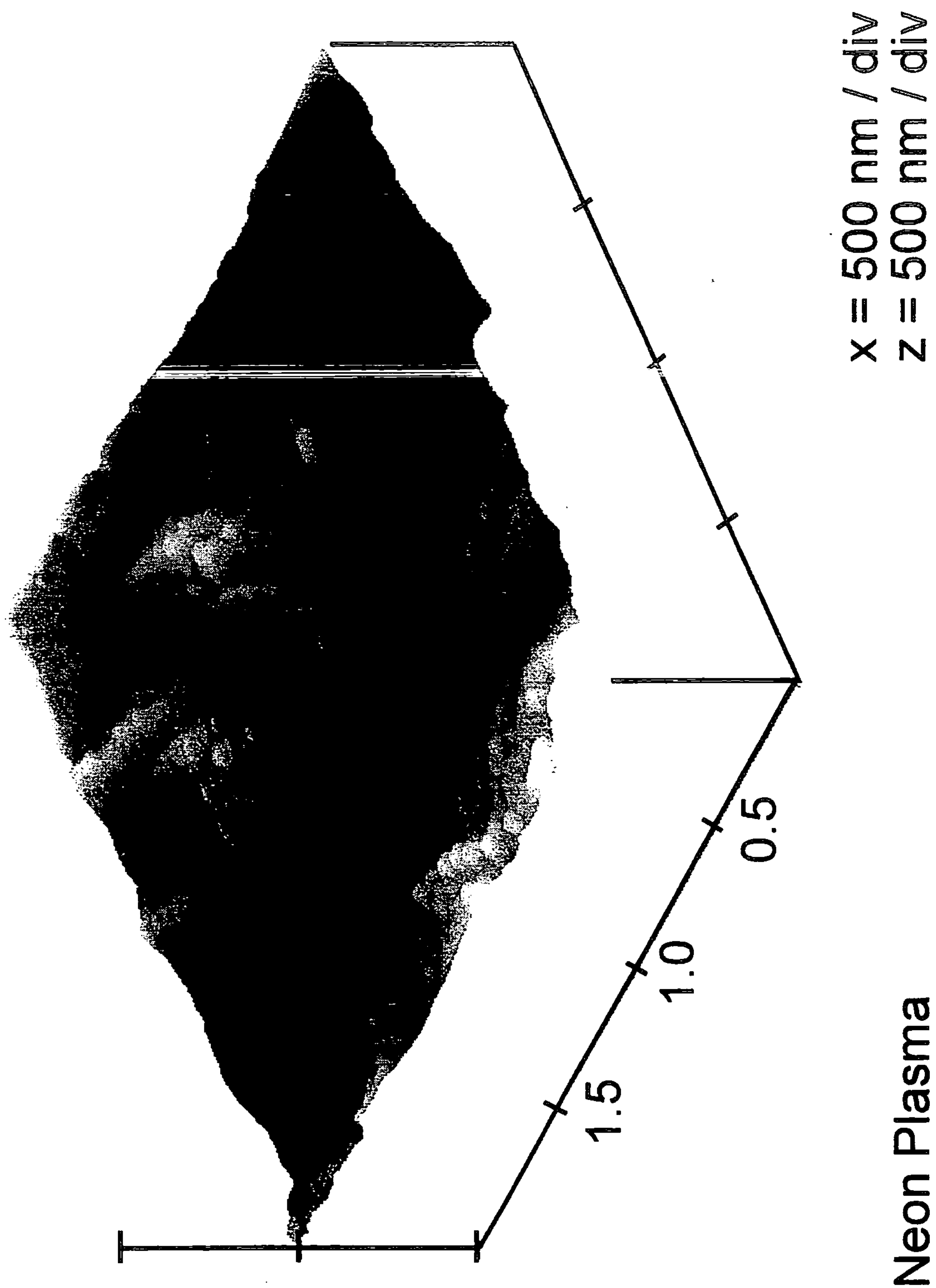

Figure 2.9

Atomic force micrograph of Ar plasma treated PTFE.

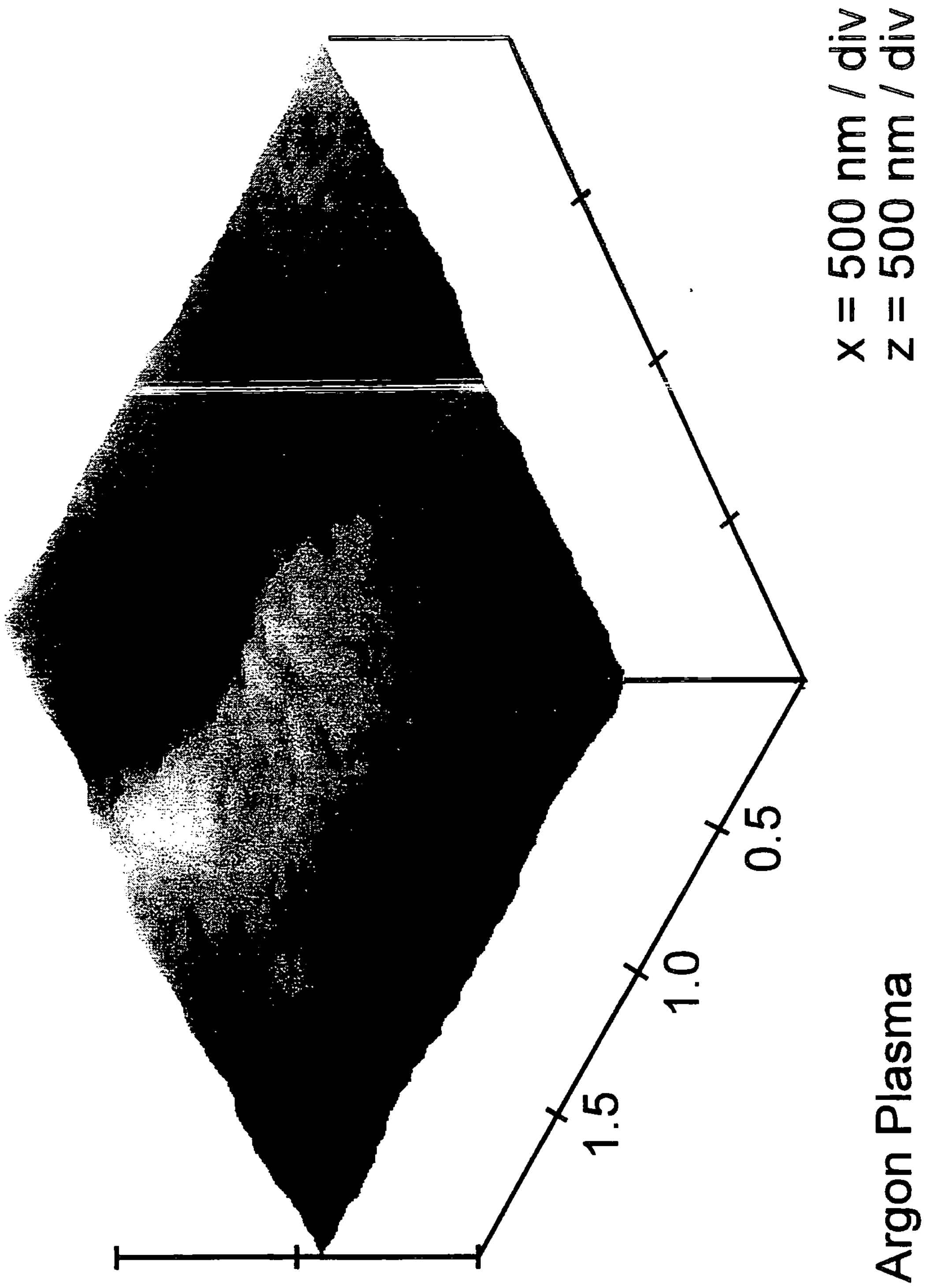

Figure 2.10

Atomic force micrograph of CF_4 plasma treated PTFE.

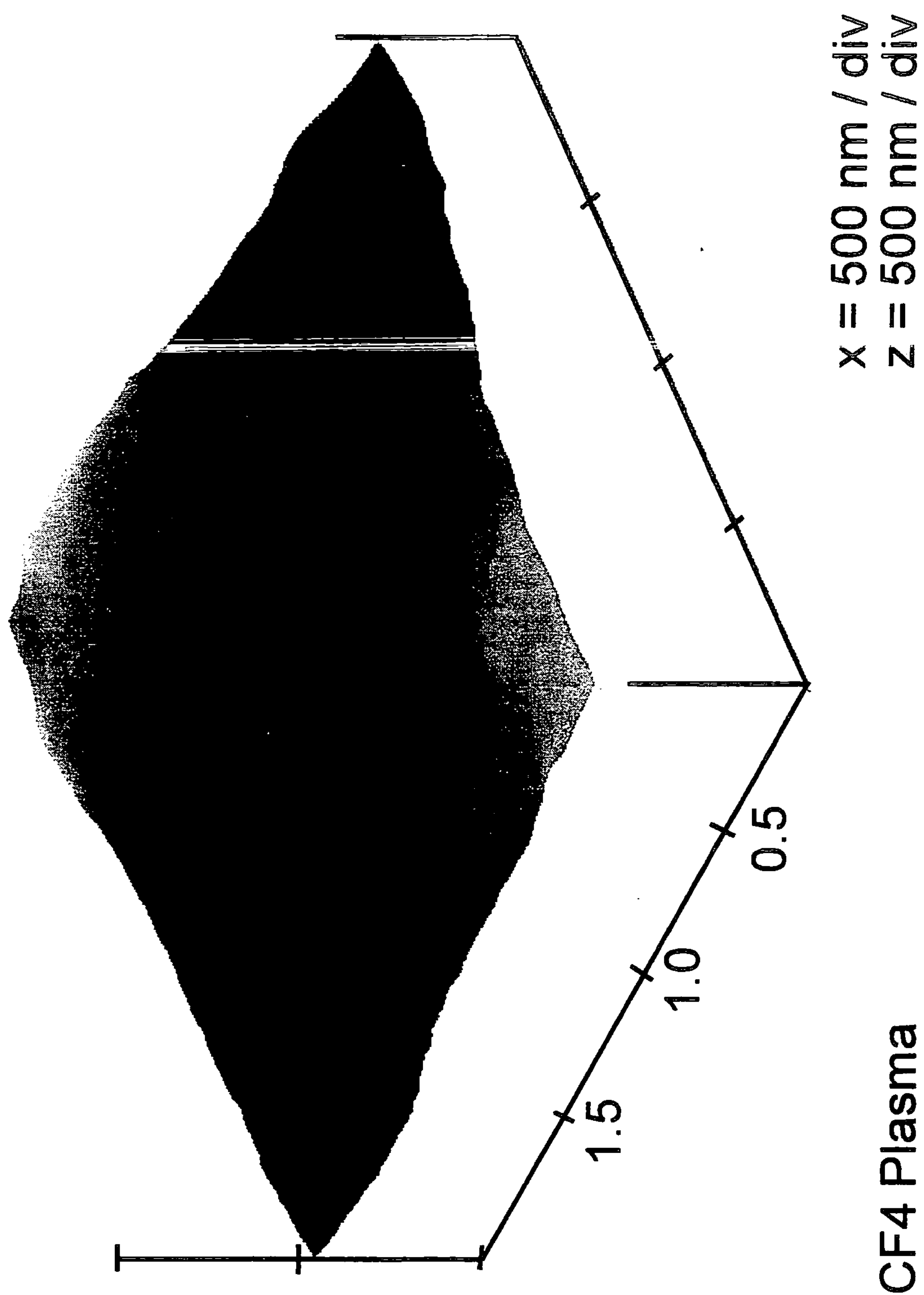

2.3.2 Oxygen Plasma Treatment

XPS shows that there is virtually no change in the chemical nature of the PTFE substrate during oxygen plasma treatment, figure 2.2(c) and table 2.1.

However there is a substantial degree of surface roughening, which is discernible in the form of a micro-roughness superimposed upon the original macro-roughness of the starting material, figure 2.4.

2.3.3 Hydrogen Plasma Treatment

Hydrogen plasma treatment of PTFE results in a dramatic defluorination of the surface[9], table 2.1. The C(1s) envelope has shifted to lower C(1s) binding energy values, which are more typical of hydrogenated carbon centres[33], figure 2.2(h). A small amount of oxygen and nitrogen was detected on the treated samples, the most likely origin for this being reaction between trapped free radical centres at the surface and the atmosphere during transport of the modified substrate from the glow discharge apparatus to the XP spectrometer[16,36].

In many ways the hydrogen and oxygen glow discharge treated PTFE surfaces are topographically very similar in appearance, except that the level of macro-roughness is less extensive for the former, figure 2.5.

2.3.4 Nitrogen Plasma Treatment

Nitrogen glow discharge treatment of PTFE results in a small amount of nitrogen incorporation together with a slight broadening of the C(1s) envelope[10-13], figure 2.1(d) and table 2.1.

Atomic force microscopy shows a fine globular texture which has wiped out the original parent polymer microstructural features, figure 2.6.

This is consistent with previous SEM studies where the PTFE topography was reported to undergo change to a fibrous pattern[11].

2.3.5 Inert Gas Plasma Treatment (Helium, Neon, and Argon)

Inert gas plasma treatment of PTFE results in a small amount of oxygen and nitrogen incorporation into the surface[7,10,36], table 2.1. This can be accounted again in terms of the activated surface undergoing reaction with the atmosphere during substrate transfer to the XP spectrometer[16,36]. The relative order of surface defluorination is He > Ar > Ne. This is accompanied by the emergence of a low binding energy shoulder on the main >$\underline{C}F_2$ C(1s) peak, which is characteristic of Mg $K\alpha_{1,2}$ components corresponding to -$\underline{C}$F-CF_n- (289.5 eV), -$\underline{C}$F- (288.3 eV), -$\underline{C}$-CF_n- (286.6 eV), and -$\underline{C}_x$- (284.6 eV) environments[37], figures 2.2(e)-(g).

The atomic force micrographs following inert gas plasma treatment, figures 2.7-2.9, are in many ways similar to the surface texture previously seen following nitrogen glow discharge modification. Fine globular features are evident in all cases. However, the way in which these are distributed varies a great deal depending upon the gas used. On moving from helium-to-neon/nitrogen-to-argon glow discharges, there appears to be a local ordering phenomenon taking place which gives rise to the formation of fibrils. These results are in contradiction with previous SEM studies which mentioned that Ar plasma treatment does not alter the PTFE surface morphology[7]. This discrepancy could be attributed to the masking of any topographical features during the metallization of the substrate prior to SEM characterization.

2.3.6 CF_4 Plasma Treatment

CF_4 plasma treatment of polytetrafluoroethylene effectively produces very little chemical change in the PTFE substrate, except for a small amount of fluorine incorporation. This leads to a slight shoulder at higher C(1s) binding energy (293.6 eV), which can be assigned to $-CF_3$ environment, figure 2.2(b).

The treated PTFE surface exhibits the smoothest texture amongst the series of feed gases under investigation, figure 2.10. Similar behaviour has been previously observed by SEM for other polymer substrates which have been exposed to pure CF_4 plasmas[38].

2.4 DISCUSSION

Differing rates of physical sputtering between amorphous and crystalline regions of PTFE cannot solely account for the observed changes in surface topography for the various plasma treatments[39,40]. A range of energy transfer mechanisms are in operation within a low pressure RF discharge, as illustrated in chapter 1. These include electron acceleration in the bulk of the plasma, electron deflection from sheath potentials, formation of energetic neutrals by charge-exchange and elastic collisions between ions and neutral gas species, and ion and electron acceleration in the wall boundary sheaths[41]. In terms of surface modification, the most important criteria of a glow discharge are the nature, the arrival rates, and the angular and energy distributions of the species impinging upon the surface[42]. Electron impact processes influence the density of ions, radicals, metastables, and photons contained within the plasma. The energy distributions for neutral and ionic species contained within a non-

equilibrium plasma correspond to approximately ambient temperature, whilst the electron temperature is considerably higher.

Non-isothermal plasmas interact with organic substrates via a direct energy transfer component arising from ions and metastables down to ~ 10 Å (10×10^{-10} m), and a radiative transfer component consisting of vacuum ultraviolet (VUV) photo-irradiation which can penetrate up to ~ 10 μm (10×10^{-6} m) below a polymer surface[18,43,44], both are illustrated in figure 2.11.

Figure 2.11

A schematic diagram of the direct and radiative energy transfer mechanisms occurring during polymer surface modification by inert gas plasmas (not to scale).

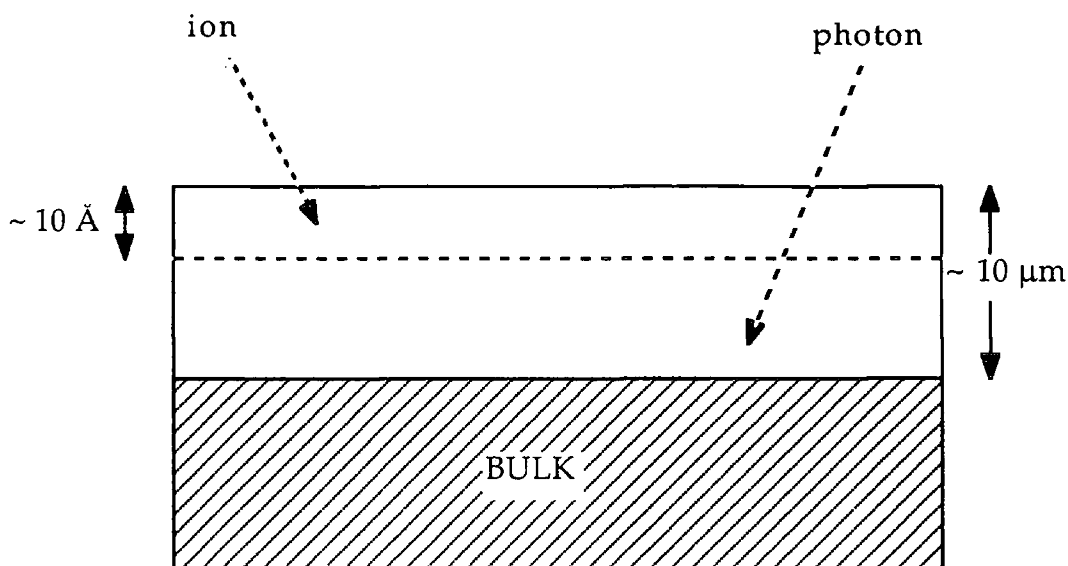

Typically, ion densities lie in the range of 10^8 - 10^{10} cm^{-3} with energies of 0 - 100 eV[45-48]; whilst mean electron energies span 0 - 20 eV with a high energy tail reaching out to 100 eV due to reflections at sheath boundaries[45,49]. Within the glow region, the plasma exists at a positive potential with respect to the substrate surface, this results in positive ions contained in the

plasma being accelerated through a space charge sheath towards the substrate[50].

Prolonged oxygen plasma treatment of PTFE results in a morphologically spongy-like surface[6,7,8]. Pure O_2 plasmas yield a much rougher surface in comparison to CF_4 glow discharge treatment of PTFE[14]. Although a large number of chemical reactions are possible in an oxygen plasma, oxygen atoms are generally regarded as being the primary reactive species in conjunction with vacuum UV surface activation[26,51,52]. Also the average potential difference between the plasma and the substrate (plasma sheath potential) is much greater for an oxygen plasma than for a CF_4 plasma[14]. Therefore, a greater level of substrate etching can be expected for the case of an oxygen plasma. The most likely initiation step during O_2 plasma treatment of PTFE is reported to be polymer radical formation during ion/photon/electron bombardment[14] to yield either:-

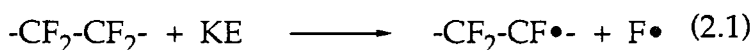

$$-CF_2-CF_2- + KE \longrightarrow -CF_2-CF\bullet- + F\bullet \quad (2.1)$$

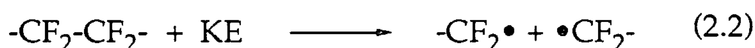

$$-CF_2-CF_2- + KE \longrightarrow -CF_2\bullet + \bullet CF_2- \quad (2.2)$$

The reaction of O atoms or O_2 with a polymer radical will inhibit cross-linking, leading to scission of the polymer backbone[53]. Fluorine abstraction from PTFE by oxygen radicals to form $OF\bullet$ is energetically unfavourable[14] and studies using atomic oxygen ($O(^3P)$) have exhibited negligible surface oxidation[54].

A hydrogen plasma defluorinates PTFE to a large extent. Low energy electron impact of H_2 produces photons in the vacuum ultraviolet region[55], but this cannot solely account for the high level of surface defluorination observed. A comparison of H_2^+ and He^+ ion bombardment of PTFE has shown that the former is better at defluorination of the surface, and this can be attributed to a chemical effect[56]. Defluorination of the PTFE surface by a hydrogen glow discharge must therefore be governed by the chemically

reducing nature of the constituent hydrogen atoms[9], whereas for the other gases, any loss of surface fluorine can only be attributed to vacuum ultraviolet (VUV) photons[57,58], ion bombardment[59], or electron impact dissociation[60,61]. Fluorine abstraction from PTFE by hydrogen atoms to form HF is known to be energetically favourable[9,14], and has been previously identified by IR emission spectroscopy[62]:-

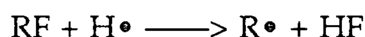

$$RF + H\bullet \longrightarrow R\bullet + HF$$

A mechanism has been proposed by Clark[9] which is thought to be initiated by abstraction of fluorine :-

$$-(CF_2\text{-}CF_2\text{-}CF_2\text{-}CF_2)- + H\bullet \longrightarrow HF + -(\dot{C}F\text{-}CF_2\text{-}CF_2\text{-}CF_2)- \quad (2.3)$$

Recombination of the polymer radical with a hydrogen atom leads to the formation of a vibrationally excited (*) chain segment that may be quenched by the lattice, or decompose with the elimination of HF.

$$\xrightarrow{M} -(CHF\text{-}CF_2\text{-}CF_2\text{-}CF_2)- \quad (2.4)$$

$$-(\dot{C}F\text{-}CF_2\text{-}CF_2\text{-}CF_2)- + H\bullet \longrightarrow -(CHF\text{-}CF_2\text{-}CF_2\text{-}CF_2)^*-$$

$$\xrightarrow{-HF^*} -(CF{=}CF\text{-}CF_2\text{-}CF_2)- \quad (2.5)$$

Any unsaturation produced could be rapidly saturated by H∘, reaction (2.6). Once hydrogen has been incorporated into the polymer chain, various reactions (2.7, 2.8, or 2.9) may occur.

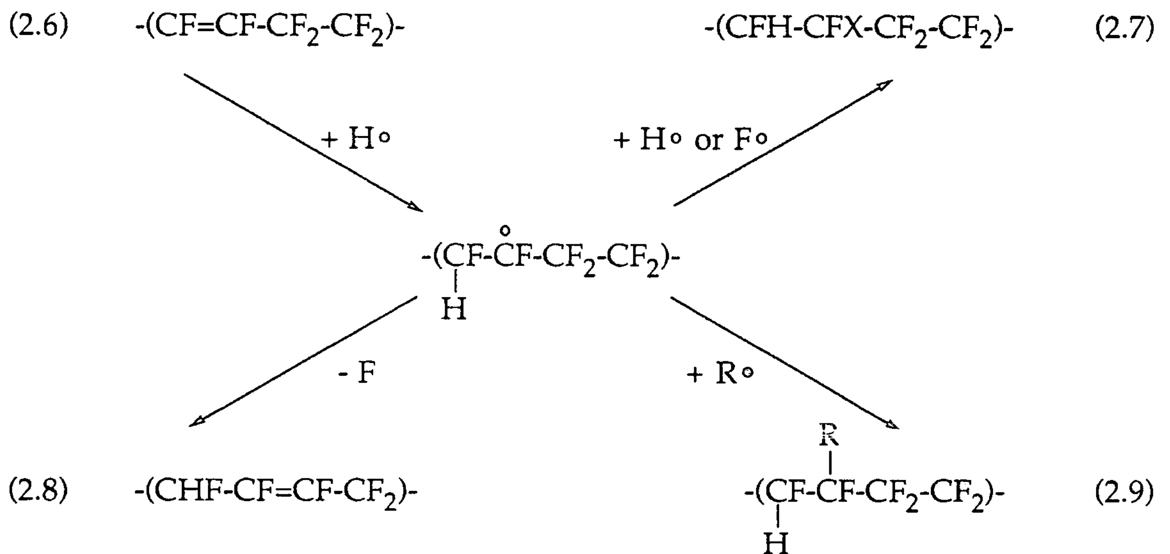

Additional reactions such as oxygen uptake and crosslinking can occur due to the interaction of residual oxygen-containing species with radicals and the recombination of radicals respectively.

Ion beam modification of PTFE is known to induce topographical and chemical changes at the surface[63-65], an area expanded upon in chapter 3. The floating potential of the substrate can be calculated to be approximately the same for the three noble gases used in this study[66]. On moving from He to Ne to Ar plasmas, the observed trend in the degree of PTFE defluorination is contrary to what might be expected in terms of a direct energy transfer perspective, where momentum transfer to the substrate should become more predominant with rising noble gas atom mass[67]. Therefore radiative energy transfer must also be taken into consideration[18,68,69]. Crossed-beam electron impact induced fluorescence studies with inert gas atoms have shown that intense vacuum ultra violet (VUV) MI emission lines are produced (where M represents the inert gas

e.g. ArI) which correspond to transitions between the lowest lying electronically excited states and the ground state of the atom (e.g. for Ar: $3s^23p^54s^1 \rightarrow 3s^23p^6$)[70,71]. These display a maximum excitation cross section at electron energies of ~ 30 eV[70]. A weaker MII line and a background radiation continuum arising from excited inert gas molecules M_2^* is also present. There is emission in the UV/visible, but the intensity is at least two orders of magnitude lower than for the VUV region. Such VUV photons typically possess energies corresponding to the order of first ionization potentials of polymers[44]. Therefore, the anomalously high defluorination of PTFE by the helium glow discharge can be accounted for, since the MI resonance lines become less energetic on descending the inert gas series[44,72], whereas momentum transfer effects will make a greater contribution for the heavier noble gas plasmas. Figure 2.12 shows how the two effects compete.

Figure 2.12

A schematic diagram showing how the VUV and direct energy transfer mechanisms change as the noble gas series is descended.

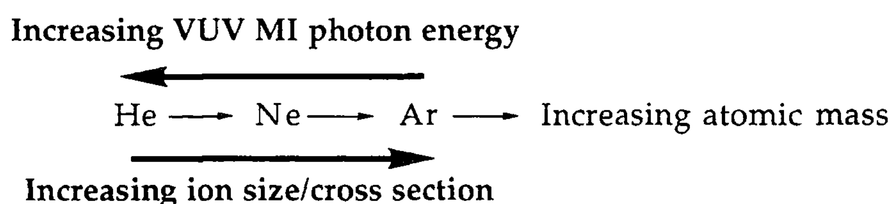

Primary processes during inert gas plasma treatment of PTFE will include rupture of the C-F bond, and main chain C-C scission followed by the chain fragments undergoing crosslinking or desorption[17]. Polymer radicals located on adjacent chains will crosslink[18], whilst radicals on neighbouring carbon atoms will form double bonds[19]. Greater fragmentation at the surface should produce a greater number of molecular fragments, with their respective mobilities decreasing with increasing chain

length and crosslinking. The C-C bond distance along a polymer backbone is much shorter than the intermolecular C-C separation between adjacent polymer chains, therefore, the net effect of crosslinking is to cause surface shrinkage[18] and internal stress. This could contribute to the observed reorganization of surface texture during noble gas glow discharge treatment of PTFE. The observed morphology in these studies is markedly different to the fine cone-like structures observed during ion sputter-etching of PTFE[73,74] and therefore cannot be ascribed to just a manifestation of ion bombardment in the conventional sense. However, since ion bombardment is dependent upon the plasma sheath and the constituent ions, any macro-roughness and / or localized charge build-up will cause a strong perturbation upon the local electric field experienced by the incident ions, leading to higher kinetic energy ions reaching the protruding and / or charged polymer regions. This can give rise to heterogeneous etching at the surface[75], and will be expected to become more evident with increasing mass of incident noble gas ion. Furthermore, agglomeration and orientation of charged low molecular weight species at the surface[76] may be influenced by such local surface electric fields. This effect would be expected to be greatest for an argon plasma, since the heavier argon ions will incur more polymer chain rupture, while its relatively weaker vacuum UV emission will yield less subsurface crosslinking, and therefore one would expect a more mobile surface in this case.

Nitrogen plasma treated PTFE experiences comparable physical and chemical changes to those observed during neon glow discharge modification. Atomic nitrogen and neon are very close to each other in the Periodic Table, thereby giving rise to similar momentum transfer behaviour (small difference in atomic mass) and VUV emission spectra (virtually equivalent atomic orbitals).

A CF_4 glow discharge can be regarded as a source of fluorine atoms with a small concentration of CF, CF_2, and CF_3 radicals[77-81]. This is

supported by electron impact experiments with CF_4, which indicate that F atoms are the primary species[82]. The identification of $-CF_3$ centres following CF_4 plasma treatment can be taken as evidence for the main PTFE backbone undergoing cleavage followed by fluorination of the $-CF_2$ radicals. The alternative explanation of $-CF_3$ functionalities attached to the main PTFE backbone can be ruled out since there are no corresponding crosslinked carbon centres present in the C(1s) spectrum at lower binding energy values from the main $-CF_2-$ peak. The contact angle of water increases during CF_4 plasma treatment[15]. This cannot be attributed to morphological changes (since Wenzels Law states 'on roughening a wettable surface becomes more wettable and a non-wettable surface becomes more non-wettable')[83,84], therefore this must be due to the extra $-CF_3$ groups. CF_4 plasmas are widely used for polymer etching, in a similar way to O_2 plasmas. However, Egitto[14] has suggested that different etching mechanisms apply, since the two treatments result in very different morphologies. Fluorine abstraction from PTFE by fluorine radicals to form F_2 is energetically unfavourable[14], whilst recombination or termination of polymer radicals with fluorine atoms will favour the formation of stable fluorocarbons species with inherently poor etch characteristics[14,85].

2.5 CONCLUSIONS

Non-equilibrium glow discharge treatment of PTFE using non-polymerizable gases results in surface modification. The chemical and topographical changes induced depend heavily on the gas used. Oxygen plasma treatment gives rise to the highest level of surface roughening together with virtually no change in chemical composition. Etching of the PTFE to reveal a chemically similar but topographically spongy-like surface is the likely mechanism. Hydrogen glow discharge treatment causes the

greatest loss of fluorine from the surface as hydrogen atoms in the plasma can react with, and abstract, fluorine from the polymer. Nitrogen and noble gas plasma treatment promotes the formation a fibrillar micro-texture. Both the direct and radiative mechanisms of energy transfer were found to play important roles, the level of which depends on the particular gas molecule. CF_4 glow discharge treatment of PTFE causes polymer chain rupture followed by fluorine atom capping to yield $-CF_3$ end groups.

Future work on *in situ* modification and chemical analysis could be performed to elucidate the origin of the surface oxygen and nitrogen incorporation. Recently apparatus has been built in this laboratory which will allow this to be studied. Use of suitable window materials should allow the substrate to be shielded from all but the VUV component of the plasma to asses its individual contribution to the modification process. Biasing of the substrate may be possible to direct selected charged particles, within the plasma, away from or towards the PTFE.

2.6 REFERENCES

1. Hansley, V. L. *Industrial and Engineering Chemistry* **1951,** *43,* 1759.
2. Nelson, E. R.; Kilduff, T. J.; Benderly, A. A. *Ind. Eng. Chem.* **1958,** *50,* 329.
3. Dousek, F. P.; Jansta, J. *Electrochim. Acta* **1975,** *20,* 1.
4. Jansta, J.; Dousek, F. P.; Patzelova,V. *Carbon* **1975,** *13,* 377.
5. Costello, C. A.; McCarthy,T. J. *Macromolecules* **1984,** *17,* 2941.
6. Morra, M.; Occhiello, E.; Garbassi, F. *Langmuir* **1989,** *5,* 872.
7. Morra, M.; Occhiello, E.; Garbassi, F. *Sur. Int. Anal.* **1990,** *16,* 412.
8. Golub, M. A.; Wydeven, T.; Cormaia, R. D. *Langmuir* **1991,** *7,* 1026.
9. Clark, D. T.; Hutton, D. R. *J. Polym. Sci., Polym. Chem. Ed.* **1987,** *15,* 2643.
10. Yasuda, H.; Marsh, H. C.; Brandt, S.; Reilley, C. N. *J. Polym. Sci., Polym. Chem. Ed.* **1977,** *15,* 991.
11. Kusabriaki, M. *Japn. J. Appl. Phys.* **1990,** *29,* 2809.
12. Golub, M. A.; Lopata, E. S.; Finney, L. S. *Langmuir* **1993,** *9,* 2240.
13. Hoshino, S.; Yumoto, M.; Sakai, T. *Proc. 11th Internat. Symp. Plasma Chem.* Loughborough, England, 1993, 1253.
14. Egitto, F. D.; Matienizo, L. J.; Schreyer, H. B. *J. Vac. Sci. Technol.* **1992,** *A10,* 3060.
15. Klausner, M.; Loh, I. H.; Baddour, R. F.; Cohen, R. E. *Proc. ACS Div. Polymeric Mater. Sci. Eng.* **1987,** *56,* 227.
16. Momose, Y.; Tamura, Y.; Ogino, M.; Okazaki, S.; Hirayama, M. *J. Vac. Sci. Technol.* **1992,** *A10,* 229.
17. Wheeler, D. R.; Pepper, S. V. *J. Vac. Sci. Technol.* **1982,** *20,* 226 and 442.
18. Clark, D. T.; Dilks, A. *J. Polym. Sci., Polym. Chem. Ed.* **1977,** *15,* 2321.
19. LeMoe, A.; Duraud, J. P.; Le Gressus, C.; Okuzumi, H. *Scanning Electron Microscopy* **1986,** 1319.

20. Hansen, R. H.; Schonhorn, H. *J. Polym. Sci. Polym. Lett.* **1966**, *4*, 203.

21. Gilman, A. B.; Goldshtein, D. V.; Potapov, V. K.; Shifrina, R. R. *High Energy Chemistry* **1988**, *22*, 393.

22. Tran, C. N. B.; Walt, D. R. *J. Colloid. Interface. Sci.* **1989**, *132*, 373.

23. Hollahan, R.; Stafford, B. B.; Falb, R. D.; Payne, S. T. *J. Appl. Polym. Sci.* **1969**, *13*, 807.

24. Clark, D. T.; Dilks, A., *J. Polym. Sci., Polym. Chem. Ed.* **1977**, *15*, 15.

25. Gerenser, L. J. *J. Adhesion Sci. Technol.* **1987**, *1*, 303.

26. Bell, A. T. In *Techniques and Applications of Plasma Chemistry;* Hollahan, J. R.; Bell, A. T. Eds.; Wiley: New York, 1974; chapter 1.

27. Boenig, H. V. *Fundamentals of Plasma Chemistry and Technology;* Technomic: Lancaster, PA, 1988.

28. Shard, A. G.; Munro, H. S.; Badyal, J. P. S. *Polym. Comm.* **1991**, *32*, 152.

29. Ehrlich, C. D.; Basford, J. A. *J. Vac. Sci. Technol.* **1992**, *A10*, 1.

30. Zhong, Q.; Inniss, D.; Kjoller, K.; Elings, V. B. *Surface Sci.* **1993**, *290*, L688.

31. Atkins, P. W. *Physical Chemistry 5th Ed*; Oxford Uni. Press: Oxford, 1994, p 29.

32. Evans, J. F.; Gibson, J. H.; Moulder, J. F.; Hammond, J. S.; Goretzki, H.P *Fresenius Z. Anal. Chem.* **1984**, *319*, 841.

33. Beamson, G.; Briggs, D. *High Resolution XPS of Organic Polymers: The Scienta ESCA300 Database* ; Wiley: Chichester, 1992.

34. Brown, H. A.; Crawford, G. H. In *The Science and Technology of Polymer Films Volume II* ; Sweeting, O. J. Ed.; Wiley: New York, 1971; pp 587-652

35. Wittman, J. C.; Smith, P. *Nature* **1991**, *352*, 414.

36. Tan, K. L.; Woon, L. L.; Wong, H. K.; Kang, E. T.; Neoh, K. G. *Macromolecules* **1993**, *26*, 2832.

37. Clark, D. T.; Feast, W. J.; Ritchie, I.; Musgrave, W. K. R.; Modena, M.; Ragazzini, M. *J. Polym. Sci., Polym. Chem. Ed.* **1974**, *12*, 1049.

38. Kogoma, M., Kasai, H., Takahashi, K., Moriwaki, T., Okazaki, S. *J. Phys. D: Appl Phys.* **1987**, *20*, 147.

39. Liston, E. M.; Rose, P. W. *Proc. 7th Internat. Symp. Plasma Chem.* Eindoven, Netherlands, 1985, 219.

40. Wheater, R. H.; Emmi, F.; White, R. F.; Bingle, W. D.; Horwath, R. S. *Proc. 4th Plasma Process Symp.* The Electrochem. Soc.: Pennington, New Jersey, 1983, 629.

41. Egitto, F. D., Matienzo, L. J. *Society of Vacuum Coaters, 36th Annual Technical Conference Proceedings* 1993, 10.

42. Chapman, B. *Glow Discharge Processes;* Wiley: New York, 1980.

43. Clark, D. T.; Dilks, A. *J. Polym. Sci., Polym. Chem. Ed.* **1977**, *16*, 911.

44. Clark, D. T., Dilks, A. *J. Polym. Sci., Polym. Chem. Ed.* **1980**, *18*, 1233.

45. Seebock, R. J., Kohler, W. E., and Romheld, M. *Contrib. Plasma Phys.* **1992**, *32*, 613.

46. Winters, H. F. *Topics in Current Chemistry* **1980**, *94*, 69.

47. Janes, J.; Huth, C. *J. Vac. Sci. Technol.* **1992**, *A10*, 3522.

48. Hopwood, J. *Appl. Phys. Lett.* **1993**, *62*, 940.

49. Godyak, V. A.; Piejak, R. B. *Phys. Rev. Lett.* **1990**, *65*, 996.

50. Thornton J. A. In *Deposition Technologies for Films and Coatings,* Bunshah, R. F., Ed.; Noyes: New Jersey, 1982, chapter 2.

51. Shard, A. G.; Badyal, J. P. S. *J. Phys. Chem.* **1991**, *95*, 9436.

52. Joubert, O.; Pelletier, J.; Arnal, Y. *J. Appl. Phys.* **1989**, *65*, 5096.

53. Smolinsky, G.; Vasile, M. J. *Eur. Polym. J* . **1979**, *15*, 87.

54. Wydeven, T.; Golub, M. A.; Lerner N. R. *J. Appl. Polym. Sci.* **1989**, *37*, 3343.

55. Ajello, J. M.; Shemansky, D.; Kwok, T. L.; Yung, Y. L. *Phys. Rev. A* **1984**, *29*, 636.

56. Cheeks, T. L.; Ruff, A. L. *Mater. Res. Soc. Symp. Proc.* **1987**, *75*, 527.

57. Egitto, F. D.; Matienzo, L. J. *Polym. Degrad. Stabil.* **1990**, *30*, 293.

58. Takacs, G. A.; Vukanovic, V.; Egitto, F. D.; Matienzo, L. J.; Emmi, F.; Tracy, D.; Chen, J. X. *Proc. 10th Internat. Symp. Plasma Chem.* Bochum, Germany, 1991, 14.

59. Sovey, J. S. *J. Vac. Sci. Technol.* **1979**, *16*, 813.

60. Youxian, D.; Griesser, H. J.; Mau, A. W.; Schmidt, R.; Liesegang, J. *Polymer* **1991**, *32*, 1126.

61. Morra, M.; Occhiello, E.; Garbassi, F. *Die Angewandte Makromolekulare Chemie* **1990**, *180*, 191.

62. Gallaher, T. N.; DeVore, T. C.; Carter III R. O.; Anderson, C. *Appl. Spectrosc.* **1980**, *34*, 408.

63. Chang, C. A.; Baglin, J. E. E.; Schrott, A. G.; Lim, K. C. *Appl. Phys. Lett.* **1987**, *51*, 103.

64. Chang, C. A. *Appl. Phys. Lett.* **1987**, *51*, 1236.

65. Wells, R. K.; Ryan, M. E.; Badyal, J. P. S. *J. Phys. Chem.* **1993**, *97*, 12879.

66. Chen, F.F. In *Plasma Diagnostic Techniques*, Huddlestone, R.H.; Leonard, S.L., Eds.; Academic: New York, 1965; p 113.

67. Fang, D; Marcus, K.M. In *Glow Discharge Spectroscopies*, Marcus, R.K., Ed.; Plenum: New York, 1993; p 28.

68. Liston, E. M. *Proc. IX Internat. Symp. on Plasma Chem.* Pugnochiuso, Italy, 1989, L7.

69. Takacs, G. A.; Vukanovic, V.; Tracy, D.; Chen, J. X.; Egitto, F. D.; Matienzo, L. J.; Emmi, F. *Polym. Degrad. Stabil.* **1993**, *40*, 73.

70. Ajello, J. M.; James, G. K.; Franklin, B.; Howell, S. *J. Phys. B* **1990**, *23*, 4355.

71. Kelly, R. L. *J. Phys. Chem. Ref. Data* **1987**, *16*, 1.

72. Samson, J. A. R. *Techniques of Vacuum Ultraviolet Spectroscopy*; Wiley: New York, 1967.

73. Yamamoto, S.; Tabata, H.; Moriuchi T. *Jap. Plastics Age* **1982**, *20*, 39.

74. Busscher, H. J.; Stokroos, I. ; Van der Mei, H. C.; Rouxhet, P. G.; Schakenaad, J. M. *J. Adhesion Sci. Technol.* **1992**, *6*, 347.

75. Ingram, S.G. *J. Appl. Phys.* **1990**, *68*, 500.

76. Strobel, J.M.; Strobel, M.; Lyons, C.S.; Dunatov, C.; Perron, S.J. *J. Adhesion. Sci. Technol.* **1991**, *5*, 119.

77. Zheng, J.X. *J. Appl. Polym. Sci.* **1993**, *48*, 231.

78. Occhiello, E.; Morra, M.; Garbassi, F.; Bargon, J. *Appl. Surface Sci.* **1989**, *36*, 285.

79. d'Agostino, R.; Cramarossa, F.; DeBenedictis, S. *Plasma Chem. Plasma Processing* **1982**, *2*, 213.

80. Truesdale, E. A.; Smolinsky, G. *J. Appl. Phys.* **1979**, *50*, 6594.

81. Plumb, I. C.; Ryan, K. R. *Plasma Chem. Plasma Processing* **1986**, *6*, 205.

82. Kay, E. *Proc. Internat. Ion Engineering Congress - ISIAT 83 & IPAT 83*, Kyoto, 1983, 1657.

83. Wu, S. *Polymer Interface and Adhesion;* Marcel Dekker: New York, 1982.

84. Kaelble, D. H. *Physical Chemistry of Adhesion;* Wiley: New York, 1971.

85. Egitto, D. F.; Vukanovic, V.; Taylor, G. N. In *Plasma Deposition, Treatment, and Etching of Polymers;* d'Agostino, R., Ed.; Academic; San Diego, 1990; chapter 5.

CHAPTER 3

MODELLING OF NON-ISOTHERMAL ARGON GLOW DISCHARGE MODIFICATION OF PTFE USING LOW ENERGY ARGON ION BEAMS

3.1 INTRODUCTION

Many methods of PTFE modification have been illustrated in the previous chapter. Surface modification was observed when using an argon plasma, a major constituent of which is argon ions. In this chapter modification using low energy argon ion beams is compared to that caused by an argon plasma in an attempt to quantify the effect ions have in plasma surface modification of polymers. Similarities and differences in the resultant surface structures are considered in terms of primary and secondary interactions between the polymer substrate and incident ion beam or plasma species.

3.1.1 Ion Beam Modification of Polymers

Most technologies based on irradiation effects in polymers make use of the fact that the chemistry of the organic film is easily changed[1]. Ion bombardment of organic films is known to result in irreversible changes, and modification of polymer surface properties has been observed using ion beams of various energies for some time[2].

3.1.1.1 Fundamentals of Ion-Polymer Interactions

Chemical modification of polymer films by ions differs to that caused by other ionizing particles in three main ways[3]:-

(i) two different mechanisms of energy deposition can occur simultaneously, electronic excitation and interparticle collisions,

(ii) the spatial distribution of reactive precursors is homogeneous,

(iii) the amount of energy deposited is greater for ions.

Each of these points will now be considered in turn.

The two energy deposition mechanisms (electronic excitation and interparticle collisions) differ because the electronic term produces excited species and radicals in the polymer which relax according to thermodynamic rules (minimization of energy), whereas the interparticle collisions are random and can produce non-thermodynamic species (highly unstable fragments)[3]. This leads to a large variety of available reactive species in the polymer surface.

The spatial distribution of reactive precursors generated by ion bombardment is important in the case of polymers compared to other materials. The primary species generated on impact may recombine or react within a larger volume than that of the ion track due to diffusion processes or propagation of radical species along the chain. In general, polymers have low thermal and electrical conductivity and radicals persist for some time, so excited states from successive impacts may interact effectively. This differs greatly to the effects observed in metals or semiconductors.

The effect of ion beams on molecular solids differs with the ion dose received. At high fluence (10^{14} atoms cm^{-2} or greater) a 'plasma-like' region along the ion tracks has been evoked, where all existing bonds are broken producing a graphitized surface. The resulting amorphous carbonaceous surface is often said to have lost all memory of the initial polymer[4]. Loss of volatile species and continuous bond rearrangement is involved in formation of the final structure. At lower fluence (10^{13} atoms cm^{-2} or less) many of the primary interactions are described as 'mild' reactions[3] which combine to give new functional groups, a different backbone and electronic structure. The modifications at low fluence produce chemically different products than those formed at high fluence. Figure 3.1 shows how typical chemical reactions and physical properties of bombarded polymers vary with increasing ion fluence[2].

Figure 3.1

The trends of ion fluence versus typical chemical reactions and related physical properties of bombarded organic polymers[4].

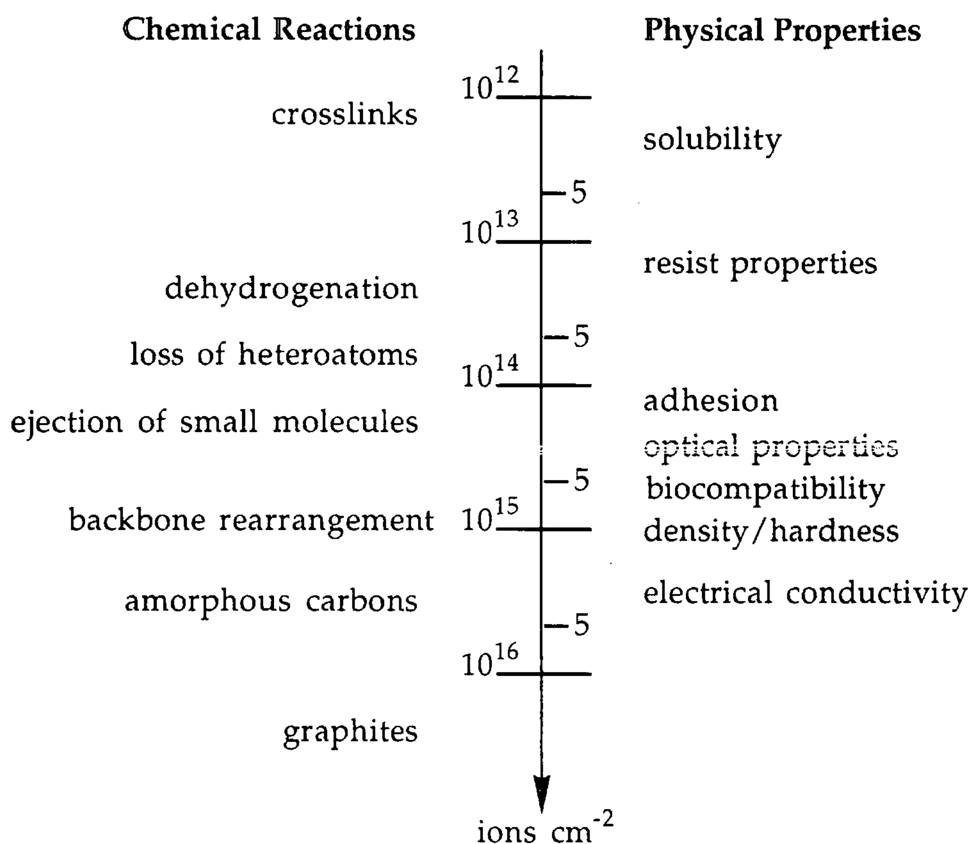

In summary ion-polymer interactions are essentially non-linear, high density energy deposition events that induce intense chemical changes such as dehydrogenation, decarbonylation, decarboxylation, ejection of other stable molecules, reduction of functional groups, loss of aromaticity via ring opening, loss of heteroatoms, backbone rearrangements, etc[4]. For the purpose of this work the effects of ion beams on PTFE are the important factor and these will now be reviewed.

3.1.1.2 Ion Beam Modification of PTFE

The modification of PTFE using energetic particles such as X-rays[5,6], electrons[7-11], atoms[12,13], lasers[14-17], and ion beams[18,19], have all been

studied. In particular, ion beams of a broad spectrum of energies and origin are reported[18-24]. Residual gas analysis of irradiated PTFE using He, N_2, and Si ion beams in the energy range 0.2 to 2.0 MeV yielded CF and CF_3 groups[18]. XPS and gas analysis performed after irradiation of PTFE with 20 MeV $^{34}Cl^{4+}$ ions[22] indicated better adhesion to thin gold films and defluorination. A reduction in the number of CF_2 groups has has also been observed after 750 eV H_2 and He ion beam exposure[19]. The enhancement of fluorine removal by H_2 ion bombardment was attributed to a chemical reaction between hydrogen atoms produced in the beam and radical sites on the polymer[19] as discussed in the previous chapter. The removal of CF_2 groups and fluorine by inert ion bombardment is believed to occur by ion beam induced desorption.

Low energy (30-3000 eV) inert gas (Ar^+ and Xe^+) ions have been shown to defluorinate PTFE without incorporation of the inert gas atom[23] and 400-1000 eV Ar^+ beams have been used to sputter PTFE targets[20], a topic that is covered in greater detail in chapter 4. The interaction of Ar^+ ions in the energy range 1-5 keV with tetrafluoroethylene/ethylene (TFE.E) copolymer and PTFE has been studied previously[24]. The rate of PTFE defluorination was found to decrease with increasing incident ion energy, which was attributed to the increased sputtering of PTFE revealing fresh polymer[24].

Modification of polymer surfaces by non-equilibrium glow discharges comprise of reaction and degradation of the substrate by ions generated in the plasma and also by other plasma species such as free radicals, excited species (i.e. metastables), electrons and electromagnetic radiation[25]. The prime objective of this study is to evaluate the relative importance of ion-substrate interactions during the argon plasma treatment of PTFE.

3.1.2 Ion Source

The ion source used in these experiments is the cold cathode electron impact type ion source[21]. This is composed of an anode surrounded by a can, the front surface of which has an aperture for ion removal figure 3.2. At the other end is mounted the cold cathode, which is held at a negative potential relative to the anode. The potential difference between the cathode and anode causes ion bombardment of the cathode resulting in secondary electron emission. The gas for the discharge (in this case argon) is introduced near the cold cathode and becomes ionized by the secondary electrons emitted from the cathode. The ions generated are accelerated by an extraction electrode and then focused into a beam after they leave the source. A minimum of two power supplies are required to operate the source, one for the anode-cathode potential and one for the extraction potential.

A cold cathode ion source differs from a hot cathode ion source because the primary ionization of the gas in the hot cathode source is by electrons emitted from a hot thermionic cathode.

Figure 3.2

Schematic of the cold cathode ion source used in these experiments[21].

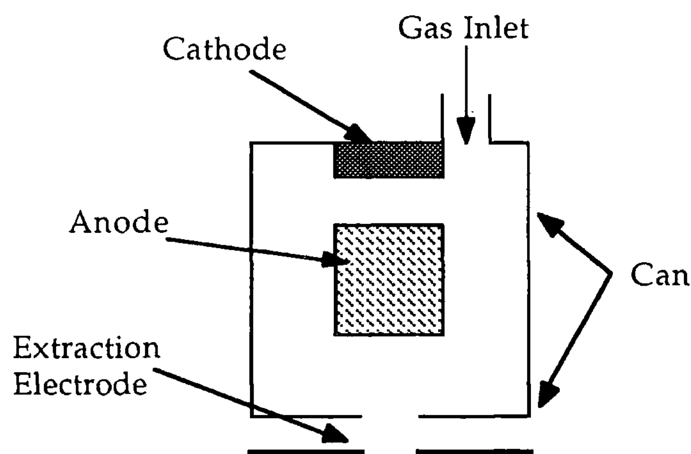

3.2 EXPERIMENTAL

3.2.1 Plasma Modification

Glow discharge experiments were carried out in a electrodeless cylindrical reactor as described in chapter 2 (section 2.2). The experimental set up and procedure was also the same as in chapter 2, and will not be repeated here. After the reactor was cleaned a large strip of PTFE was inserted into the centre of the reactor, which was then pumped down to its base pressure. Subsequently argon was introduced into the reaction chamber at 2 x 10^{-1} Torr pressure, and a flow rate (F_V) of approximately 1.0 cm^3 min^{-1}. After allowing 5 min for purging, the glow discharge was ignited at 50 W for 20 min. Upon termination of modification, the RF source was switched off, and argon was allowed to continue flowing through the reactor for another 5 min. Finally the system was let up to atmosphere and XPS analysis was performed as detailed in chapter 2 (section 2.2.1).

3.2.2 Ion Beam Modification

In situ Ar^+ ion irradiation/XPS studies were performed in a Vacuum Generators ESCALAB instrument (base pressure 2 x 10^{-11} Torr). A cold cathode ion gun (Vacuum Generators AG21) with a 1-2 % energy spread was used. A constant flux of Ar^+ ions was maintained by keeping the ion beam current hitting the substrate fixed at 5 x 10^{-10} A with the ion energy at 0.8, 1.4, 3.0, or 4.0 keV for each successive experimental run. Ion irradiation times were successively doubled between each exposure i.e. 30 s, 1 min, 2 min, 4 min, etc. The low ion current was due to the defocused nature of the ion beam, which covered the whole sample surface (1 cm^2). The angle of incidence of the ion beam to the sample surface was 20°, which was identical to the take off angle for the photo-electrons emitted from the sample. XPS

analysis was carried out using Magnesium Kα radiation as the photo-excitation source and constant analyser energy mode (CAE, 50 eV pass energy) photoelectron detection.

3.3 RESULTS

3.3.1 Argon Plasma Modification

Clean PTFE displays a main C(1s) peak at 291.2 eV, and a weak Mg K$\alpha_{3,4}$ satellite at lower binding energy, figure 3.3.

The C(1s) XP spectra of each treated surface was fitted with six Mg K$\alpha_{1,2}$ components having equal FWHM corresponding to -$\underline{C}_X$- (284.6 eV), -$\underline{C}$-CF_n- (286.6 eV), -$\underline{C}$F- (288.3 eV), -$\underline{C}$F-CF_n- (289.5 eV), -$\underline{C}F_2$- (291.2 eV),-$\underline{C}F_3$ (293.6 eV) environments[26]. Additional Mg K$\alpha_{3,4}$ satellites[27] (with a different fixed FWHM) were also taken into consideration.

Negligible variation in the C(1s) envelope throughout the R.F. coil region was observed during argon glow discharge modification of PTFE. The plasma treated surface composition was calculated to be 53.6% C, 36.7% F, 8.3% O, and 1.3 % N (oxygen and nitrogen containing groups are most likely to arise from reaction between trapped free radicals at the surface and the atmosphere during sample transfer to the XP spectrometer[28], as seen in the last chapter). Clearly a high degree of surface defluorination (F:C = 0.69) has taken place during the argon plasma treatment of PTFE, figure 3.4. The modification is much greater than that for argon plasma treatment in chapter 2. However, this is not too surprising after considering the longer treatment time and higher plasma power employed here.

Figure 3.3

C(1s) XP spectrum of clean PTFE.

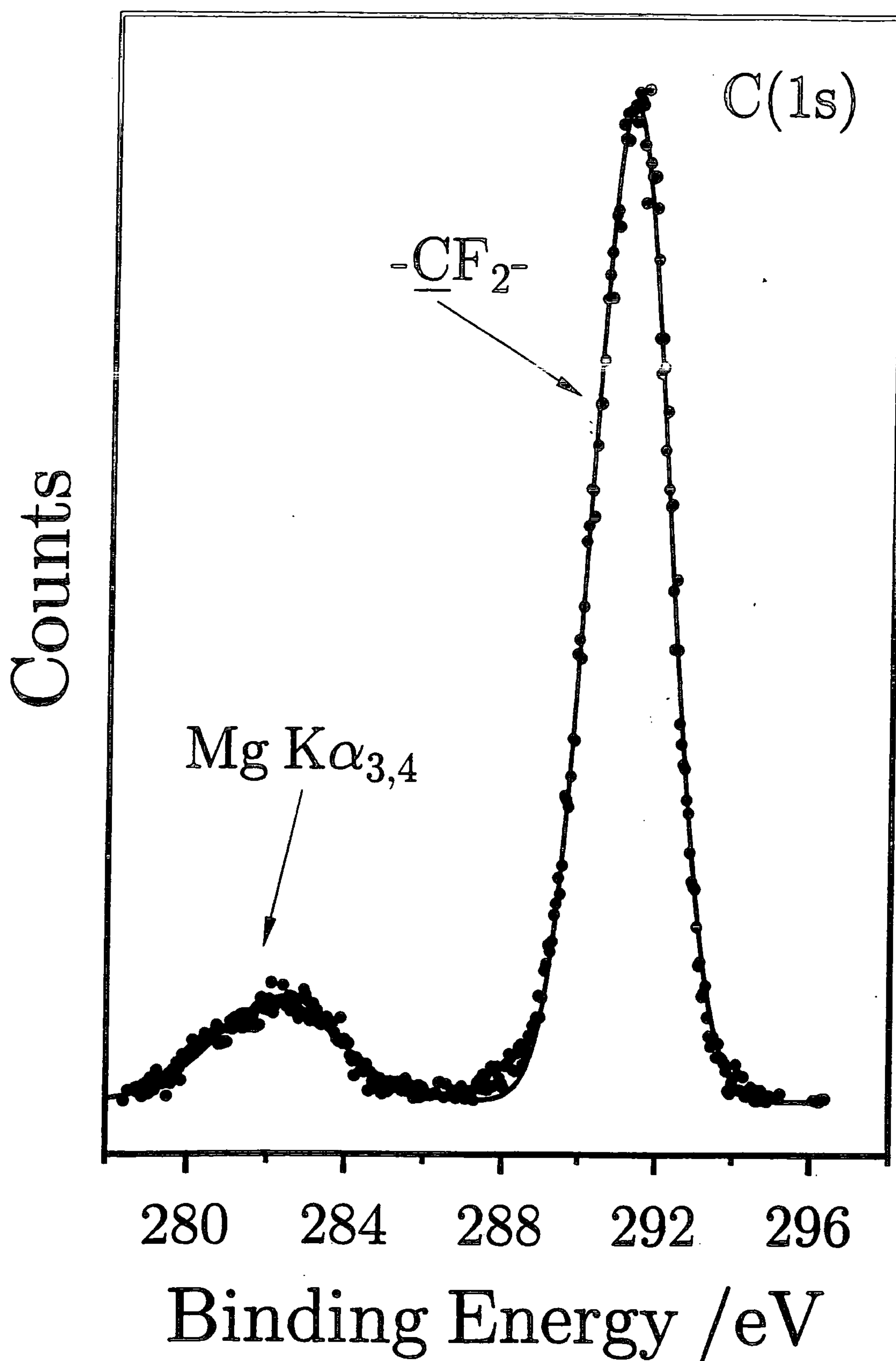

Figure 3.4

C(1s) XP spectrum of argon plasma modified PTFE (50 W, 20 min).

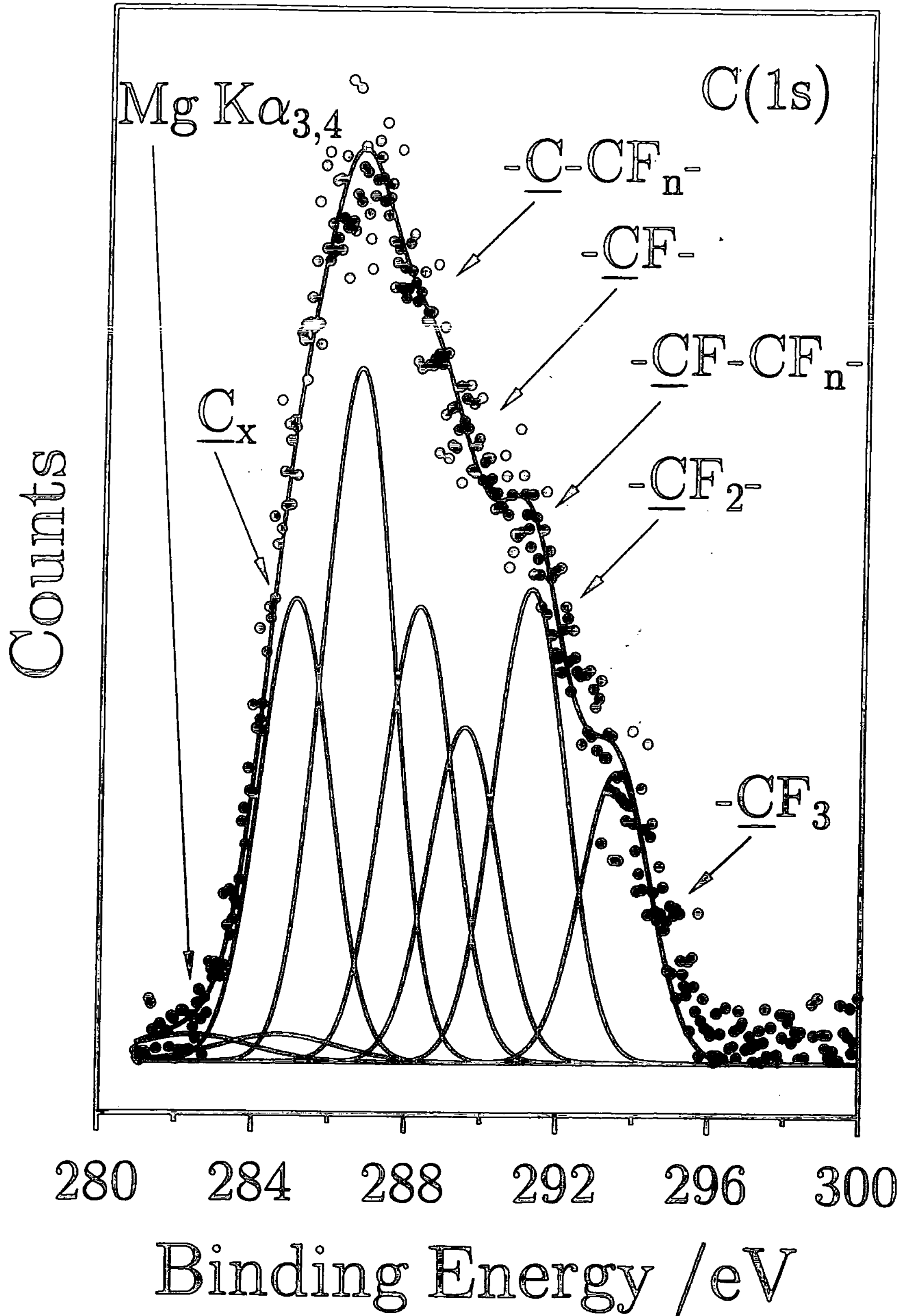

3.3.2 Argon Ion Beam Modification

F(1s) : C(1s) ratios plotted against Ar^+ ion dose (ions cm^{-2}), figure 3.5, show that the extent of surface defluorination of PTFE increases with ion dose (i.e. irradiation time), and in the energy range investigated the lower energy ion beams appear to be more effective in promoting defluorination. The most defluorinated surface (F : C = 0.63) was generated during a lengthy exposure (total of 128 min) to a low energy Ar^+ ion beam (0.8 keV), in this case the low binding energy side of the C(1s) envelope predominates, figure 3.6. Higher energy Ar^+ ion beams cause much less defluorination; for instance, 4 keV energy ions yield a F : C ratio of 1.37 after the same exposure time. This is in common with Huttons[24] results, who also found the modification to be uniform throughout the sampling depths for C(1s) electrons excited by Mg Kα radiation. It has been reported that argon ions, in the energy range used in the present work, have a penetration depth of about 10 nm in Teflon[29] which is greater than the sampling depth of the XPS experiment. Trapped argon within the polymeric matrix was not detected by XPS, and all of the modified surfaces were found to be stable with respect to ageing under an ultra high vacuum environment.

Figure 3.5

A plot of F : C ratios against ion dose (ions cm^{-2}).

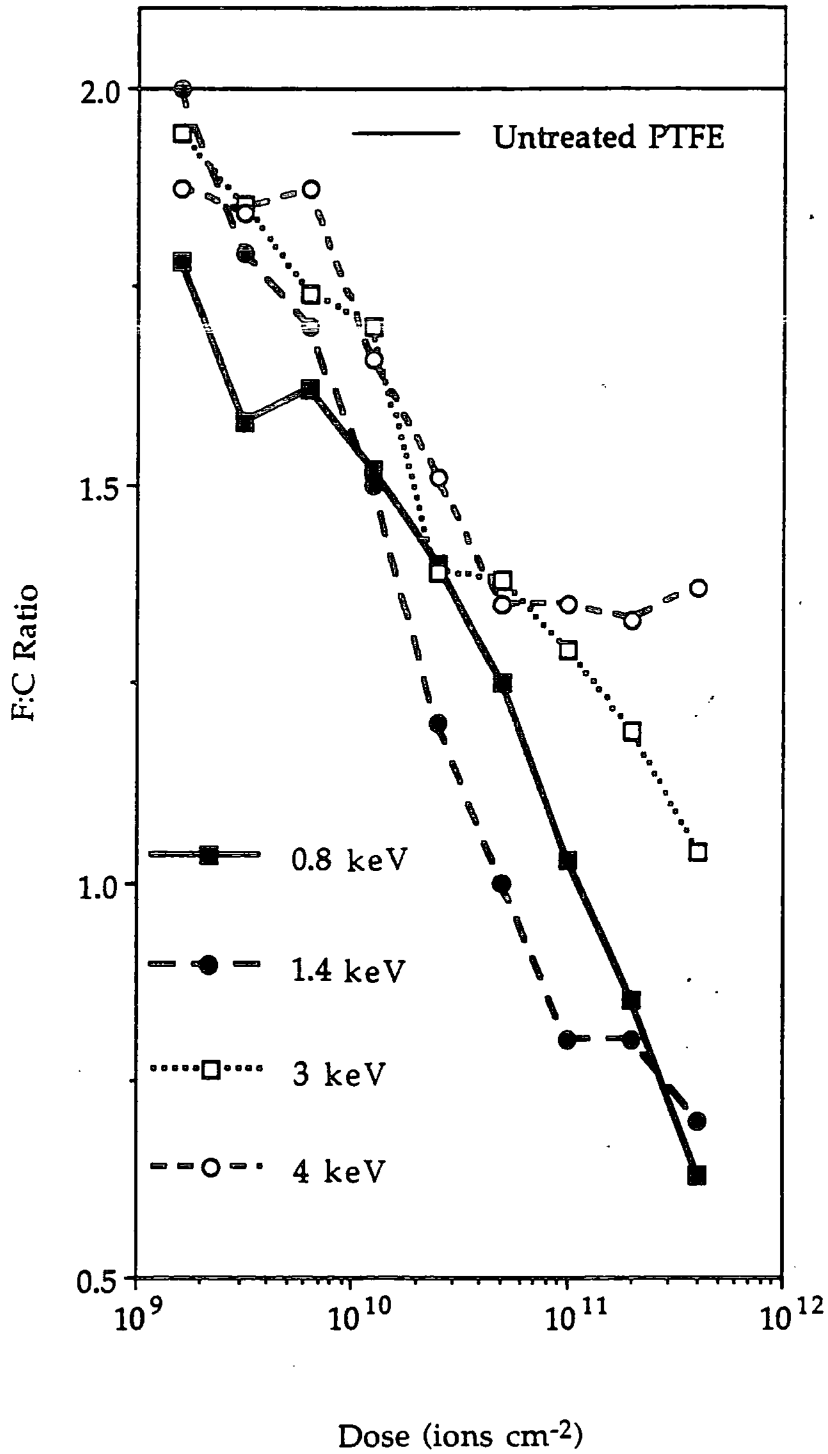

Figure 3.6

C(1s) XP spectrum of argon ion beam modified PTFE (0.8 keV, 128 min).

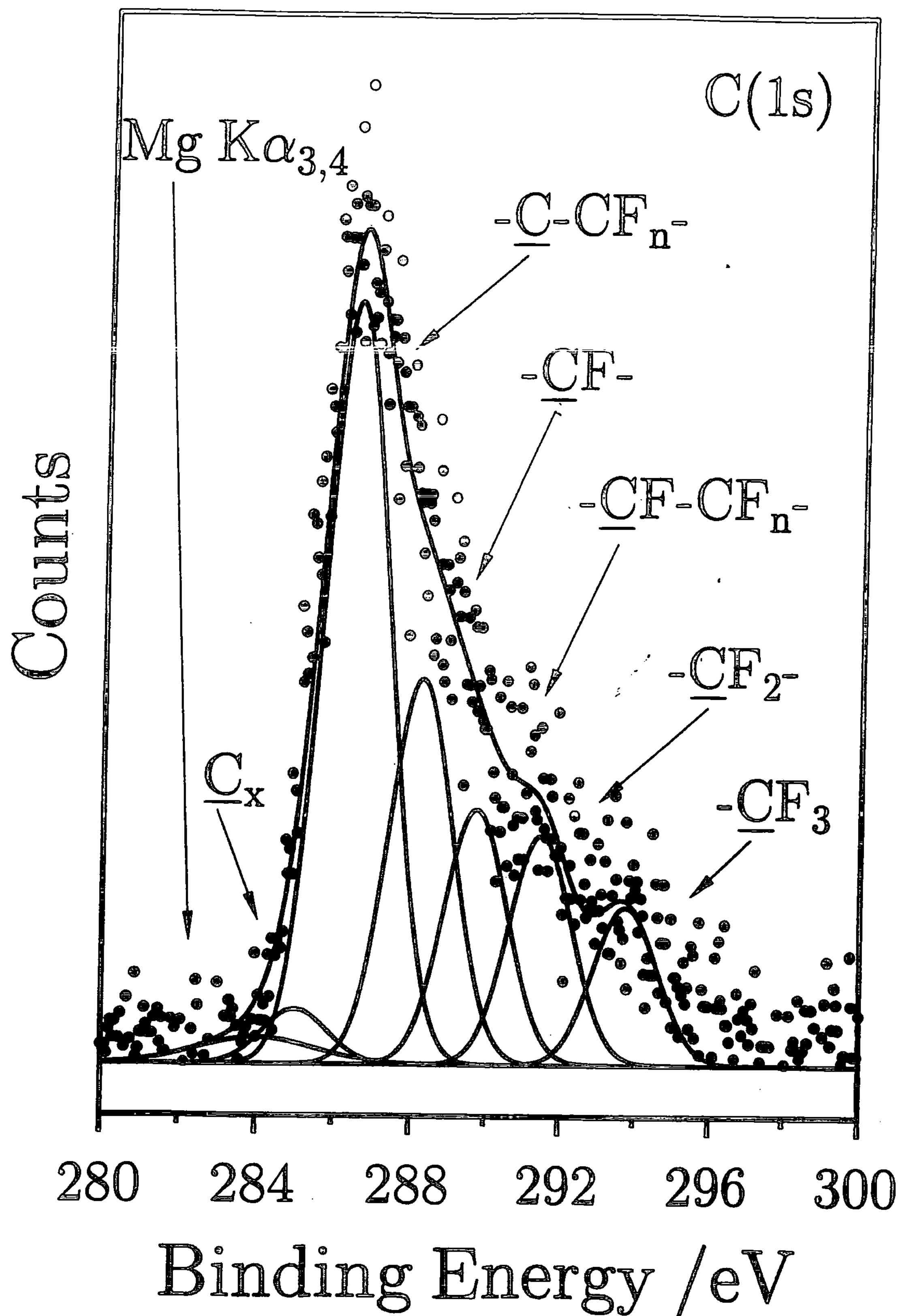

3.4 DISCUSSION

Surface modification of PTFE by plasma techniques is appealing as a dry process for altering the polymer substrates hydrophobicity[30]. Ion beam modification of polymer surfaces can result in crosslinking, defluorination, backbone rearrangement, and the formation of amorphous carbon, graphite, and diamond-like-carbon[2,31] as detailed in the introduction. Such treatments can yield desirable electrical, optical, abrasive, and adhesive properties[2,22,32-34]. In the case of argon, there appears to be a strong chemical similarity between the PTFE surface created by plasma and low energy ion beam treatments.

Generally, treatment of PTFE with a noble gas ion beam results in loss of fluorine in the surface region (as studied by XPS)[24,35]. The XPS C(1s) envelope initially consists of a single narrow peak for $-\underline{C}F_2-$, which broadens upon ion bombardment, with a concomitant decrease in the F(1s) signal. The presence of $-\underline{C}F_3$ functionality is reported to originate from the recombination of chain fragments and fluorine atoms[24]. Differences between the relative amounts of fluorinated functionalites seen in the plasma treated surface and ion beam treated surface may be due to modification induced by the additional species present in the argon plasma. The shorter times required for plasma treatment could be again due to the effect of additional plasma species or may indicate that the plasma generates a greater dose per unit time (flux) of ions. The ion dose was seen to be an important factor regarding the level of defluorination in the ion beam experiment.

Ion bombardment results in the emission of electrons, neutrals, ions, and photons[36] at comparable energies to those typically found in non-isothermal glow discharges. The maximum energy of ions bombarding a substrate during plasma exposure is equal to the difference between the plasma potential and the surface potential, which can range from tens to

hundreds of eV[37,38]. Therefore low energy Ar^+ ion beam irradiation of PTFE may serve as a good model for argon glow discharge modification (where ion-surface interactions are regarded as being a predominant process). However, at higher Ar^+ ion beam energies, extensive sputtering occurs leading to the continuous unveiling of fresh PTFE[24].

Static secondary ion mass spectrometry (SSIMS), a recently developed method of polymer surface analysis, is based on the mass analysis of ejected species after surface irradiation with a low density ion beam. Low beam currents, 10^{-11} to 10^{-8} A cm^{-2}, and energies, 0.5 to 4 keV, are used[39] which are of the order of the argon ion beams used in this study ($5x10^{-10}$ A cm^{-2}, 0.8 - 4 keV). Therefore, modification of a polymer surface following primary ion burial[36] is an important feature which needs to be taken into consideration when interpreting SSIMS spectra of polymeric substrates.

3.5 CONCLUSIONS

Clearly a number of similarities are evident between argon plasma treatment of PTFE and the low energy Ar^+ ion beam experiments. These can be explained in terms of similar physicochemical phenomena occurring at the polymer surface during argon glow discharge modification and low energy Ar^+ ion burial into PTFE.

Further work could include *in situ* plasma modification/XPS which will soon be possible in this laboratory to compare with the *in situ* ion beam modification. Similar modelling studies using different polymer substrates and ion/plasma environments may lead to further mechanistic details of ion-polymer interactions occurring in plasmas. For instance, Groning[40] has recently shown that noble gas plasma and low energy ion beam treatment of PMMA produce exactly the same chemical modifications at the surface.

3.6 REFERENCES

1. Venkatesan, T.; Calcagno, L.; Elman, B. S.; Foti, G. In *Ion Beam Modification of Insulators* Eds. Mazzoldi, P.; Arnold, G. W. Elsevier: Amsterdam, 1987; chapter 8.
2. Pignataro, S.; Marletta, G. In *Mettalized Plastics 2* Ed. Mittal, K. L., Plenum: New York, 1991; p 269.
3. Marletta, G. *Nuc. Inst. and Meth. in Phys. Res.* **1990**, *B46*, 295.
4. Pignataro, S. *Surf. Inter. Anal.* **1992**, *19*, 275.
5. Wheeler, D. R.; Pepper, S. V. *J. Vac. Sci. Tech. A* **1982**, *20*, 442.
6. Rye, R. R.; Arnold, G. W. *Langmuir* **1989**, *5*, 1331.
7. Rye, R. R. *J Polym. Sci., Polym. Phys. Ed.* **1993**, *31*, 357.
8. Chakrabarti, N.; Jacobus, J. *Macromolecules* **1988**, *21*, 5487.
9. Sessler, G. M.; West, J. E.; Ryan, F. W.; Schonhorn, H. J. *J. Polym. Sci.* **1973**, *17*, 3199.
10. Kelber, J. A.; Rogers, J. W.; Ward, S. J. *J. Mater. Res.* **1986**, *1*, 717.
11. Michael, R.; Stulik, D. *J. Vac. Sci. Tech. A* **1986**, *4*, 1861.
12. Tasker, S.; Chambers, R. D.; Badyal, J. P. S. *J. Phys. Chem.* **1994**, *98*, 12442.
13. Michael, R.; Stulik, D. *J. Vac. Sci. Tech. A* **1986**, *4*, 1861.
14. Dickinson, J. T.; Shin, J. J.; Jiang, W.; Norton, M. G. *J. Appl. Phys.* **1993**, *74*, 4729.
15. Blanchet, G. *Science* **1993**, *262*, 719.
16. Blanchet, G.; Fincher, C. R. *Advanced Materials* **1994**, *6*, 881.
17. Novis, Y.; Demeulemeester, R.; Chtaib, M.; Pireaux, J. J.; Caudano, R *Brit. Polym. J.* **1989**, *21*, 147.
18. Lewis, M. B.; Lee, E. H. *Nuc. Inst. and Meth. in Phys. Res.* **1991**, *B61*, 457.
19. Cheeks, T. R.; Ruoff, A. L. *Mater. Res. Soc. Symp. Proc.* **1987**, *75*, 527.

20. Quaranta, F.; Valentini, A.; Favia, P.; Lamendola, R.; d'Agostino, R. *Appl. Phys. Letts.* **1993**, *63*, 10.

21. Wilson, R. G.; Brewer, G. R. *Ion Beams with Applications to Ion Implantation* ;Wiley: New York, 1973; p 58.

22. Ingemarsson, P. A.; Keane, M. P.; Gelius, U. *J. Appl. Phys.* **1989**, *66*, 3548.

23. Taylor, J. A.; Lancaster, G. M.; Rablais, J. W. *Appl. Surf. Sci.* **1978**, *1*, 503.

24. Hutton, D. R. *Ph.D. Thesis*; 1983, University of Durham.

25. Boenig, H. V. *Fundamentals of Plasma Chemistry and Technology*; Technomic Publ. Co. Inc.: Lancaster, PA, 1988.

26. Clark, D. T.; Feast, W. J.; Ritchie, I.; Musgrave, W. K. R.; Modena, M.; Ragazzini, M. *J. Polym. Sci., Polym. Chem. Ed.* **1974**, *12*, 1049.

27. Wagner, C. D.; Riggs, W. M.; Davis, L. E.; Moulder, J. F.; Muilenberg, G. E. *Handbook of X-Ray Photoelectron Spectroscopy*, Perkin-Elmer Corporation: Eden Prairie Mi, 1978; p 13.

28. Yasuda, H.; Marsh, H. C.; Brandt, S.; Reilley, C. N. *J. Polym. Sci., Polym. Chem. Ed.* **1977**, *15*, 991.

29. Tan, B. J.; Fessehaie, M.; Suib, S. L. *Langmuir* **1993**, *9*, 740.

30. Kusabiraki, M. *Jap. J. Appl. Phys.* **1990**, *29*, 2809.

31. Ryan, M. E.; Badyal, J. P. S. *Macromolecules*, **1995**, *28*, 1377.

32. Fink, D.; Muller, M. *Nuc. Inst. and Meth. in Phys. Res.* **1988**, *B32*, 125.

33. Hirvonen, J. K. *Annu. Rev. Mater. Sci.* **1989**, *19*, 401.

34. Ingemarsson, P. A. *Nuc. Inst. and Meth. in Phys. Res.* **1990**, *B44*, 437.

35. Gossedge, G. M.; Cadman, P. *J. Mat. Sci.*, **1979**, *14*, 2672.

36. Lipinsky, D.; Jede, R.; Ganschow, O.; Benninghoven, A. *J. Vac. Sci. Technol.* **1985**, *A3*, 2007.

37. Winters, H. F. *Topics in Current Chemistry* 1980, 94, 69.

38. Janes, J.; Huth, C. *J. Vac. Sci. Technol.* **1992**, *A10*, 3522.

39. Briggs, D.; Brown, A.; Vickerman, J. C. *Handbook of Static Secondary Ion Mass Spectrometry* ; Wiley: Chichester, 1989; p 8.

40. Groning, P.; Kuttel, O. M.; Collaud-Coen, Dietler, G.; Schlapbach, L. *Appl. Sur. Sci.* **1995**, *89*, 83.

CHAPTER 4

PLASMA POLYMERIZATION OF SPUTTERED PTFE

4.1 INTRODUCTION

The last two chapters concentrated on plasma modification of PTFE surfaces. In this chapter the same RF glow discharges are utilized to synthesize 'PTFE like' thin films. Non-equilibrium plasmas are useful for a variety of chemical reactions, these include the generation of atoms[1], radicals[2], isomerization[3], rearrangement[4], etching[5], and polymerization[6]. Polymeric layers can be prepared by introducing saturated or polymerizable solid forming species into such low temperature glow discharges as outlined in chapter 1. Plasma polymerized fluoropolymer films offer many potential applications, including use as non-wettable surfaces[7], dielectrics[8], optical layers[9], and wear resistant coatings[10]. The most popular preparative route for manufacturing these materials has been the injection of a fluoromonomer into a non-isothermal glow discharge. Alternatively, radio frequency (RF) sputtering of a PTFE substrate[8,11,12] can be used. Such RF sputtering of PTFE is understood to evolve C_2F_4 (tetrafluoroethylene)[11-13], which subsequently undergoes plasma polymerization in the RF sputter field[14].

4.1.1 Plasma Sputter Deposition

Although plasma polymerization was introduced in chapter 1, the concept of plasma sputter deposition has not yet been touched on. It is the purpose of the next section to review this area.

Sputtering is a process where material is dislodged and ejected from the surface of a target due to momentum exchange associated with surface bombardment by energetic particles. Substrates are positioned in front of the target so that they intercept the flux of sputtered atoms. The most common method of providing the ion bombardment is by use of a plasma. Since the ejected species are created by physical rather than chemical or thermal

processes, virtually any material can be sputter deposited. This has led to many applications particularly in the electronics industry, e.g. in the production of oxide microcircuit insulation layers[15], piezo-electric transducers[16], photoconductors[17] and luminescent films[18] for display devices, and photolithographic mask blanks[19].

Generation of the plasma required for sputter deposition can be achieved using several methods, for instance DC glow discharges, magnetron devices, and RF plasmas. Of these RF plasmas are the most popular because they can be used with conducting, semiconducting or insulating targets.

4.1.2 Sputter Deposited PTFE

Sputtered PTFE has been studied for many years[14,20,21] with a recent resurgence in the area[22,23]. Depending on deposition conditions, these polymer films can exhibit excellent properties comparable to PTFE[21,24]. The growth mechanism of fluorocarbon materials synthesized by PTFE sputtering is not well understood. The stoichiometry of a $(CF_x)_n$ polymer film depends on the mass distribution of the molecular fragments arriving at the substrate surface. During sputtering of a PTFE target by ions, low weight fragments are ejected and further molecular dissociations may occur in the plasma. As a result RF sputtered films exhibit a fluorine deficiency[22] compared to PTFE.

Growth of plasma polymerized films has been described by the activated growth model (AGM) in which film deposition occurs only at specific polymer sites that have been 'activated' by energy transfer from the plasma to the polymer site, typically by ion bombardment[25,26]. Measurable differences in film composition with substrate material have recently been observed, which is consistent with the AGM model in that plasma-surface interactions during initial stages of deposition dominate and establish the

growth mechanism and characteristics of the film[27]. It has been suggested that both sputtered PTFE and plasma polymerized fluorocarbon films grown in a similar manner have closely related structure[14], although it's now believed this may be an over simplification[20]. There has never previously been a systematic study of the influence of sputter gas on the character of the resultant plasma polymer film. In this chapter, plasma polymerization of RF sputtered PTFE is examined in the context of to what extent the chemical nature of the deposited fluoropolymer layer is influenced by the carrier gas (He, Ne, Ar, N_2, H_2) used in the glow discharge. The chemical composition of the plasma phase has been monitored by ultraviolet emission spectroscopy during PTFE sputtering and correlated with the chemical nature (as evaluated by X-ray photoelectron and infrared spectroscopy) of the obtained fluorocarbon deposits.

4.2 EXPERIMENTAL

4.2.1 Glow Discharge Experiments

The experimental set-up and procedure were the same as in chapter 2. The cleaning plasma treatment (50 W air plasma for 40 min) was carried out in the presence of glass substrates, but in the absence of any polymer film. After cleaning, the entire inside of the glass reactor was lined with fresh PTFE film (Mupor Ltd) using a PTFE covered glass support and the reactor was pumped down to its base pressure. Subsequently the carrier gas of interest was introduced into the reaction chamber at 2 x 10^{-1} Torr pressure, and a flow rate (F_v) of approximately 1.0 $cm^3\ min^{-1}$. After allowing 5 min for purging, the glow discharge was ignited at 50 W for 20 min. Upon termination of deposition, the radio frequency source was switched off, the

carrier gas was allowed to purge the system for 5 min, and then vented to atmosphere before immediate analysis of the deposited film.

4.2.2 Analysis

A Kratos ES200 spectrometer was used for (XPS) analysis as described in chapter 2 (section 2.2.1). This was operated in the fixed analyser transmission (FAT) mode, at a pass energy of 65 eV. Instrumentally determined sensitivity factors for unit stoichiometry were taken as C(1s) : O(1s) : F(1s) : N(1s): Si(2p) equals 1.00 : 0.46 : 0.33 : 0.37 : 1.31.

A FTIR Mattson Polaris instrument was used for transmission infrared analysis of RF plasma sputtered fluorocarbon layers deposited onto pressed potassium bromide (KBr) discs. A reference infrared spectrum of PTFE substrate was obtained by using a variable angle attenuated total reflection (ATR) cell fitted with a KRS-5 crystal; an incident beam angle of 45° resulted in 14 internal reflections. Typically, 100 scans were acquired at a resolution of 4 cm^{-1}.

A home-built UV emission spectrometer based upon a Czerny-Turner type monochromator was used for plasma glow analysis. A computer was used to rotate the grating via a stepping motor, and also to accumulate the counts from the photomultiplier tube detector. This instrument could scan continuously from 180 to 500 nm at 0.5 nm resolution.

4.3 RESULTS

4.3.1 X-ray Photoelectron Spectroscopy

Clean PTFE displays a main C(1s) peak at 291.2 eV, and a weak Mg $K\alpha_{3,4}$ satellite shifted by approximately 9 eV towards lower binding energy, figure 4.1(a). For each type of glow discharge treatment investigated, there was negligible variation in the C(1s) envelope across the region of the RF coils, which reflects a homogeneous chemical composition. This observation is consistent with the whole of the reactor being lined with PTFE, and therefore being able to provide a uniform source of polymerizable species. The absence of any Si(2p) signal from the underlying glass substrate was taken as being indicative of complete coverage by the plasma polymer. A small amount of oxygen was detected, the most likely origin for this being reaction between trapped free radical centres at the surface and the atmosphere during transport of the deposited layer from the glow discharge apparatus to the XP spectrometer[28] (contamination within the bulk of the deposited fluoropolymer layer can be ruled out since oxygenated carbon functionalities were absent in the transmission infrared analysis of these films).

The C(1s) XP spectra of each coating was fitted with six Mg $K\alpha_{1,2}$ components having equal FWHM corresponding to $-\underline{C}_x-$ (284.6 eV), $-\underline{C}-CF_n-$ (286.6 eV), $-\underline{C}F-$ (288.3 eV), $-\underline{C}F-CF_n-$ (289.5 eV), $-\underline{C}F_2-$ (291.2 eV), and $-\underline{C}F_3$ (293.6 eV) environments[29], figure 4.2. Additional Mg $K\alpha_{3,4}$ satellites[30] shifted by approximately 9 eV towards lower binding energy (with a different fixed FWHM) were also taken into consideration. Table 4.1 summarizes the relative proportions of fluorinated carbon centres present for each glow discharge treatment. Surprisingly, no fluoropolymer deposition was observed for the hydrogen carrier gas experiments.

Fluoropolymer deposits resulting from the noble gas plasmas displayed a gradual loss in fluorine content with increasing atomic mass of the carrier gas, whilst nitrogen plasma sputtering of PTFE produced the greatest $-CF_2-$ component. The XP spectrum of fluorocarbon film produced with argon carrier gas shows a strong resemblance to the argon plasma modified PTFE investigated in the last chapter.

Table 4.1

Summary of C(1s) XPS peak fits (NB [Total $-\underline{C}-$] = [$-\underline{C}-$] + [$-\underline{C}-CF_n-$], and [Total $-\underline{C}F-$] = [$-\underline{C}F-$] + [$-\underline{C}F-CF_n-$]).

	F:C Ratio	Total $-\underline{C}-$	Total $-\underline{C}F-$	$-\underline{C}F_2-$	$-\underline{C}F_3$	% C	% F	% N	% O
PTFE	2.00	0.0	0.0	100.0	0.0	33.7	66.3	0.0	0.0
Nitrogen	1.21	14.6	37.5	34.9	13.1	40.1	48.6	8.7	2.5
Helium	1.02	25.6	39.9	25.4	9.2	45.3	46.0	3.1	5.6
Neon	0.82	38.8	33.4	20.2	7.5	50.7	41.3	1.0	7.0
Argon	0.78	39.7	33.2	18.9	8.0	52.0	40.4	0.9	6.8

Figure 4.1

C(1s) XP spectra of: (a) clean PTFE; (b) nitrogen sputter deposited fluoropolymer; (c) helium sputter deposited fluoropolymer; (d) neon sputter deposited fluoropolymer; and (e) argon sputter deposited fluoropolymer.

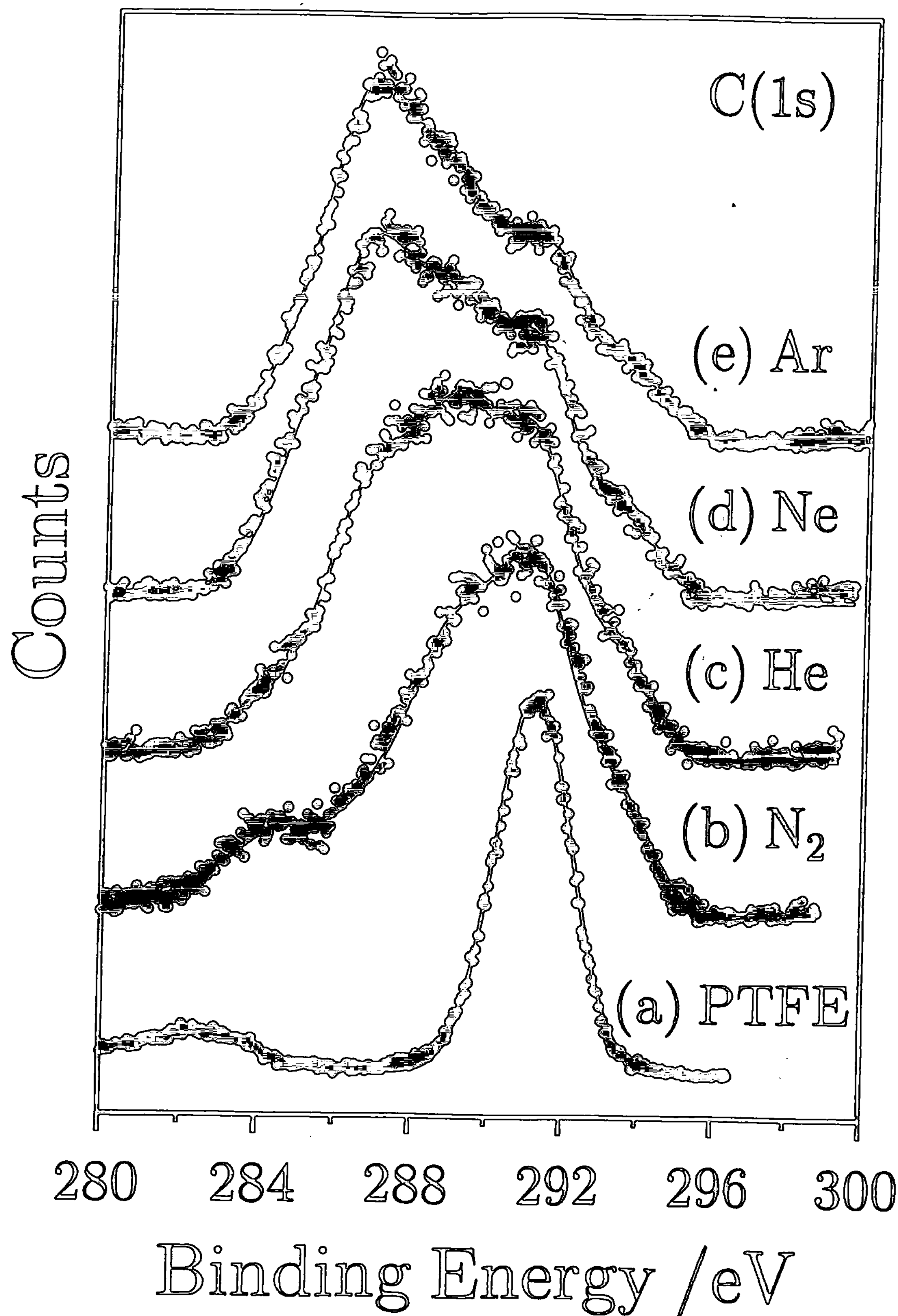

Figure 4.2

Typical C(1s) XPS peak fit (argon glow discharge, 50 W 20 min).

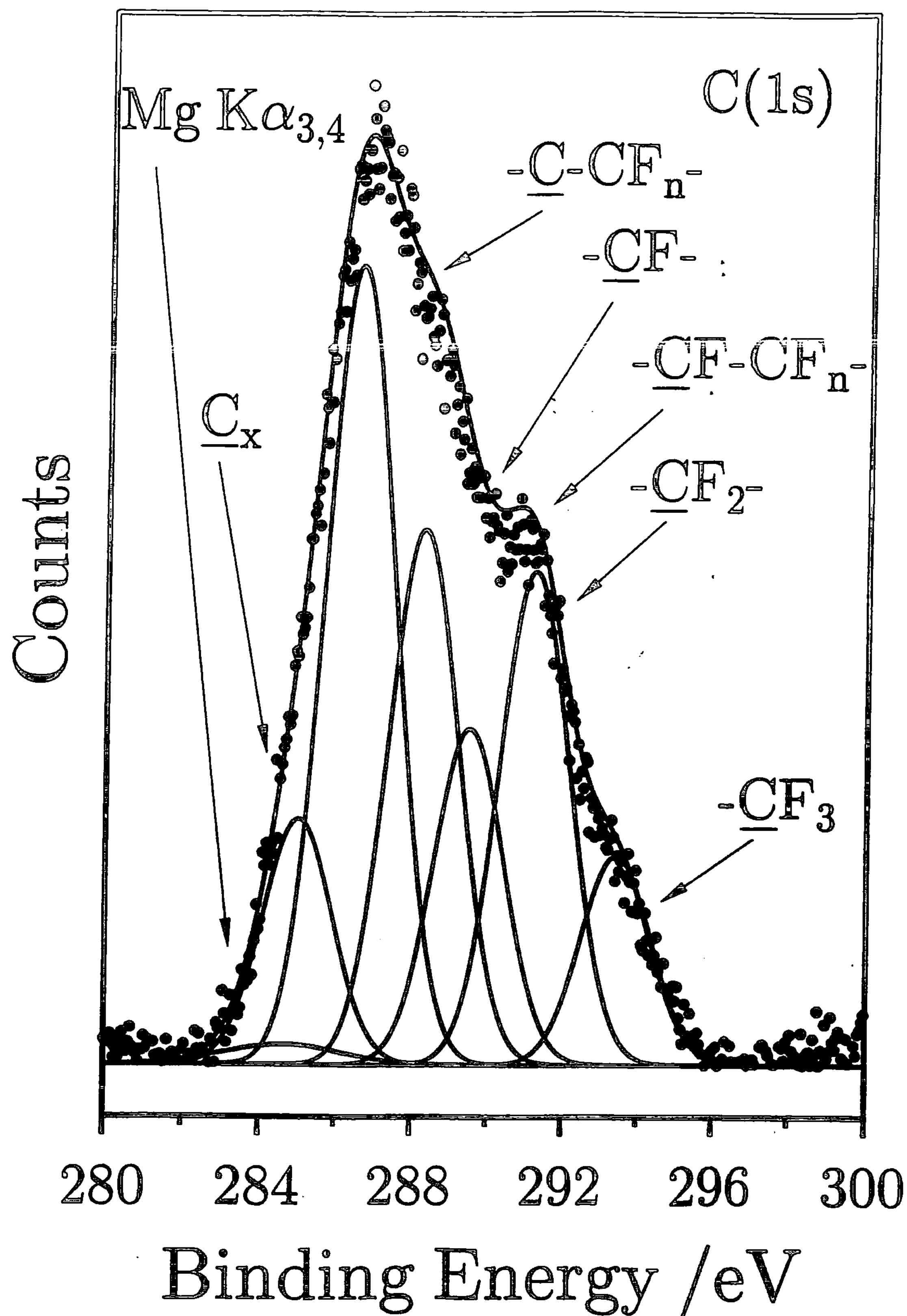

4.3.2 Infrared Spectroscopy

Absorption bands in the ATR-FTIR spectrum of clean PTFE, figure 4.3(a), can be assigned as follows[31]: 514 cm^{-1} (CF_2 wagging), 556 cm^{-1} (CF_2 rocking) and 640 cm^{-1} (CF_2 rocking), 1152 cm^{-1} (asymmetric C-F stretch), 1208 cm^{-1} (symmetric C-F stretch). Infrared absorption bands in the sputter deposited fluoropolymer layers, figure 4.3(b)-(e), were assigned as follows: 740 cm^{-1} ($-CF_3$ stretching deformation[32] and/or symmetric CF_2 vibration which becomes active due to distortion of $(-CF_2-)_n$ chains[33]), 1000 - 1400 cm^{-1} (C-F stretching[34-36]), 1515 cm^{-1} (absorption bands in this region have been previously observed for plasma polymers prepared from perfluorobenzene[37]), 1626 cm^{-1} (-CF=C< stretch in a crosslinked environment[34,38]), 1730 cm^{-1} (-CF=CF- stretch[34,35,38,39]), and 2077 cm^{-1} (-CF=C=CF- stretching - fluorine substitution causes a shift to higher vibrational frequencies away from the usual 2000-1900 cm^{-1} region[34,38]). On moving from nitrogen, to helium, to neon, to argon, the 1515 cm^{-1} absorbance bands rises in intensity at the expense of the 1626 cm^{-1} and 1730 cm^{-1} features, this is consistent with a greater number of crosslinked / aromatic environments.

4.3.3 UV Emission Spectroscopy

Common methods used for identifying and monitoring the intermediates within fluorocarbon plasmas include mass spectrometry and emission spectroscopy. Mass spectrometry can be used to sample ions and radicals or analyze stable end products in the effluent[40-42]. Emission spectroscopy is useful for identifying excited intermediates within the plasma phase although the determination of absolute concentrations requires knowledge of the relative amounts of ground and excited state species[43]. Since the optical diagnostic tool is external to the reactive plasma

chamber, this makes it a non-intrusive technique enabling the direct observation of short lived species[44]. Previous conclusions obtained by effluent mass spectrometry for fluorocarbon discharges tie in with the appropriate optical emission spectra[44]. For instance, CF_2 species are believed to play an important role in fluorocarbon plasmas[41,45-49], the rate of plasma polymerization has been shown to correlate with the CF_2 radical concentration in the glow discharge[50-52].

Assignment of emission spectra from fluorocarbon plasmas can be complicated[53]. A number of bands in the 197-420 nm UV region are reported to be characteristic of CF, CF_2, and CF_3 radical species[53-56], these provide a basis for identification of emission bands obtained in the present study. UV emission spectra were acquired for excited glow discharges of helium, neon, argon, and nitrogen gas in the absence and presence of PTFE, figures 4.4 to 4.7. Two UV band systems are observed for CF: these being ($A^2\Sigma^+$-$X^2\Pi$) and ($B^2\Delta$-$X^2\Pi$) transitions in the 220-295 nm[55,56] and 197-220 nm[56,57] ranges respectively. The CF_2 ($^1B_1$-$^1A_1$) band system at 240-325 nm[54] has been previously noted for tetrafluoroethylene (C_2F_4), perfluoropropene (C_3F_6), and perfluorobutene (C_4F_8) glow discharges[48,53,54,58-61]. There is some overlap here with the CF ($A^2\Sigma^+$-$X^2\Pi$) transition between 220-295 nm. UV emission features for CF_3 radicals are reported to have been observed by Suto[62-64] in the 180-300 nm region; however a theoretical analysis by Larrieu[65] raises some ambiguities concerning this assignment of CF_3 bands. In fact the main UV emission features for CF_3 radicals occurs in the 450-750 nm region[62], whilst atomic F lines appear in the 680-720 nm region[66-69]. Unfortunately for both of these species, there is no overlap with the scan range available in the present study. The disappearance of any lines from the pure gas glow discharge during PTFE sputter plasma polymerization can be explained in terms of the absorption of these lines by sputtered fluorocarbon species.

Figure 4.3

FTIR absorbance spectra of: (a) clean PTFE; (b) nitrogen sputter deposited fluoropolymer; (c) helium sputter deposited fluoropolymer; (d) neon sputter deposited fluoropolymer; and (e) argon sputter deposited fluoropolymer.

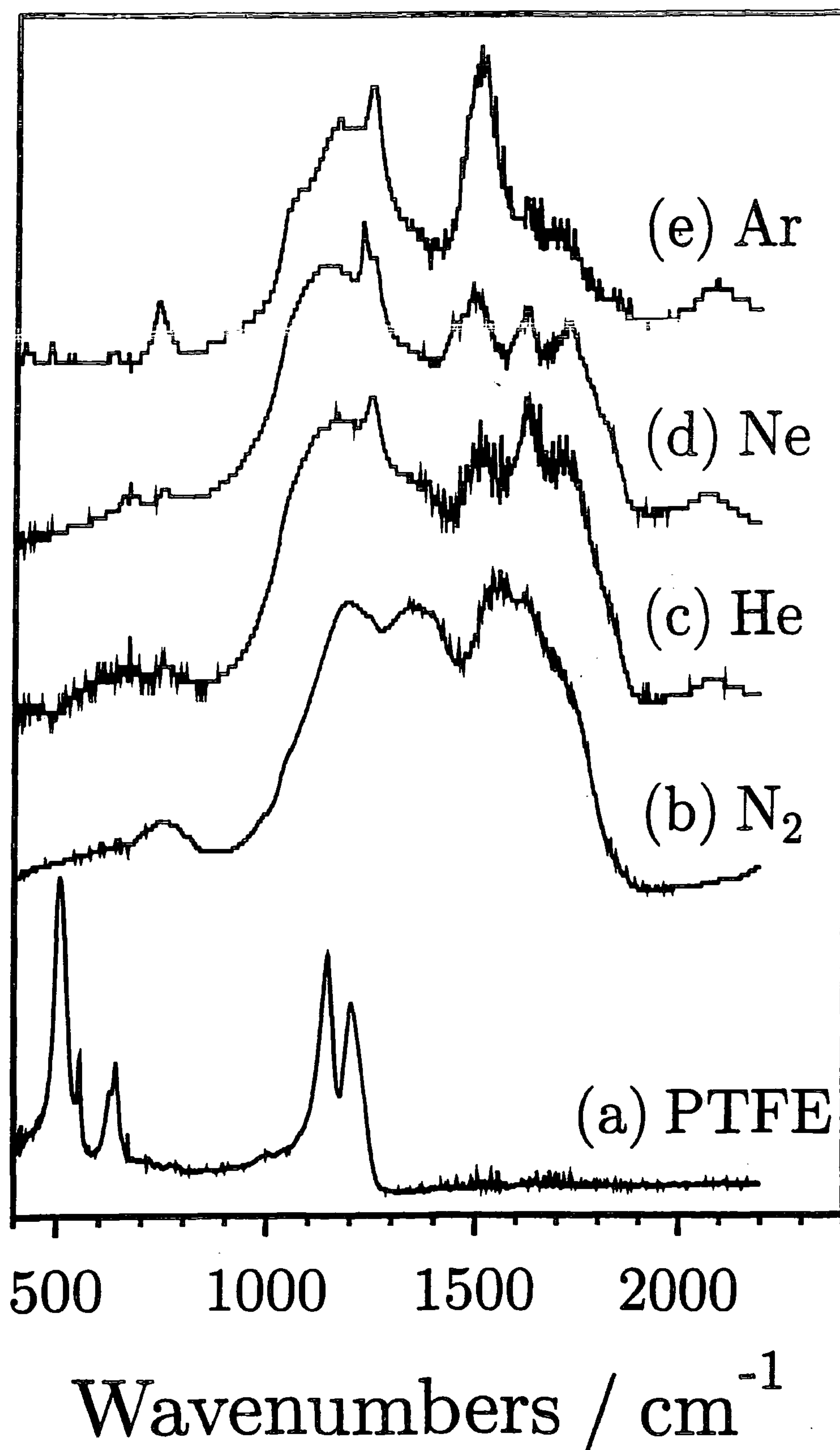

Figure 4.4

UV emission spectra of He glow discharge in the absence (lower) and presence (upper) of PTFE film in the 180-500 nm region.

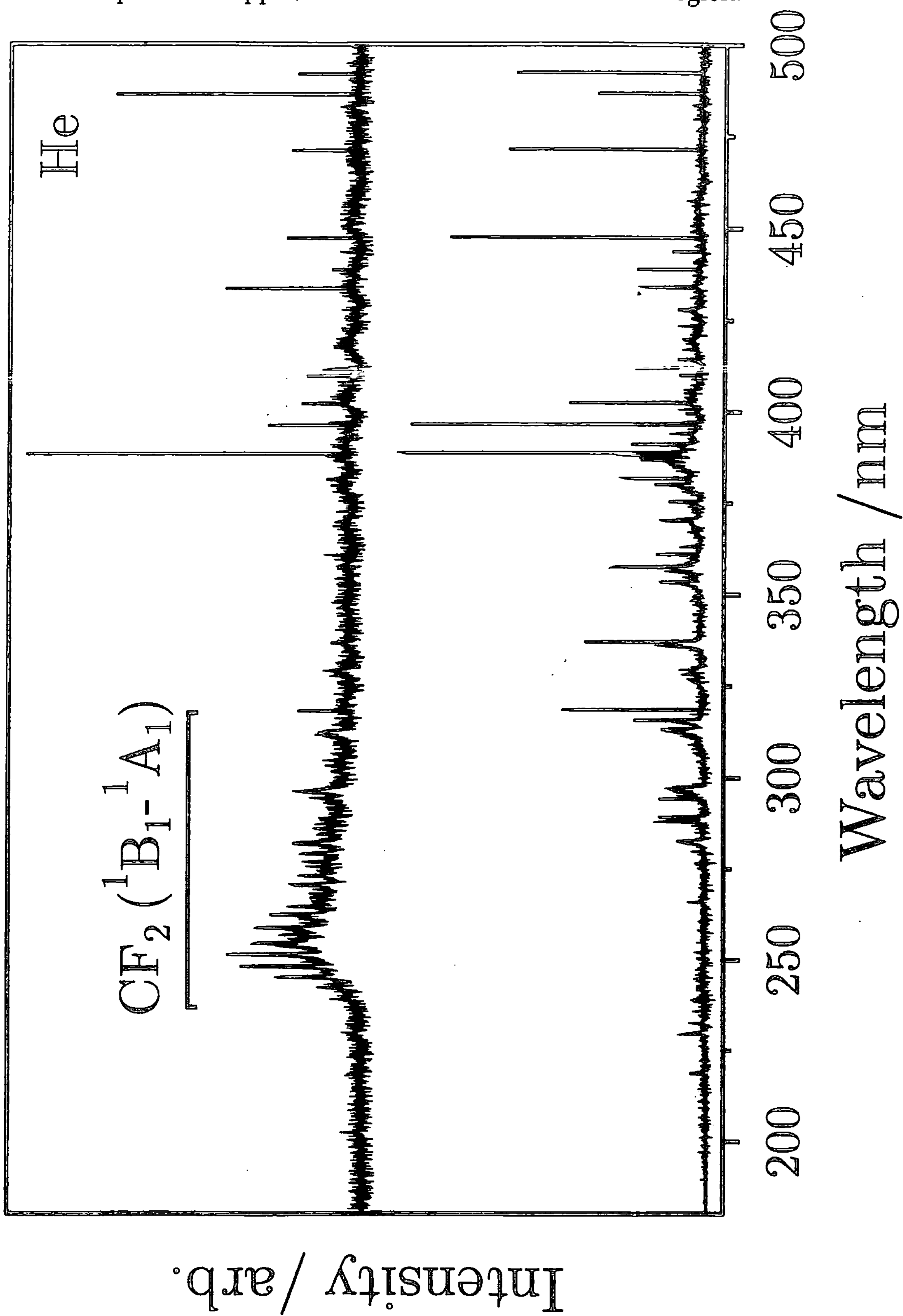

Figure 4.5

UV emission spectra of Ne glow discharge in the absence (lower) and presence (upper) of PTFE film in the 180-500 nm region.

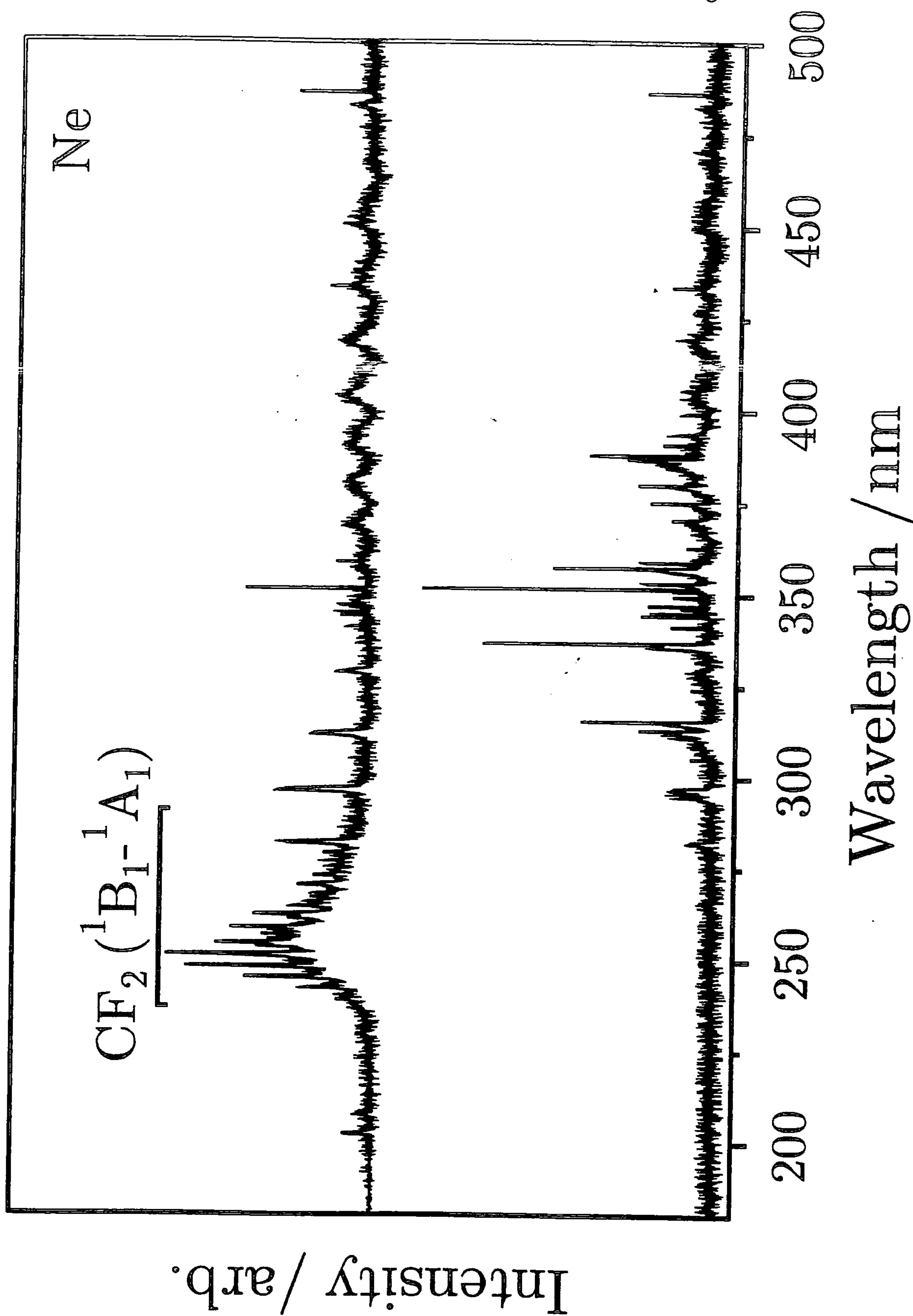

Figure 4.6

UV emission spectra of Ar glow discharge in the absence (lower) and presence (upper) of PTFE film in the 180-500 nm region.

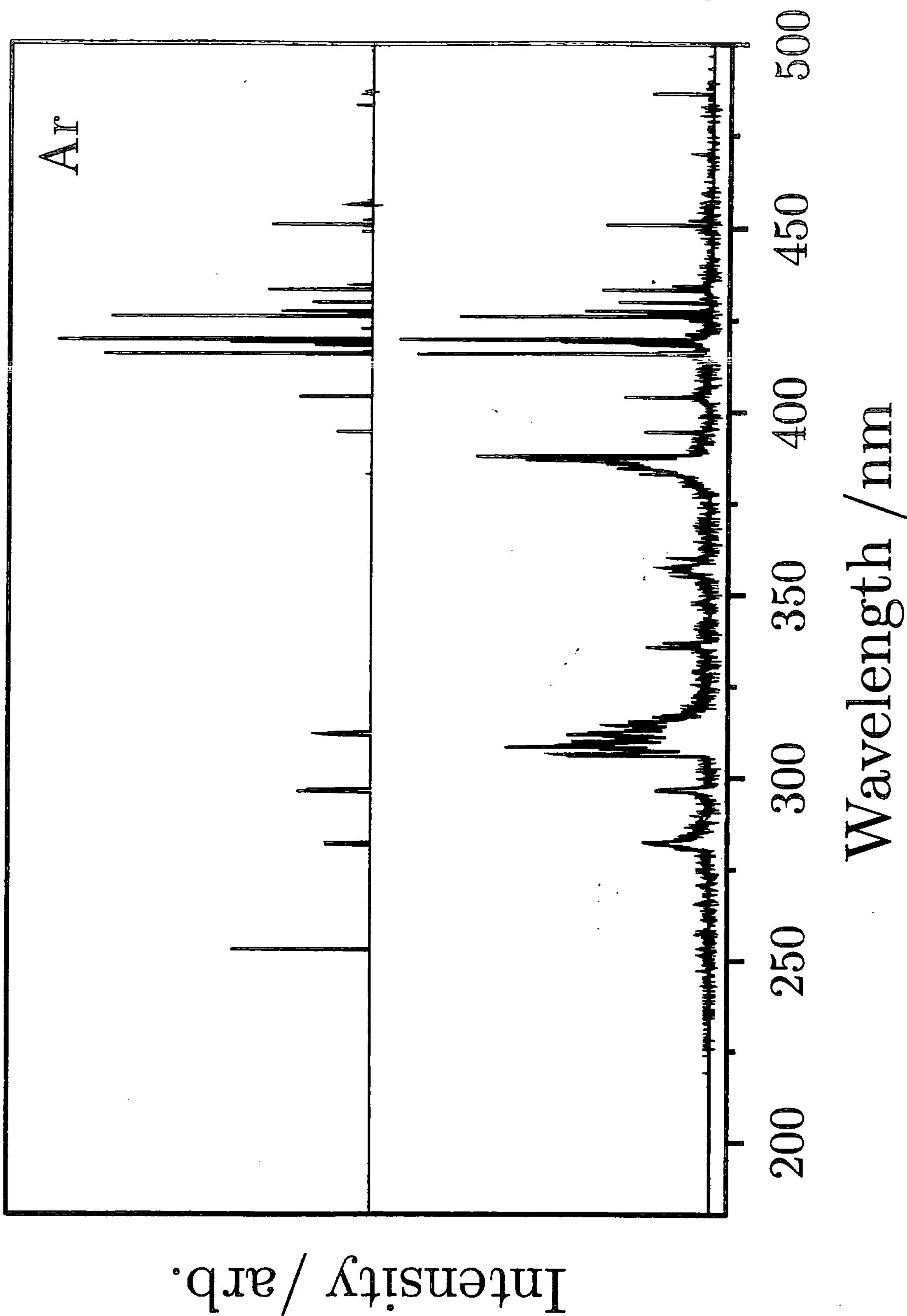

Figure 4.7

UV emission spectra of N_2 glow discharge in the absence (lower) and presence (upper) of PTFE film in the 180-500 nm region.

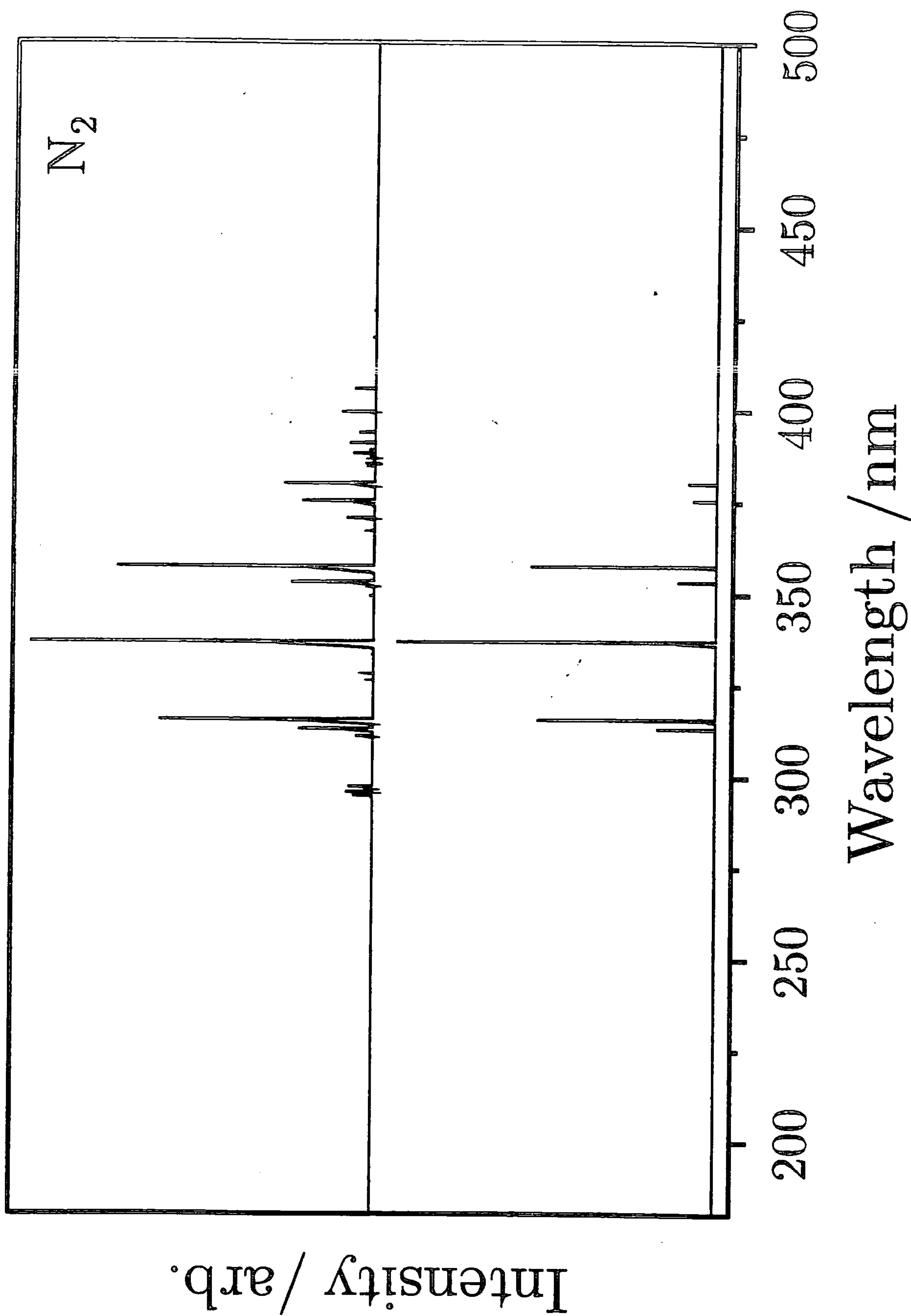

In the case of helium plasma treatment of PTFE, all peaks between 320 and 500 nm can be assigned to helium, figure 4.4. Forty-four lines in the CF_2 ($^1B_1$-$^1A_1$) band system are evident between 240 and 320 nm (many more than for neon) and only one CF band is evident at 202.3 nm ($B^2\Delta$-$X^2\Pi$ transition). Furthermore, fourteen of the lines which appeared in the pure helium glow discharge are absent during sputter deposition.

The UV emission peaks measured during neon glow discharge sputtering of PTFE spectrum can be assigned to neon, CF_2 or CF transitions, figure 4.5. All of the bands in the 280-500 nm range are characteristic of a clean neon plasma. The intense feature between 240 and 280 nm can be resolved into thirty lines of the CF_2 ($^1B_1$-$^1A_1$) band system. The lines at 229.6 and 223.2 nm are CF ($A^2\Sigma^+$-$X^2\Pi$) transitions, and those at 207.7 and 202.4 are CF ($B^2\Delta$-$X^2\Pi$) transitions. Twelve of the UV emission bands seen for the pure neon glow discharge were found to disappear during RF sputtering of PTFE.

Apart from one intense line at 253.3 nm which is difficult to precisely assign, all of the UV emission bands identified during argon plasma sputtering of PTFE originate from the argon glow discharge, figure 4.6. Three characteristic bands of the pure argon plasma at 388.0 nm, 357.4 nm and 336.9 nm were also absent during glow discharge sputtering of PTFE.

Most of the peaks observed during nitrogen glow discharge sputtering of PTFE can be assigned to those characteristic of pure nitrogen plasmas[70], figure 4.7. Additional bands are present at 394.0 nm, 370.8 nm, 297.6 nm, 296.1 nm and 295.7 nm, the last three of these fall in the CF_2 ($^1B_1$-$^1A_1$) region, although exact assignment is difficult. It is of interest to note that the overall absolute UV spectral intensity was greatest for the pure nitrogen glow discharge, this can be explained in terms of each nitrogen molecule effectively dissociating to form two excitable nitrogen atoms.

4.4 DISCUSSION

Decomposition of PTFE during glow discharge sputtering results mainly in the evolution of tetrafluoroethylene (C_2F_4). These species undergo plasma polymerization in the vicinity of the electromagnetic sputter field[11,13,71]. High deposition rates occur when a carrier gas (such as argon) is used during RF sputtering of PTFE[20], this behaviour may be attributed to greater momentum transfer (substrate etching) by the heavier argon species[72]. Modification of the PTFE substrate itself has been shown in the previous chapters to take place during exposure to inert gases, nitrogen, and hydrogen plasmas[73,74].

XPS analysis of the sputtered films has shown that the fluorine content drops on moving from helium to neon to argon glow discharges, this appears to be a direct manifestation of momentum transfer phenomena[23,72]. The $-CF_2-$ wagging and rocking vibrations in the infrared fingerprint region of PTFE are not evident in the plasma polymer spectra, this can be taken as being indicative of a highly crosslinked fluorocarbon network. Since the CF_2 ($^1B_1$-$^1A_1$) UV emission band system is evident for all the noble gas sputter plasma polymerization experiments, it is instructive to compare the number of lines present in the CF_2 ($^1B_1$-$^1A_1$) band system for each gas, although no conclusions can be made from the absolute line intensities because these will depend on the type of noble gas atom used. On moving from helium to neon to argon it is found that during glow discharge sputtering of PTFE there is a decrease in the number of lines contained in the CF_2 ($^1B_1$-$^1A_1$) band system, which can be attributed to absorption of the emitted CF_2 ($^1B_1$-$^1A_1$) band system lines by unsaturated fluorocarbon species, resulting in their effective absence. Overall, a direct correlation exists between the level of defluorination in the coating as measured by XPS, the FTIR absorbance strength of the carbon-rich/cross-linked/aromatic species, and the observed attenuation in the number of

lines contained in the CF_2 ($^1B_1$-$^1A_1$) band system due to photoabsorption by unsaturated fluorocarbon moieties. The nitrogen glow discharge UV emission results are anomalous due to the very intense lines of nitrogen itself, which effectively masked out any fluorocarbon features.

The stark contrast in deposition behaviour between hydrogen and helium carrier gas experiments is slightly puzzling at first glance. Since both gases are very light, yet no plasma polymer was generated in the case of hydrogen. There are two possible explanations for this paradox: either the sputter rate is very low for a hydrogen glow discharge; or the evolved species may not readily succumb to plasma polymerization but prefer to form stable by-products, e.g. HF and CH_4. Surface modification of PTFE by a hydrogen plasma was seen, in chapter two, to result in defluorination of the polymer substrate via HF elimination[70] (i.e. hydrogen atom exchange with the PTFE backbone[73]). Indeed, very low concentrations of carbon-containing moieties are evolved during the exposure of a fluoropolymer surface to a hydrogen glow discharge, whereas all noble gases (including helium) eject a variety of fluorocarbon species into the plasma phase[70].

Fluoropolymer films deposited from nitrogen glow discharge sputtering of PTFE appears to yield the highest F:C ratio. Since atomic nitrogen (atomic mass = 14) does not differ significantly from neon (atomic mass = 20), this anomalous behaviour by the nitrogen plasma can be attributed to either a greater density of sputtering moieties (dissociation of each nitrogen molecule in the glow discharge will generate two nitrogen atoms), or some type of chemical interaction between excited nitrogen species and the PTFE substrate (e.g. the formation of excimers).

The argon sputter polymerized film bears a strong resemblance to the argon plasma modified PTFE in the last chapter. It was shown that the ion component of the plasma was very important in the modification of PTFE surfaces. The correlation here with the argon sputter polymerized films suggests ion interactions are important in plasma polymerization and in fact

the influence of ion bombardment on the growth mechanism of plasma polymerized films has been apparent in several studies[75-77].

4.5 CONCLUSIONS

Non-equilibrium glow discharge treatment of polytetrafluoroethylene results in the simultaneous sputtering of the substrate accompanied by plasma polymerization of ablated fluorocarbon species. In the case of noble gases, the extent of fragmentation and defluorination can be accounted for in terms of a simple momentum transfer model; whereas additional chemical factors may be in play in the case of hydrogen and nitrogen glow discharges.

The nature of the carrier gas strongly influences the composition of the resulting fluoropolymer. For the inert gases a correlation is observed between the presence of CF_2 in the plasma and the amount of CF_2 incorproated into the final polymer film.

4.6 REFERENCES

1. Wagner, H. G.; Wolfrum, J. *Angew. Chem.* **1971**, *83*, 561.
2. Suhr, H. *Plasma Chem. Plasma Processing* **1983**, *3*, 1.
3. Suhr, H.; Schucher, U. *Synthesis* **1970**, 431.
4. Wells, R. K.; Drummond, I. W.; Robinson, K. S.; Street, F. J.; Badyal, J. P. S. *J. Chem. Soc., Chem. Commun.* **1993**, *6*, 549.
5. Egitto, F. D.; Vukanovic, V.; Taylor, G. N. In *Plasma Deposition, Treatment, and Etching of Polymers* ; d'Agostino, R., Ed.; Academic; San Diego, 1990; chapter 5.
6. Biederman, H.; Osada, Y. *Adv. Polym. Sci.* **1990**, *95*, 59.
7. Yasuda, H. *Plasma Polymerization*; Academic; London, 1985.
8. Pratt, I. H.; Lausman, T. C. *Thin Solid Films* **1972**, *10*, 151.
9. Martinu, L.; Biederman, H. *Vacuum* **1986**, *36*, 477.
10. Sugimoto, I.; Miyake, S. *J. Appl. Phys.* **1991**, *70*, 2618.
11. Morrison, D. T.; Robertson, T. *Thin Solid Films* **1973**, *15*, 87.
12. Jackson, N. F.; Harrop, P. J. Br. Patent 1226946, 1971.
13. Mathias, E.; Muller, C. H. *J. Phys. Chem.* **1967**, *71*, 2673.
14. Tibbitt, J. M.; Shen, M.; Bell, A. T. *Thin Solid Films* **1975**, *29*, L43.
15. Schreiber, H. U.; Froschle, E. *J. Electrochem. Soc.* **1976**, *123*, 30.
16. Hickernall, F. S. *J. Vac. Sci. Technol.* **1976**, *12*, 879.
17. Fraser, D. B. *Thin Solid Films* **1972**, *13*, 407.
18. Maple, T. G.; Buchanen, R. A. *J. Vac. Sci. Technol.* **1973**, *10*, 616.
19. Mei, L.; Greene, J. E. *J. Vac. Sci. Technol.* **1975**, *11*, 149.
20. Holland, L.; Biederman, H.; Ojha, S. M. *Thin Solid Films* **1976**, *35*, L19.
21. Biederman, H.; Osada, Y. *Thin Solid Films* **1977**, *41*, 329.
22. Marechal, N.; Pauleau, Y. *J. Vac. Sci. Technol.* **1992**, *A10*, 447.
23. Yamada, Y.; Kurobe, T. *Jpn. J. Appl. Phys.* **1993**, *32*, 5090.
24. Harrop, R.; Harrop, P. J. *Thin Solid Films* **1969**, *3*, 109.

25. d'Agostino, R.; Capezzuto, P.; Bruno, G.; Cramarossa, F. *Pure Appl. Chem.* **1985,** *57,* 1287.
26. Yasuda, H. K.; Yeh, H. S.; Fusselman, S. *Pure Appl. Chem.* **1990,** *62,* 1689.
27. O'Keefe, M. J.; Rigsbee, J. M. *J. Appl. Polym. Sci.* **1994,** *53,* 1631.
28. Sharma, A. K.; Yasuda, H. *J. Appl. Polym. Sci.* **1989,** *38,* 741.
29. Clark, D. T.; Feast, W. J.; Ritchie, I.; Musgrave, W. K. R.; Modena, M.; Ragazzini, M. *J. Polym. Sci., Polym. Chem. Ed.* **1974,** *1* , 1049.
30. Wagner, C. D.; Riggs, W. M.; Davis, L. E.; Moulder, J. F.; Muilenberg, G. E. *Handbook of X-Ray Photoelectron Spectroscopy;* Perkin-Elmer Corporation, 1978; p 13.
31. Starkweather, H. W.; Ferguson R. C.; Chane D. B.; Minor J. M. *Macromolecules* **1985** , *18,* 1684.
32. Haque, Y.; Ratner, B.D. *J. Polym. Sci., Polym. Phys. Ed.* **1988,** *27,* 3965.
33. Giegengack, H.; Hinze, D. *Phys. Statis Solidi* **1971,** *A8,* 513.
34. Bellamy, L. J. *The Infra-Red Spectra of Complex Molecules Vol. 1;* Wiley: New York, 1975.
35. Buzzard, P. D.; Soong, D. S.; Bell, A. T. *J. Appl. Polym. Sci.* **1982,** *27,* 3965.
36. Sugimoto, I. *Macromolecules* **1991,** *24,* 1480.
37. Inagaki, N.; Kibayashi, N.; Matsushima, M. *J. Membrane Sci.* **1988,** *38,* 85.
38. Silverstein, R. M.; Bassler, G. C.; Morrill, T. C. *Spectrometric Identification of Organic Compounds* ; Wiley: New York, 1981.
39. Dias, A. J.; McCarthy, T. J. *Macromolecules* **1985,** *18,* 1826.
40. Studniarz, S. A. In *Ion-Molecule Reactions Vol. 2;* Franklin, J. L., Ed.; Plenum; New York, 1972; pp 647- 671.
41. Vasile, M. J.; Smolinsky, G. *J. Phys. Chem.* **1977,** *81,* 2605.
42. Smolinsky, G.; Vasile, M. J. *Eur. Polym. J.* **1979,** *15,* 87.

43. Miller, T. A. In *Annual Review of Physical Chemistry Vol. 27*; Rabinovich, B. S.; Ed.; Annual Review; California, 1976; pp 127-152.

44. Millard, M. M.; Kay, E. *J. Electrochem. Soc.* **1982**, *129*, 160.

45. Powell, F. X.; Lide, D. R. *J. Chem. Phys.* **1966**, *45*, 1067.

46. Bass, A. M.; Mann, D. E. *J. Chem. Phys.* **1962**, *36*, 3501.

47. Dyke, J. M.; Golob, L.; Johnathan, N.; Morris, A.; Okuda, M. *J. Chem. Soc., Faraday Trans. 2* **1974**, *70*, 1828.

48. King, D. S.; Schenck, P. K.; Stephenson, J. C. *J. Mol. Spec.* **1979**, *78*, 1.

49. Smith, O. E.; Jacox, M. E.; Milligan, D. E. *J. Mol. Spec.* **1976**, *60*, 381.

50. Kay, E.; Coburn, J. W.; Kruppa, G. *LeVide* **1976**, *183*, 89.

51. Kay, E.; Dilks, A.; Coburn, J. In *Topics in Current Chemistry*; Veprek, S.; Venugopalan, M., Eds.; Springer Verlag; Berlin, 1980; pp 1-54.

52. Dilks, A.; Kay, E. In *Plasma Polymerization* ; Shen, M.; Bell, A. T., Eds.; ACS Symposium Series; American Chemical Society: Washington, D C, 1979; pp 195-218.

53. Koda, S. *Chem. Phys. Lett.* **1978**, *55*, 353.

54. Venkateswarlu, P. *Phys. Rev.* **1950**, *77*, 676.

55. Porter, T. L.; Mann, D. E.; Acquista, N. *J. Mol. Spectros.* **1965**, *16*, 228.

56. Pearse, R. W. B.; Gayson, A. G. *The Identification of Molecular Spectra*; Chapman and Hall: London, 1976.

57. Andrews, E. B.; Barrow, R. F. *Proc. Phys. Soc., London* **1951**, *A64*, 481.

58. Mathews, C. W. *Can. J. Phys.* **1967**, *45*, 2355.

59. Marsigny, L.; Ferran, J.; Lebreton, J.; Legrange, R. *C. R. Acad. Sci., Paris, Ser. C* **1968**, *266*, 9 and 507.

60. Gilbert, R.; Thoret, A. *J. Phys. Chem.* **1976**, *80*, 1017.

61. Trung, Q.; Durocher, G.; Sauvageau, P.; Dorfy, C. *Chem. Phys. Lett.* **1977**, *47*, 404.

62. Suto, M.; Washida, N. *J. Chem. Phys.* **1983**, *78*, 1007.

63. Suto, M.; Washida, N. *J. Chem. Phys.* **1983**, *78*, 1012.

64. Suto, M.; Washida, N.; Akimoto, H.; Nakamura, M. *J. Chem. Phys.* **1983**, *78*, 1019.

65. Larrieu, C.; Chaillet, M.; Dargelos, A. *J. Chem. Phys.* **1992**, *96*, 3732.

66. Harshbarger, W. R.; Porter, R. A.; Miller, T. A.; Norton, P. *Appl. Spectros.* **1977**, *31*, 201.

67. Mogab, C. J.; Adams, A. C.; Flamm, D. L. *J. Appl. Phys.* **1978**, *49*, 3796.

68. Frieser, R. G.; Nogay, J. *Appl. Spec.* **1980**, *34*, 31.

69. Donnelly, V. M.; Flamm, D. L. *Abstract 123*, The Electrochemical Society Extended Abstracts, St. Louis, 1980; p 323.

70. Gallaher, T. W.; De Vore, T. C.; Carter, R. O.; Anderson, C. *Appl. Spectrosc.* **1980**, *34*, 408.

71. Coburn, J. W.; Eckstein, E. W.; Kay, E. *J. Vac. Sci. Technol.* **1975**, *12*, 151.

72. Thornton J. A. In *Deposition Technologies for Films and Coatings*, Bunshah, R. F., Ed.; Noyes: New Jersey, 1982, chapter 2.

73. Clark, D. T.; Hutton, D. R. *J. Polym. Sci., Polym. Chem. Ed.* **1987**, *25*, 2643.

74. Yasuda, H.; Marsh, H. C.; Brandt, S.; Reilley, C. N. *J. Polym. Sci., Polym. Chem. Ed.* **1977**, *15*, 991.

75. d'Agostino. R.; Cramarossa, F.; Fracassi, F.; Desimoni, E.; Sabbatini, L.; Zambonin, P. G.; Caporiccio, G. *Thin Solid Films* **1986**, *143*, 163.

76. d'Agostino. R.; Cramarossa, F.; Illuzzi, F. *J. Appl. Phys.* **1987**, *61*, 2754.

77. d'Agostino. R.; Favia, P.; Fracassi, F.; Illuzzi, F. *J. Polym. Sci. Polym. Chem Ed.* **1990**, *28*, 3387.

CHAPTER 5

PULSED PLASMA POLYMERIZATION OF MALEIC ANHYDRIDE

5.1 INTRODUCTION

The method of plasma polymerization described in the last chapter is relatively unusual for thin film synthesis. Normally, instead of sputtering a solid substrate into the gas phase, a monomer vapour is introduced into the plasma. During polymerization, significant fragmentation of the molecule occurs, leading to a highly crosslinked material containing few of the functionalities that the monomer possessed. In this chapter control of plasma excitation is used to dictate the polymerization pathway and composition of resulting polymer.

Maleic anhydride is a widely used organic reagent which contains two types of reactive site: the anhydride functionality and the >C=C< double bond, structure 5.1.

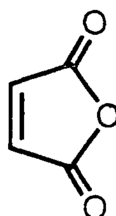

Structure 5.1

This molecule can participate in a variety of reactions including: the Diels-Alder reaction[1] (i.e. a [4 +2] cycloaddition), attack on an allylic hydrogen atoms to form asymmetric carbon centres[2], photochemical reactions[3-5], and polymerization. Conventional polymerization[6], copolymerization[7-14], and graft polymerization[15] of maleic anhydride have been extensively studied. In general, maleic anhydride functionalized polymers are sought for their improved interfacial adhesion[16], polymer/polymer compatability[17], and their ability to undergo subsequent surface reactions[18]. Homopolymerization of the monomer can be initiated by a variety of means which include γ-radiation[19], UV radiation[20], free radicals[21], ionic catalysts[22], or the application of high pressure[23]. In addition, maleic

anhydride can participate in condensation polymerization to form unsaturated polyesters[24]. Copolymerization of maleic anhydride with a variety of other monomers can lead to random addition[7-10], alternating addition[11-14], and graft copolymers[25-30].

In the this study, the homopolymerization of maleic anhydride using an RF glow discharge is investigated using both continuous wave (CW) and pulsed excitation. This solventless method can be used to deposit polymeric layers with a whole spectrum of chemical and physical properties depending upon the specific electrical discharge parameters deployed during plasma polymerization (e.g. input power, feed gas ratio, monomer pressure, substrate temperature, and substrate position). The number and lifetimes of the various reactive species contained within the plasma (ions, radicals, electrons, metastables and photons) influence which reaction pathways are pursued during glow discharge polymerization. Hence, there is considerable scope for structural and compositional tailoring of growing polymeric films. For instance, average input power is recognised as being a critical parameter which can be varied by either altering the peak power in a continuous wave (CW) electrical discharge or alternatively by pulsing the applied RF voltage. The latter technique has been mostly overlooked in the past, yet it offers scope for the optimization of reactive intermediates as well as access to conventional polymerization reaction pathways during the duty cycle off-period.

5.1.1 Pulsed Plasma Polymerization

An important aspect of CW plasma polymerization is the extensive fragmentation of the monomer that occurs. It is this feature that allows saturated molecules to be polymerized and leads to plasma deposited coatings differing significantly from conventional polymers. Although these new materials are extremely useful[31] greater control is often required

over their resultant chemical structure. Reduction of the RF power can reduce the extent of gas-phase fragmentation and generate a closer similarity between the plasma and conventionally polymerized monomer. However, this has limitations as a minimum absorbed power is required to ignite and maintain the plasma and uniform films are generally obtained only over relatively restricted power regimes for a given monomer under specific flow conditions[32]. Other approaches to controlling film composition include reduced substrate temperatures[33] and variation of substrate position, for example location downstream of the plasma[34].

Pulsed power is of interest because it enables control over the rate at which reactive species (radicals) are generated and it allows time for these species to react without additional fragmentation during the time that the power is off[35]. In the event that there are species present that can polymerize by a chain mechanism (e.g. vinyl bonds) it would be expected that pulsed power would lead to a greater contribution of this mechanism and result in a plasma polymer that more closely resembles the parent monomer and its conventional polymer[35]. A more complete understanding of the pulsed plasma polymerization process should introduce a new dimension of controllability over the final polymeric film.

5.2 EXPERIMENTAL

At room temperature maleic anhydride has a vapour pressure of approximately 0.2 Torr[36]. Briquettes of maleic anhydride (Aldrich, 99% purity) were ground into a fine powder and loaded into a monomer tube. Plasma polymerization experiments were carried out in the same reactor as used in chapter 2 (section 2.2) except that the gas inlet was replaced by a monomer tube containing maleic anhydride. A glass substrate was located in the centre of the coils. For the pulsed power experiments, the RF supply

was triggered by a signal generator, and a cathode ray oscilloscope was used to monitor the pulse width and amplitude. The pulse rise and fall time was limited by the response of the RF generator to 0.5 μs. The peak power (P_p) delivered to the glow discharge spanned 5-90 W. Pulse on-times (t_{on}) and off-times (t_{off}) could be varied between 20-800 μs and 20-1200 μs respectively. The average power $\langle P \rangle$ delivered to the system during pulsing was calculated using the following expression[37]:

$$\langle P \rangle = P_p \times \{t_{on}/(t_{on}+t_{off})\}$$

where $t_{on}/(t_{on}+t_{off})$ is defined as the duty cycle.

After cleaning using detergent and an air plasma (30 min at 50 W) the reactor was evacuated back down to its base pressure. Subsequently the monomer vapour was introduced into the reaction chamber at a pressure of approximately 0.2 Torr (which is the vapour pressure of maleic anhydride at room temperature), and at a flow rate of approximately 1.59×10^{-9} kg s^{-1}. Then the plasma was ignited and allowed to run for 10 min to provide sufficient plasma polymer for XPS analysis, or 30 min to generate films thick enough for infrared characterization. Upon completion of deposition, the RF generator was switched off, and the system flushed with monomer for 5 min prior to venting up to atmospheric pressure. Each plasma polymer layer was characterized immediately after electrical discharge treatment by X-ray photoelectron spectroscopy or infrared analysis.

XPS surface analysis was performed as detailed in section 2.2.1. Instrumentally determined sensitivity factors for unit stoichiometry were taken as being C(1s) : O(1s) equals 1.00 : 0.55. Uniform plasma polymer coverage was determined by the absence of any Si(2p) XPS signal from the underlying glass substrate.

A FTIR Mattson Polaris instrument was used for transmission infrared analysis of maleic anhydride precursor mixed with potassium bromide, as well as the respective continuous wave and pulsed plasma polymer layers deposited onto pressed potassium bromide discs. Typically, 100 scans were acquired at a resolution of 4 cm^{-1}.

5.3 RESULTS

5.3.1 Continuous Wave Plasma Polymerization

The C(1s) XPS envelope obtained from a low power (5 W) continuous wave plasma polymerization experiment can be curve fitted with five Mg $K\alpha_{1,2}$ components having equal FWHM corresponding to 55% $\underline{C}_xH_y$ (285.0 eV)[38], 10% >$\underline{C}$-C(O)=O (285.7 eV)[38], 14% >$\underline{C}$-O (286.6 eV)[38], 11% >$\underline{C}$=O / O-$\underline{C}$-O (287.9 eV)[38], and 10% -C(O)=O (289.4 eV)[39] environments, figure 5.1. Hydrocarbon/cross-linked carbon, $\underline{C}_xH_y$, is found to be the predominant carbon centre in the C(1s) envelope, with smaller amounts of oxygenated functionalities. This is significantly different from the equal contributions expected from just the >$\underline{C}$-C(O)=O and -$\underline{C}$(O)=O environments if the monomer had undergone conventional polymerization.

Table 5.1 summarises the infrared assignments for maleic anhydride. A comparison of the infrared spectra for the maleic anhydride precursor, and the 5 W CW plasma polymer shows that the sharp spectral features characteristic of the monomer are broadened (and in some cases lost), figure 5.2. This can be attributed to a high level of cross-linking[31]. Certain bands are still discernible in the CW plasma polymer: 2995 cm^{-1} (C-H stretch), 1860 cm^{-1} (asymmetric C=O stretch), 1780 cm^{-1} (symmetric C=O stretch), 1647 cm^{-1} (C=C stretch), 1240 cm^{-1} (C-O stretch), 1053 cm^{-1} (C-H deformation), and 920 cm^{-1} (C-H out of plane bending).

Figure 5.1

Typical C(1s) XPS peak fit for a 5 W CW maleic anhydride plasma polymer.

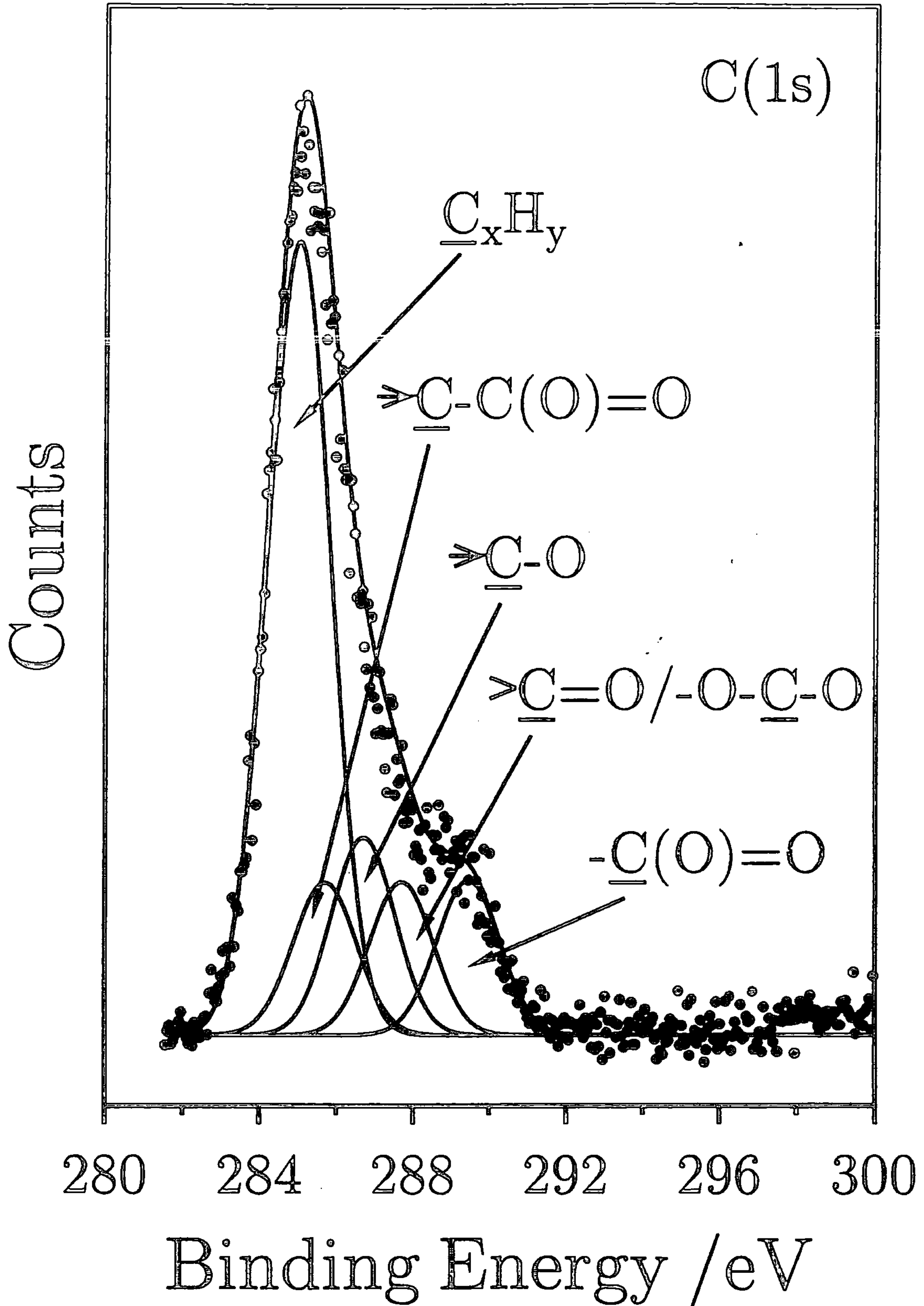

Figure 5.2

Infrared spectra of: (a) maleic anhydride monomer: (b) 5 W CW plasma polymer; and (c) pulsed plasma polymer (on-time = 20 μs, off-time = 1200 μs, and peak power = 5 W).

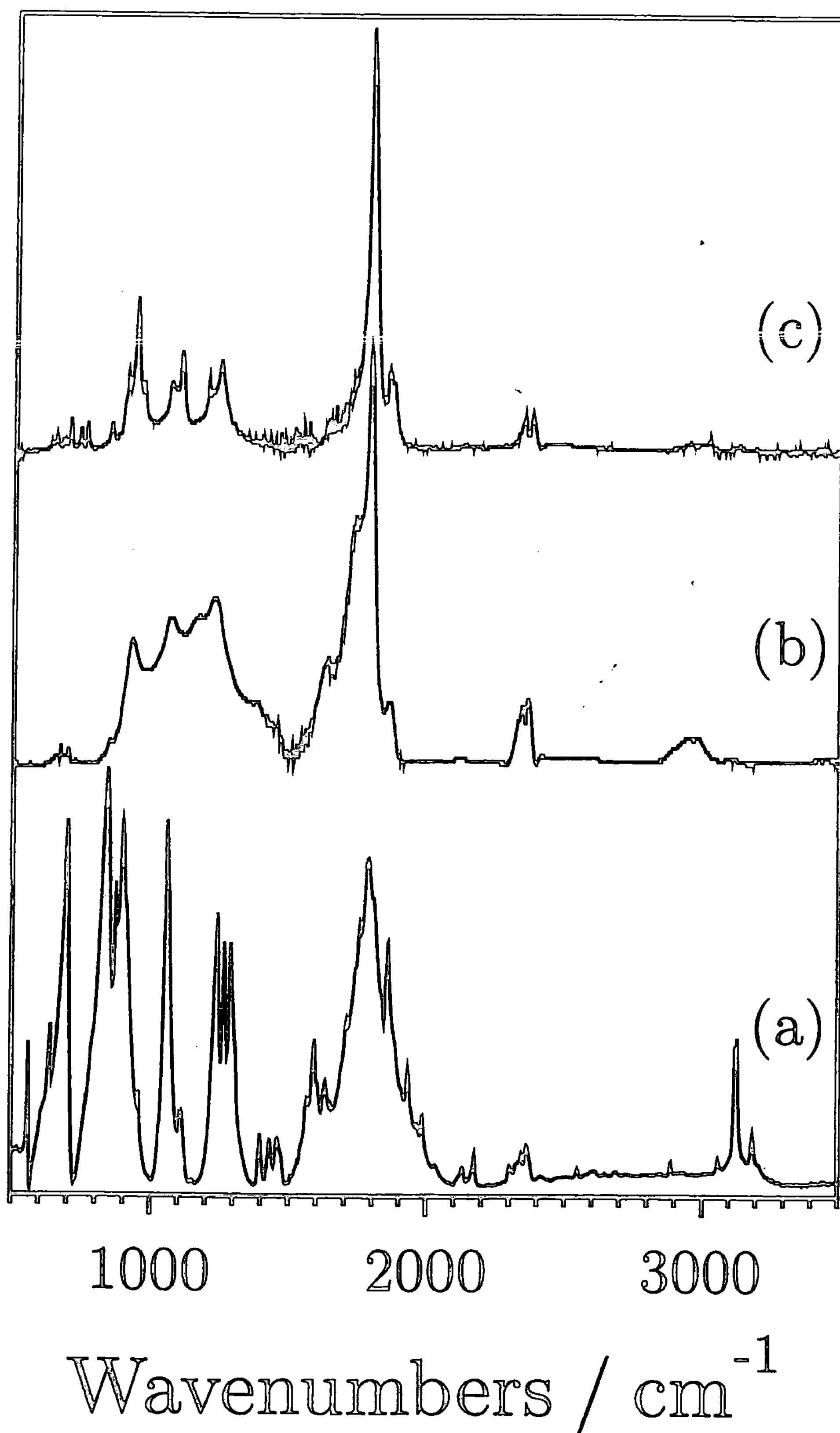

Table 5.1

Assignment of infrared absorbance bands for maleic anhydride monomer[40].

Wave number / cm^{-1}	Assignment
3190	ν(C-H) (adjacent to CH_2)
3131	ν(C-H) (adjacent to CH)
1858	νa(C=O)
1782	νs(C=O)
1593	ν(C=C)
1280	ν(C-O)
1242	δ(C-H)
1059	δ(C-H)
897	ν(C-C)
839	δ(C-H)
698	δ(maleic anhydride ring)
564	δ(C=O)

ν = stretching, δ = deformation, a = asymmetric, s = symmetric.

5.3.2 Pulsed Plasma Polymerization

The variation in anhydride group retention was investigated as a function of duty cycle parameters (on-time, off-time), and peak power. A fixed duty cycle off-period of 1200 μs, and peak power of 5 W produced a significant enhancement of the -$\underline{C}$(O)=O anhydride group C(1s) component at 289.4 eV at the expense of cross-linked carbon/hydrocarbon ($\underline{C}_xH_y$) species with decreasing on-times down to 20 μs, beyond which incomplete coverage of the glass substrate was observed, figure 5.3(a). Curve fitting of the C(1s) envelope also shows that there is an insignificant variation in the amount of >$\underline{C}$-O groups, whilst the >$\underline{C}$=O / O-$\underline{C}$-O concentration is reduced at shorter

on-periods, figure 5.3(b). This is accompanied by an increase in the total oxygen : carbon ratio, figure 5.3(c).

Similarly, for a constant duty cycle on-time (20 μs) and peak power (5 W), the -$\underline{C}$(O)=O anhydride group concentration rises with longer off-times at the expense of $\underline{C}_xH_y$ and >$\underline{C}$=O / O-$\underline{C}$-O centres together with a parallel increase in oxygen to carbon ratio, figures 5.4 (a) to (c).

It can be concluded that anhydride functionality incorporation is favoured by short on-times and long off-times. In both cases, this amounts to a lower average power input. Therefore a further study was undertaken in which the on- and off-times were kept fixed whilst the peak power was varied, figures 5.5 (a) to (c). The -$\underline{C}$(O)=O anhydride group feature at 289.4 eV in the C(1s) spectrum disappears at higher peak powers. This suggests that retention of the anhydride functionality also depends on the average power as well as the duty cycle parameters (t_{on} and t_{off}).

Infrared analysis of the pulsed plasma polymer layers unveils a closer resemblance to the maleic anhydride monomer absorption spectrum compared to the CW plasma polymer, figure 5.2. Bands in the 1250-900 cm^{-1} region are sharper indicating less cross-linking. The >C=C< stretch seen at 1647 cm^{-1} for the CW plasma polymer is absent. Hydrolysis of the anhydride functionality by air can be ruled out in the plasma polymer films because of the lack of any infrared absorbance due to C=O acid stretching[40] at 1708 cm^{-1}.

Figure 5.3 (a)

C(1s) XP spectra of pulsed plasma polymerization experiments with variable on-time (peak power = 5 W, and off-time = 1200 μs).

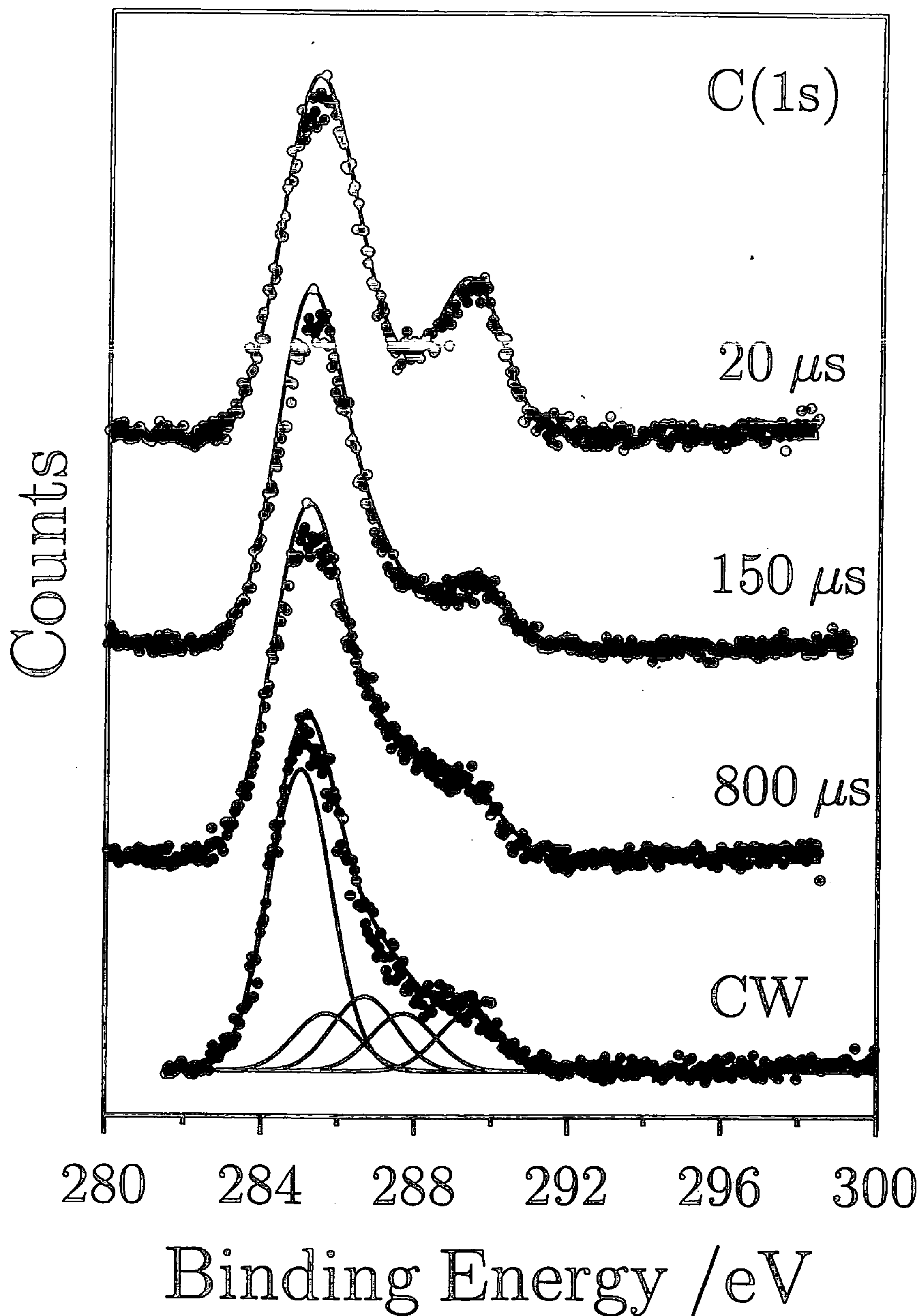

Figure 5.3 (b)

Variation of C(1s) functionalities for pulsed plasma polymerization experiments with variable on-time

(peak power = 5 W, and off-time = 1200 μs).

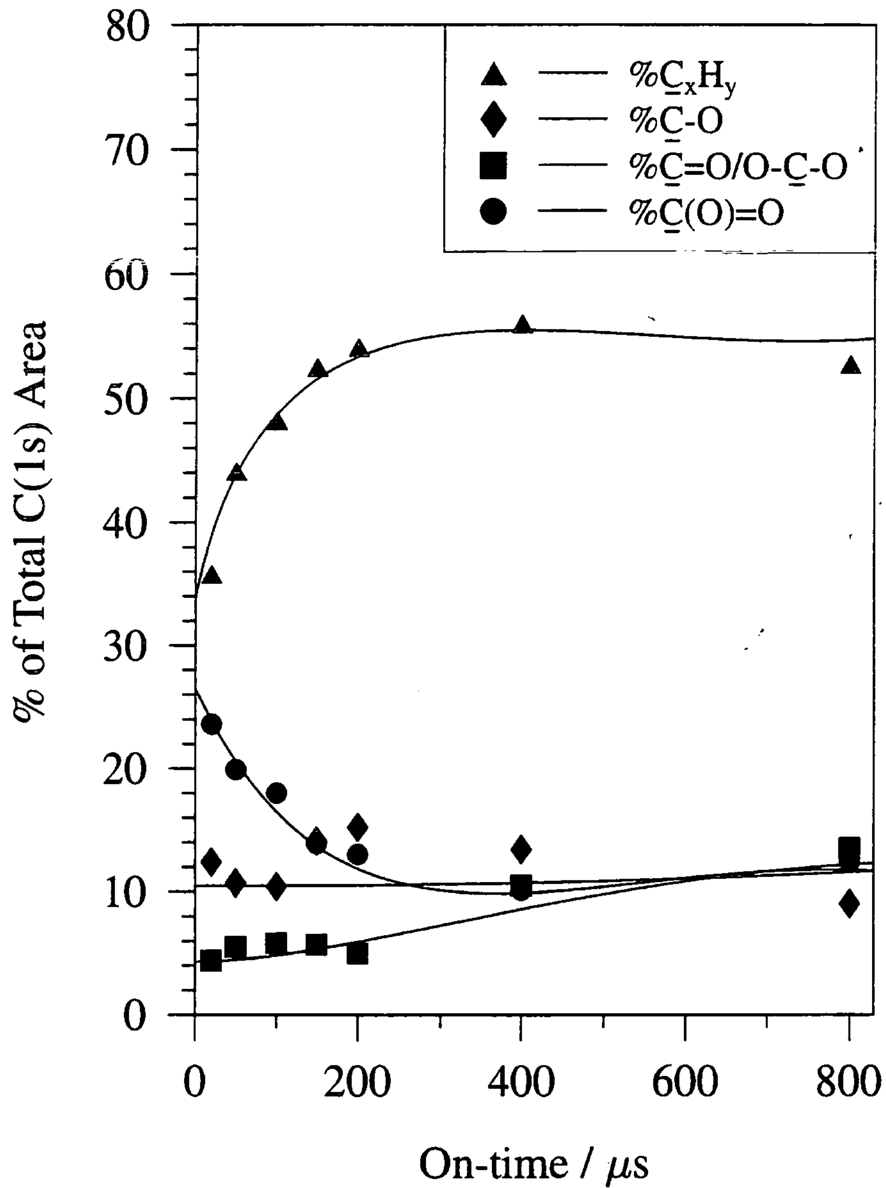

Figure 5.3 (c)

Variation of oxygen to carbon ratio for pulsed plasma polymerization experiments with variable on-time

(peak power = 5 W, and off-time = 1200 μs).

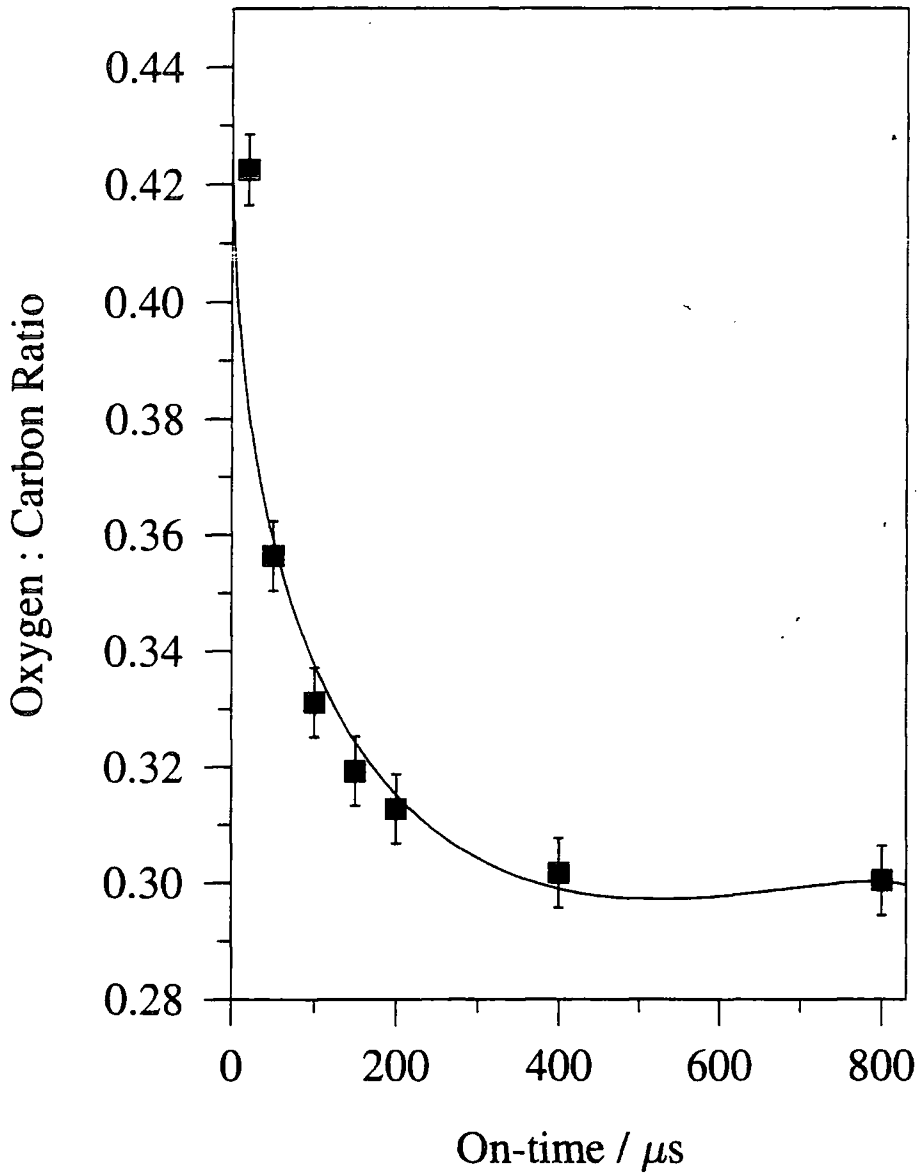

Figure 5.4 (a)

C(1s) XP spectra of pulsed plasma polymerization experiments with variable off-time (peak power = 5 W, and on-time = 20 μs).

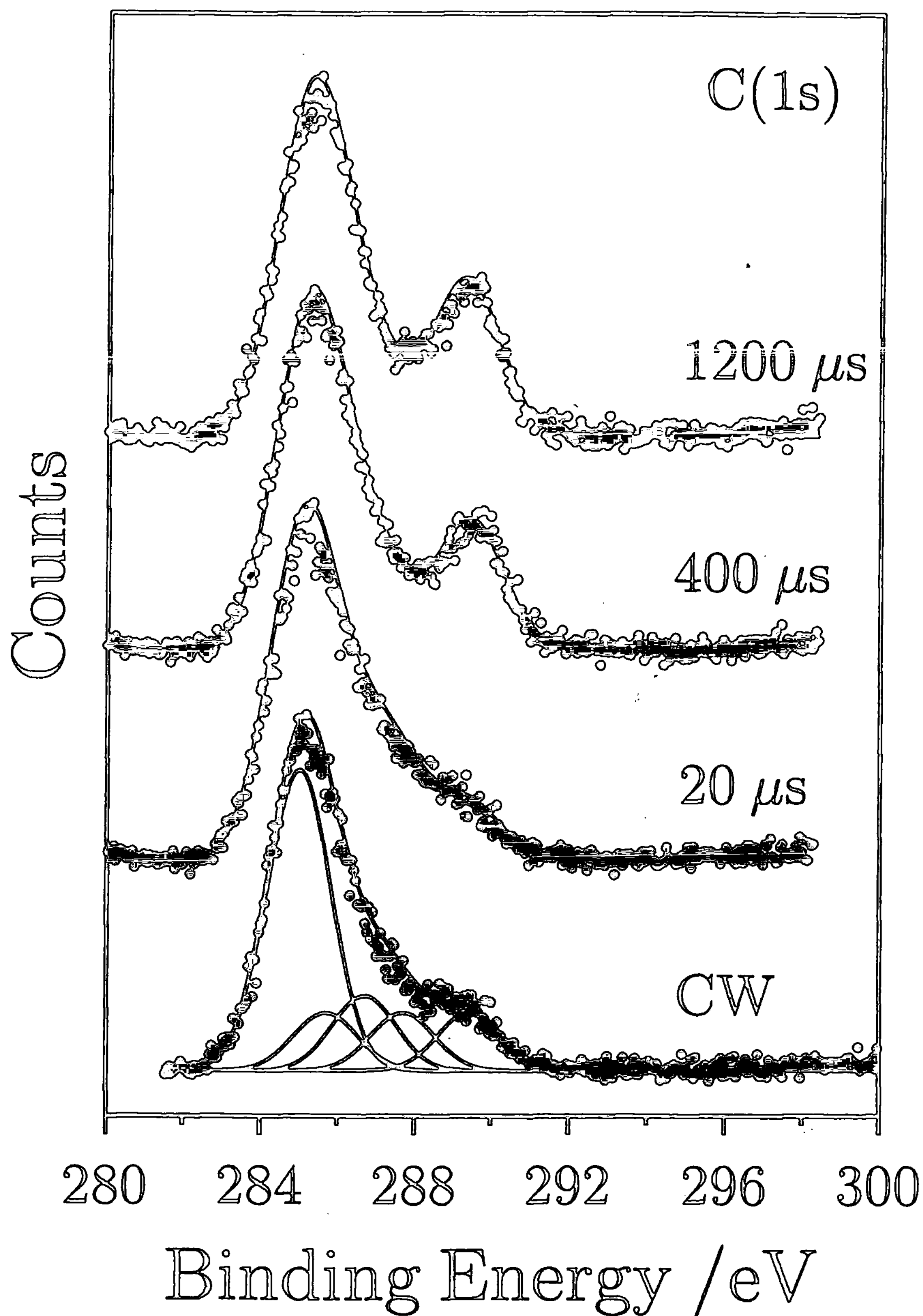

Figure 5.4 (b)

Variation of C(1s) functionalities for pulsed plasma polymerization experiments with variable off-time (peak power = 5 W, and on-time = 20 μs).

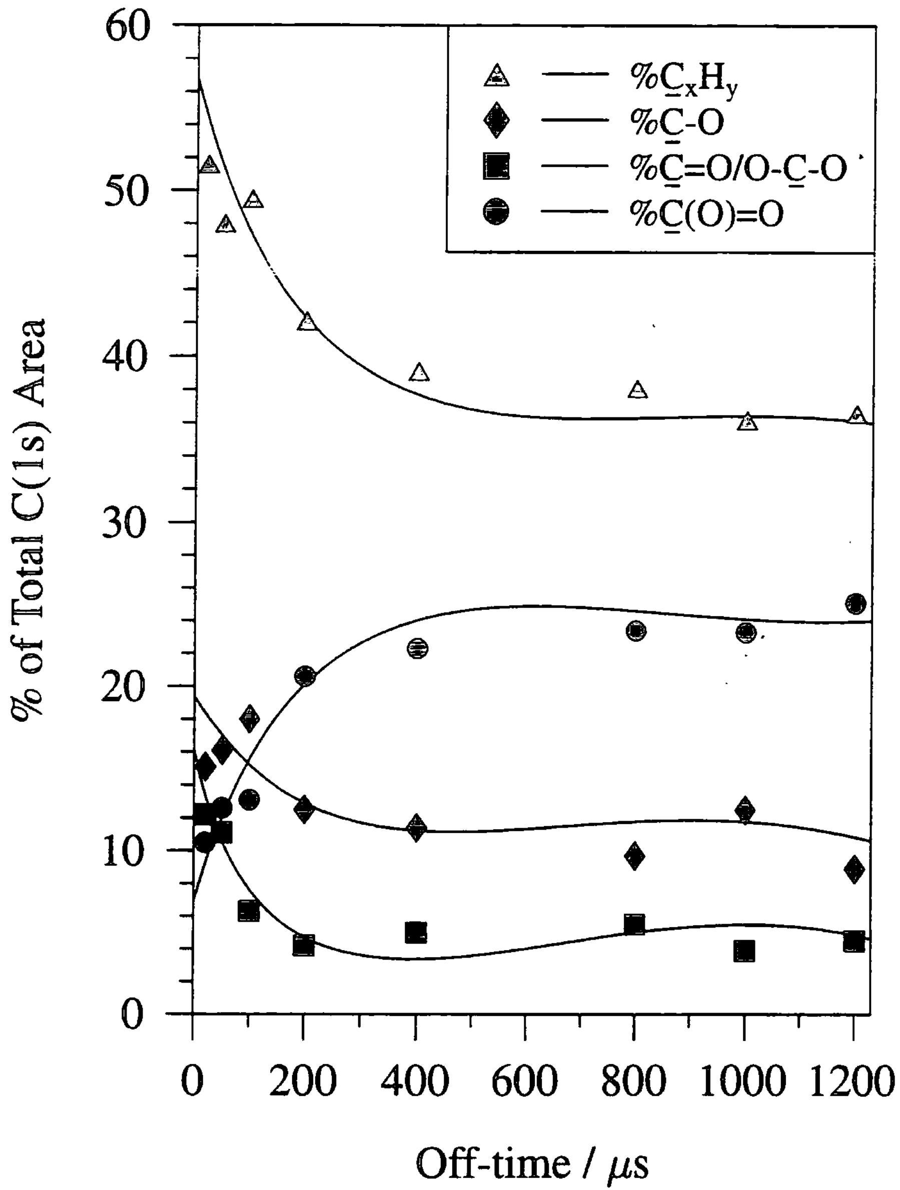

Figure 5.4 (c)

Variation of oxygen to carbon ratio for pulsed plasma polymerization experiments with variable off-time (peak power = 5 W, and on-time = 20 μs).

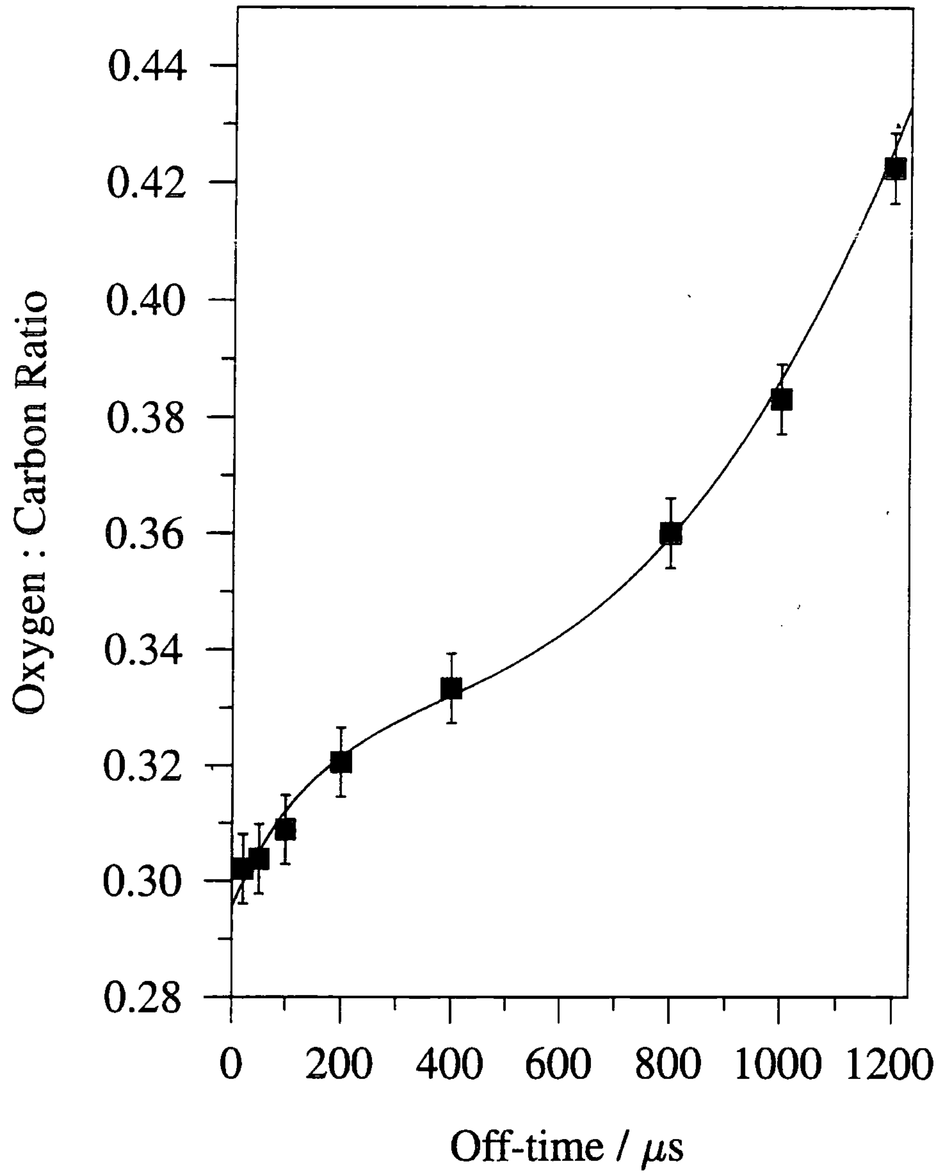

Figure 5.5 (a)

C(1s) XP spectra of pulsed plasma polymerization experiments with variable peak power (off-time = 1200 μs, and on-time = 20 μs).

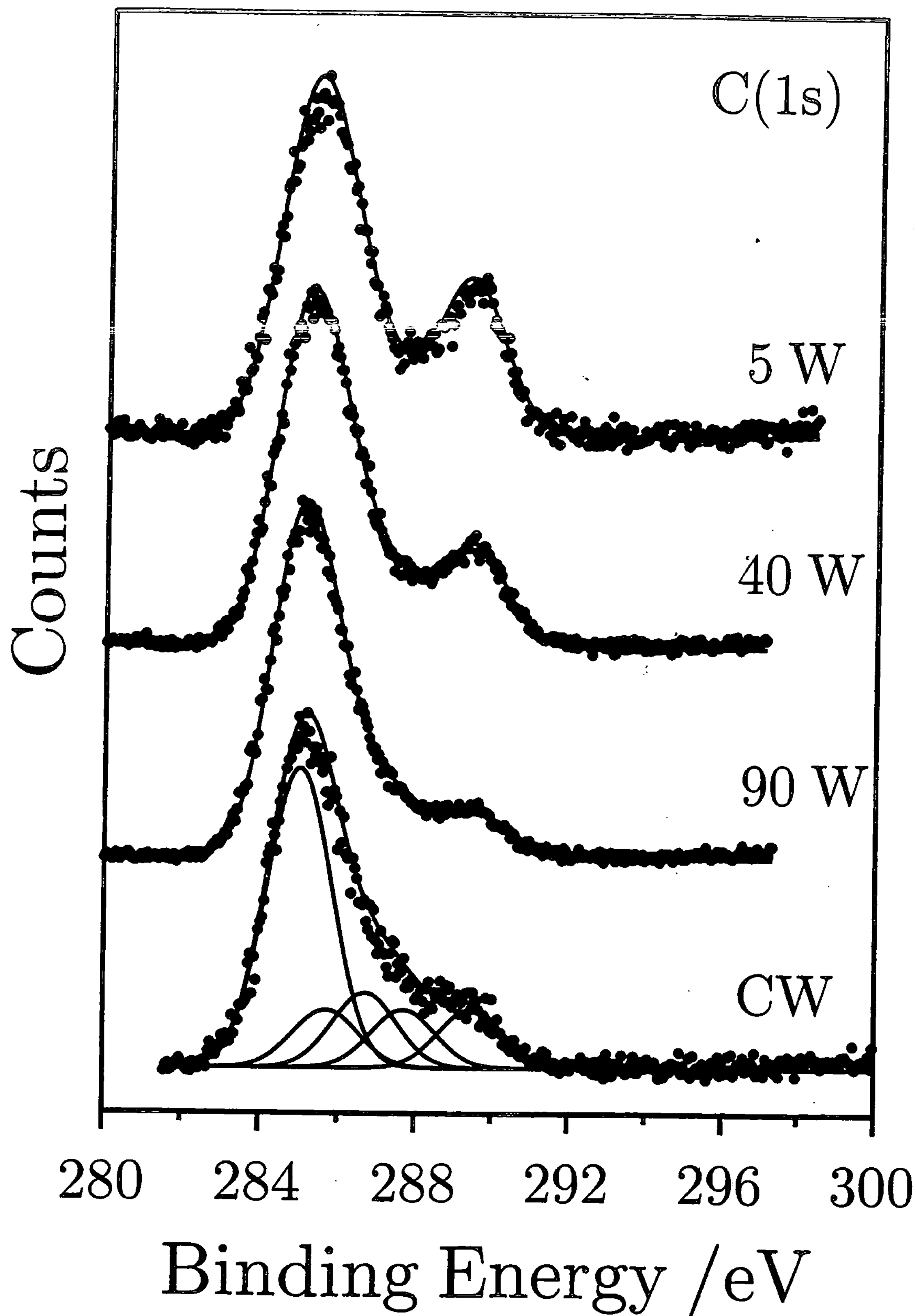

Figure 5.5 (b)

Variation of C(1s) functionalities for pulsed plasma polymerization experiments with variable peak power

(off-time = 1200 μs, and on-time = 20 μs).

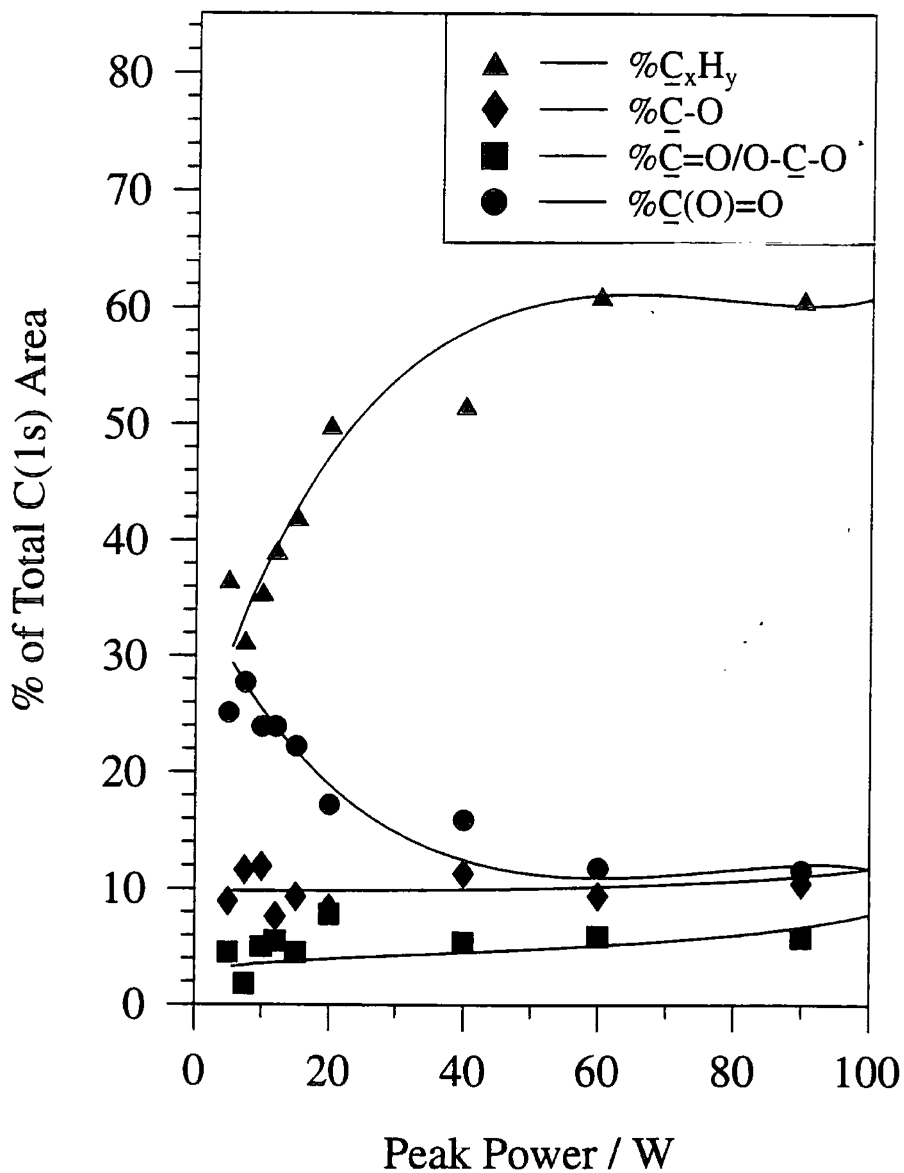

Figure 5.5 (c)

Variation of oxygen to carbon ratio for pulsed plasma polymerization experiments with variable peak power

(off-time = 1200 μs, and on-time = 20 μs).

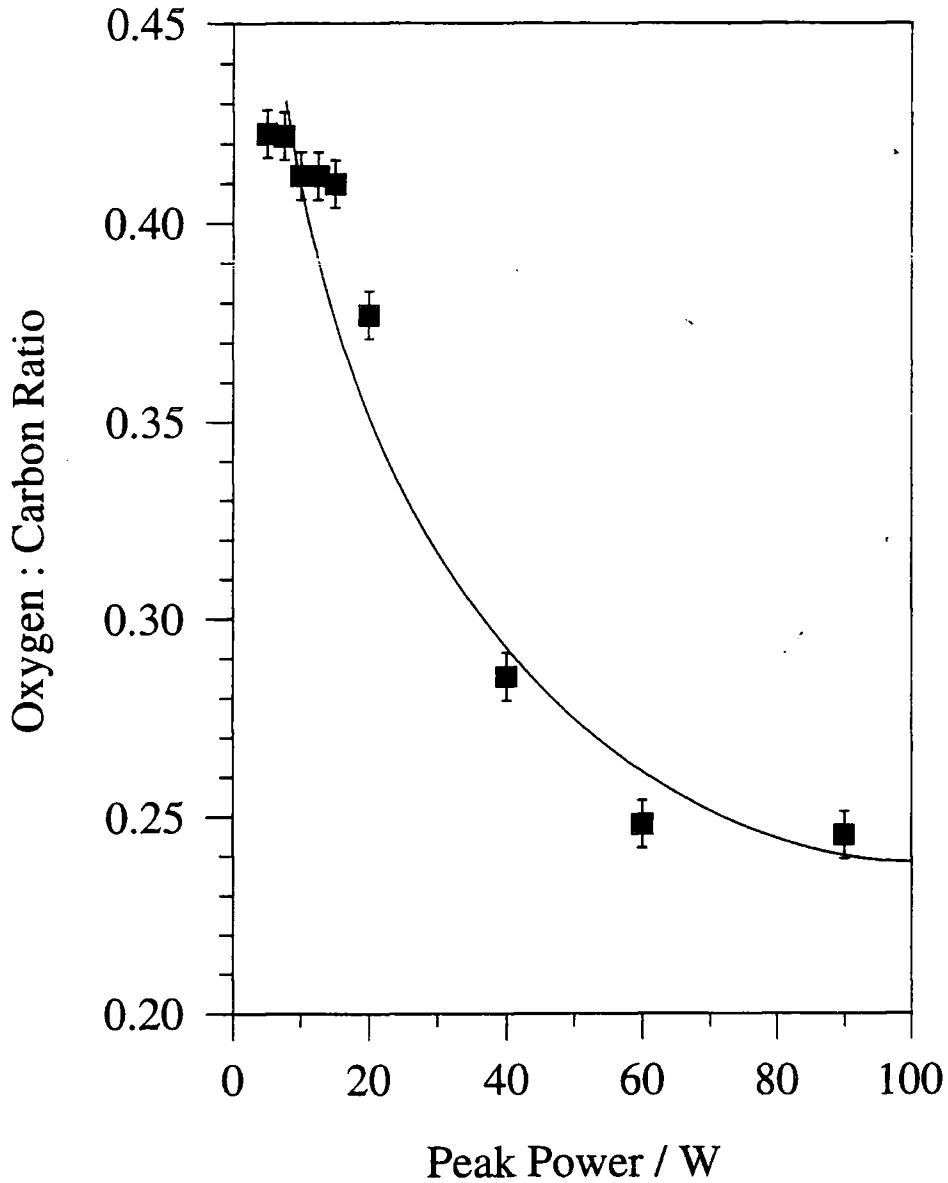

5.4 DISCUSSION

Continuous wave glow discharge polymerization of maleic anhydride yields a material which is predominantly a hydrocarbon network with a small level of oxygenation. This is in agreement with other studies which have shown that oxygen-containing organic precursors generally tend to form plasma polymers with a low oxygen content[31]. For instance, maleic anhydride has been previously shown to undergo plasma polymerization using a CW microwave energy source[40].

Pulsed plasma polymerization leads to greater functional group retention[32]. Indeed this is found to be the case in the present study where anhydride group incorporation into the plasma polymer is governed by the duty cycle parameters, with greater chemical selectivity being attained at short on-periods and long off-times. Electron impact, ion bombardment, and VUV irradiation by the electrical discharge will result in the formation of free radical centres at the growing film surface and in the vapour phase[41]. These can subsequently act as initiation centres for conventional chain growth polymerization during the duty cycle off-time:

On-time: Plasma polymerization → R• (incorporated into plasma polymer)

Off-time: Radical initiated chain growth:-

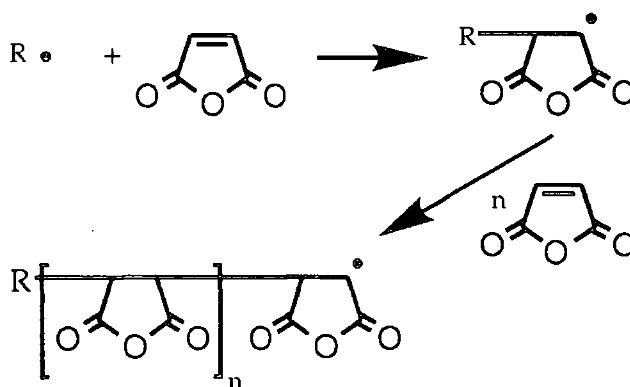

The maleic anhydride end-group on the growing polymer chain will be stabilized by a resonance effect[15]:

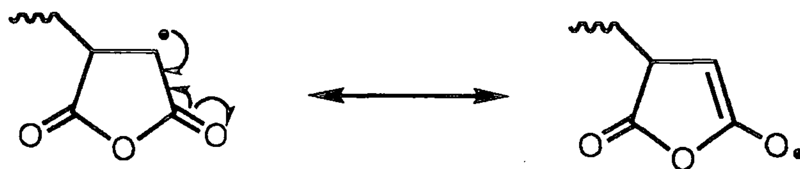

Effectively, the maleic anhydride monomer undergoes plasma initiated graft polymerization during the duty cycle off-period[18]. The lack of any alkene C-H stretching (3200 - 3100 cm^{-1}) bands[40] in the infrared spectrum of the pulsed plasma polymer materials is consistent with the free radical initiated unzipping of maleic anhydride double bonds during the duty-cycle off-time. On a theoretical basis, one would expect a 50% contribution from the -$\underline{C}$(O)=O anhydride functionality towards to the C(1s) envelope if a conventional maleic anhydride polymer had been synthesized. Pulsed plasma polymerization is capable of generating 28% anhydride centres, which is a 167% improvement compared to continuous wave plasma polymerization of maleic anhydride at 5 W. A plot of anhydride concentration versus the average power, shows that a drop in average power (obtained by any combination of on-time, off-time, and peak power) enhances the anhydride group incorporation, figure 5.6. Previous CW studies using an olefinic carboxylic acid precursor have also demonstrated that there is greater retention of the acid groups at lower powers which can be attributed to less monomer fragmentation[42]. A drop in plasma sheath potential at lower powers reduces ion bombardment of the growing film[43], accompanied by less VUV irradiation[44]; both of these effects will help to minimise the occurrence of excessive surface damage during the plasma on-time. Furthermore any suppression of monomer fragmentation at lower input energies will reduce surface etching by atomic oxygen by-products[35].

Figure 5.6

Variation in anhydride selectivity with average power (using different combinations of peak power, off-time, and on-time).

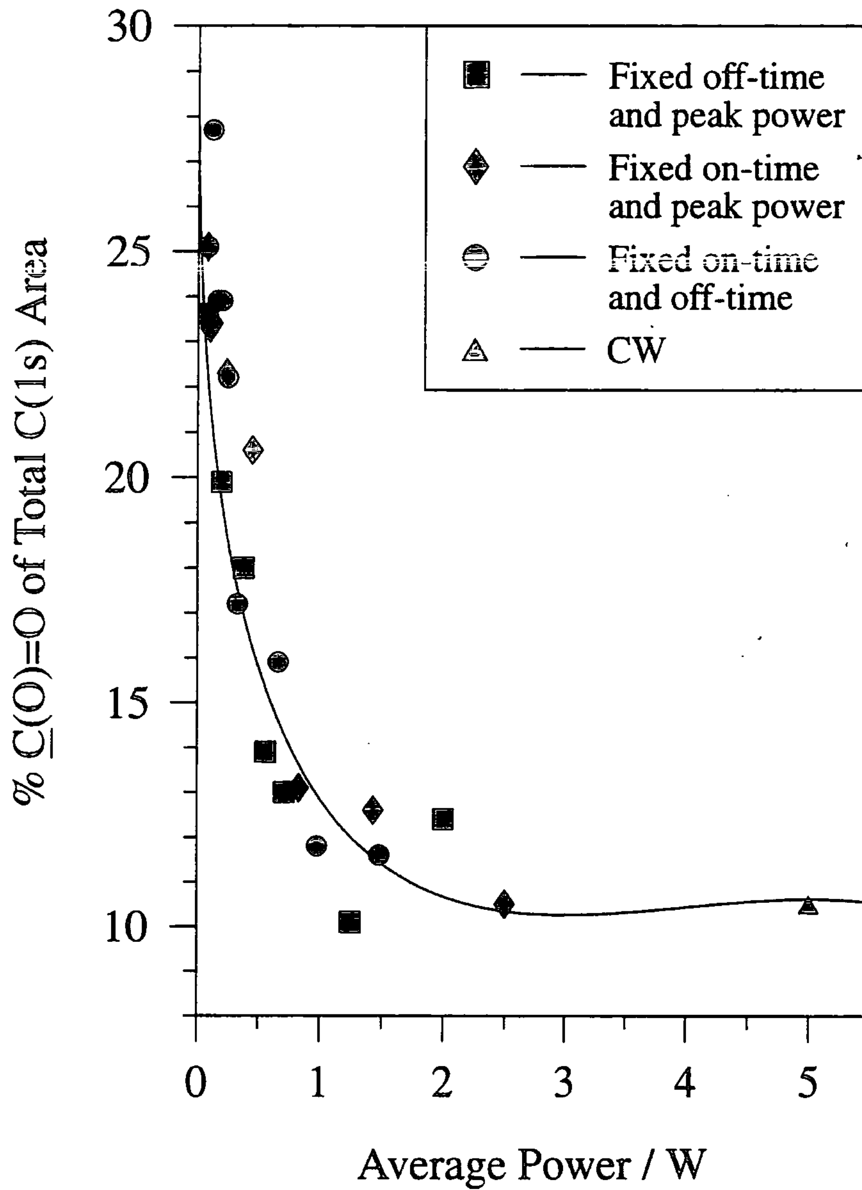

5.5 CONCLUSIONS

A comparison between continuous wave and pulsed plasma polymerization of maleic anhydride has shown that there is greater retention of the anhydride functionality originating from the parent monomer during pulsing of the electrical discharge. This can be explained in terms of lower average powers resulting in less fragmentation of the precursor molecule and reduced beam damage of the growing plasma polymer layer during the duty cycle on-time combined with radical initiated polymerization of maleic anhydride during the off-period.

5.6 REFERENCES

1. McMurry, J. *Organic Chemistry*; Brooks/Cole: Pacific Grove, 1988; p 468.
2. March, J. *Advanced Organic Chemistry 4th edn*; Wiley: New York, 1992; p 794
3. Angus, H. J. F.; Bryrce-Smith, D. *Proc. Chem. Soc.* **1959**, 326.
4. Schenck, G. O.; Steinmetz, R. *Tetrahedron Lett.* **1960**, 1.
5. Grovenstein, E.; Rao, D. V.; Taylor, W. J. *J. Am. Chem. Soc.* **1961**, *83*, 1705.
6. Sahu, U. S. *Polym. Comm.* **1983**, *24*, 61.
7. Schneier, B. *J. Polym. Sci.* **1972**, *B10*, 245.
8. Suh, K. W.; Corbett, J. M. *J. Appl. Polym. Sci.* **1968**, *12*, 2359.
9. Caze, C.; Loucheux, C. *J. Macromol. Sci. Chem.* **1978**, *A12*, 1501
10. Pellon, J. J.; Smyth, N. M.; Kugel, R. L.; Thomas, W. M. *J. Appl. Polym. Sci.* **1966**, *10*, 421.
11. Bartlett, P. D.; Nozaki, K. *J. Am. Chem. Soc.* **1946**, *68*, 1495.
12. DuPlessis, T. A.; Lustigand, A.; Greyling, E. *J. Macromol. Sci. Chem.* **1977**, *11*, 1015.
13. Kokubo, T.; Iwatsuki, S.; Yamashita, Y. *Makromol. Chem.* **1969**, *123*, 256.
14. Fujimori, K.; Schiller, W. S.; Craven, I. E. *Makromol. Chem.* **1991**, *192*, 959.
15. Roover, B. D.; Sclavons, M.; Carlier, V.; Devaux, J.; Legras, R.; Momtaz, A. *J. Polym. Sci. Polym. Chem. Ed.* **1995**, *33*, 829.
16. Hindryckx, F.; Dubois, P.; Patin, M.; Jerome, R.; Teyssie, P. *J. Appl. Polym. Sci.* **1995**, *56*, 1093.
17. Oostenbrink, A. J.; Gaymans, R. J.; *Polymer*, **1992**, *31*, 3086.
18. Gaboury, S. R.; Urban, M. W. *Langmuir*, **1994**, *10*, 2289.
19. Heseding, C.; Schneider, C. *Eur. Polym. J.* **1977**, *13*, 387.

20. Kellou, M. S.; Jenner, G. *Eur. Polym. J.* **1977,** *13,* 9.

21. Kellou, M. S.; Jenner, G. *Eur. Polym. J.* **1976,** *12,* 883.

22. Murahashi, S.; Nozakura, S.; Yasufuku, K. *Bull. Chem. Soc. Jap.* **1966,** *39,* 1338.

23. Bradbury, M. G.; Hamann, S. D.; Linton, M. *Aust. J. Chem.* **1970,** *23,* 511.

24. Fisher, R. F. *J. Appl. Polym. Sci.* **1963,** *7,* 1451.

25. Gabara, W.; Porejko, S. *J. Polym. Sci.* **1967,** *5,* 1547.

26. Minoura, Y.; Ueda, M.; Mizunuma, S.; Oba, M. *J. Appl. Polym. Sci.* **1969,** *13,* 1625.

27. Ho, R. M.; Su, A. C.; Wu, C. H.; Chen, S. *Polymer,* **1993,** *34,* 3264.

28. Rengaragin, R.; Parameswaran, V. R.; Lee, S.; Rinaldi, P. L. *Polymer,* **1990,** *31,* 1703.

29. Ruggeri, G.; Aglielto, M.; Pecragnani, A.; Ciardelli, F. *Eur. Polym. J.* **1983,** *19,* 863.

30. Gancaraz, I.; Laskawski, W. *J. Polym. Sci. Polym. Chem. Ed.* **1979,** *17,* 683.

31. Yasuda, H. *Plasma Polymerization;* Academic: London, 1985.

32. Savage, C. R.; Timmons, R. B.; Jacob, W. L. In *Structure-Property Relations in Polymers;* Urban, M. W.; Craver, C. D. Eds.; American Chemical Society: Washington DC, 1993; chapter 32.

33. Lopez, G.; Ratner, B. *ACS Polym. Mater. Sci. Eng.* **1990,** *62,* 14.

34. O'Kane, D. F.; Rice, D. W. *J. Macromol. Sci. Chem.* **1976,** *A10,* 567.

35. Hwu, W.; Zurawsky, W. P. *J. Polym. Sci. Polym. Chem. Ed.* **1992,** *30,* 409.

36. Trivedi, B. C.; Culbertson, B. M. *Maleic Anhydride;* Plenum: New York, 1982.

37. Nakajima, K.; Bell, A. T.; Shen M. *J. Polym. Sci. Polym. Chem. Ed.* **1979,** *23,* 2627.

38. Greenwood, O. D.; Tasker, S.; Badyal, J. P. S. *J. Polym. Sci. Polym. Chem. Ed.* **1994,** *32,* 2479.

39. Beamson, G.; Briggs, D. *High Resolution XPS of Organic Polymers The Scienta ESCA300 Database;* Wiley: Chichester, 1992; p 146.

40. Gaboury, S. R.; Urban, M. W. *Langmuir,* **1993,** *9,* 3225.

41. O'Keefe, M. J.; Rigsbee, J. M. *J. Appl. Polym. Sci.* **1994,** *53,* 1631.

42. Ward, R. J. *Ph.D. Thesis,* University of Durham, 1989.

43. Panchalingam, V.; Chen, X.; Huo, H.; Savage, C. R.; Timmons, R. B.; Eberhart, R. C. *ASAIO Journal,* **1993**, 39, M305

44. Yasuda, H.; Hsu, T. *J. Polym. Sci. Polym. Chem. Ed.* **1977,** *15,* 81.

CHAPTER 6

CONTINUOUS WAVE AND PULSED PLASMA POLYMERIZATION OF 2-IODOTHIOPHENE

6.1 INTRODUCTION

The effect of pulsed plasmas on the retention of monomer structure and functional groups in a plasma polymer was illustrated in the last chapter. The behaviour of a different molecular system is now studied under continuous wave and pulsed plasma conditions. 2-iodothiophene, structure 6.1, is a 5-membered aromatic heterocycle with iodine substituted at the α position. The thiophene family of polymers has been conventionally synthesised by either chemical[1-3] or electrochemical[2,4-6] routes; but more recently attempts have been made to employ non-isothermal plasma techniques because of the potential benefits of dry application to any substrate geometry[7-12]. Most plasma polymerized organic thin films are dielectric in nature, possessing good electrical insulating properties[13]. Exceptions to this general rule include plasma polymers synthesized from acetonitrile[14], thiophene[7,8], 1-benzothiophene[15], 2-chloroacrylonitrile[16], and p-xylene[17] precursors. Post doping of these materials with elements such as iodine can further improve their electrical conductivities by up to six orders of magnitude[8]. Recently, 2-iodothiophene has been polymerized using microwave frequency discharges in an attempt to simultaneously synthesize and dope the growing polymer layer[9,10,18]. This should in principle lead to a chemically more homogeneous material. In this chapter the radio frequency plasma polymerization of 2-iodothiophene is examined in order to compare the resultant plasma polymer film stoichiometry with previously reported studies employing microwave (MW) excitation[9,10,18].

Structure 6.1

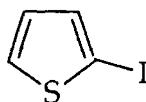

6.1.1 Polymerization of Thiophene

Two techniques are used to conventionally synthesize polythiophene and its derivatives, chemical and electrochemical polymerization. The chemically produced polymer is found to be in its undoped insulating state, whereas electrochemically produced polymer is obtained in the oxidized conducting state[19].

Thiophene has been chemically polymerized with a variety of initiators e.g. sulfuric acid, iron chloride and Zeigler catalyts[19]. Kossmehl[20] has also synthesized poly(five membered heterocycles) by bringing together the monomer and the complex AsF_5 generating black insoluble polymers. The mechanism is believed to proceed as follows:-

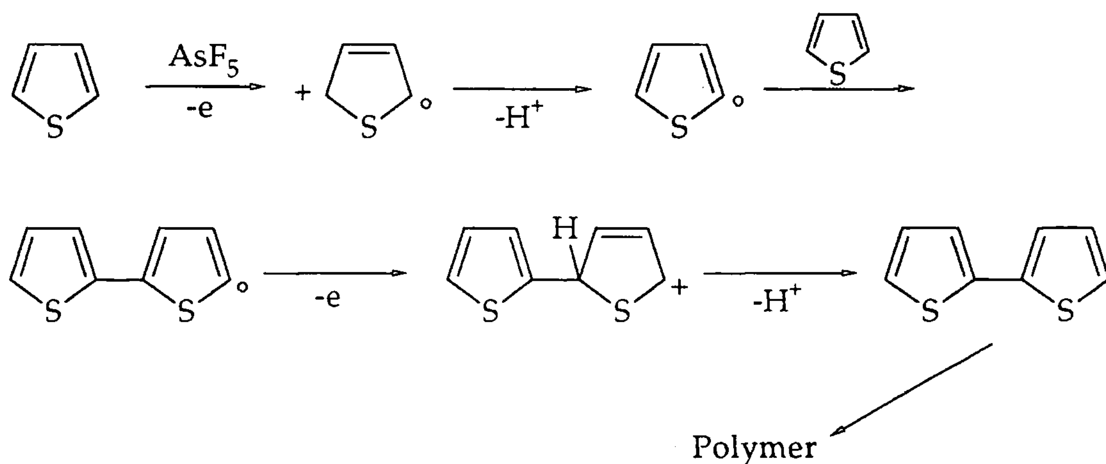

Electrochemical polymerization is carried out in a single-compartment cell with the classic three electrode configuration[19,21-23]

working electrode:	Pt, Au, or glass coated with SnO_2 or In_2O_3,
reference electrode:	saturated calomel electrode (SCE),
auxiliary electrode:	Pt, Ni, or C electrode.

The electrolytic medium typically consists of an organic solvent (THF), a supporting electrolyte (M^+X^-) and the monomer. The general mechanism proposed is:-

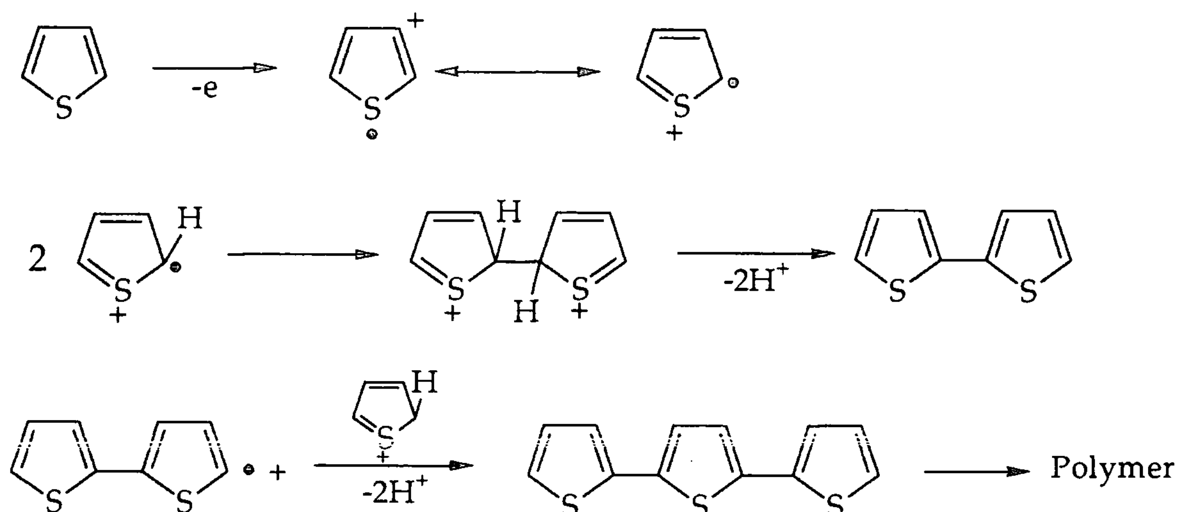

Glow discharges are now beginning to be employed in the polymerization of thiophene with some success. Films of insoluble, black material can be obtained which show promising electronic properties after doping with iodine. The stiochiometry of these polymers is very different to the monomer or conventional polymer and the mechanism of formation is poorly understood.

6.2 EXPERIMENTAL

Plasma polymerization experiments were carried as detailed in the last chapter (section 5.2). The monomer tube was filled with 2-iodothiophene (Aldrich, 98+%) which was further purified by using freeze-pump-thaw cycles. After the reactor was cleaned and evacuated down to its base pressure the monomer vapour was introduced at a pressure of approximately 0.1 Torr, and at a flow rate of approximately 2.14×10^{-8} kg s^{-1}. Then the electrical discharge was ignited and allowed to run for the

Then the electrical discharge was ignited and allowed to run for the following times: 1 min in order to provide sufficient plasma polymer material for XPS analysis; 10 min to generate films thick enough for infrared characterization; and 1 hr to deposit enough material for X-ray absorption spectroscopy. Upon completion of deposition, the RF generator was switched off, and the system flushed with monomer vapour for 5 min prior to venting the system up to atmospheric pressure. Each plasma polymer layer was then characterized by the respective analytical technique. Pulsed plasma experiments were performed by the method described in chapter 5. The pulse times, t_{on} and t_{off}, could be varied over the range 50-1000 µs. The peak power (P_p) delivered to the glow discharge spanned 5-40 W. These films were only analyzed by XPS and IR.

XPS surface analysis was performed as before (section 2.2.1). Instrumentally determined sensitivity factors for unit stoichiometry were taken as being C(1s) : I($3d_{5/2}$) : S(2p) : O(1s) equals 1.00 : 0.11 : 0.54 : 0.55. Uniform plasma polymer coverage was confirmed by the absence of any Si(2p) XP signal showing through from the underlying glass substrate. The iodine region was always run first in order to minimize any potential loss of molecular iodine under UHV conditions

XAS characterization was performed at the EPSRC Daresbury Synchrotron facility in Warrington UK, operating at 2 GeV energy and with electron currents between 100 mA and 200 mA. The sulfur K edge spectra were collected (beamline station 3.4) using total electron yield measured directly from the isolated sample holder. Plasma polymer and reference samples (sulfur and 2,5-diiodothiophene) were prepared by grinding a 90% graphite / 10% sample mixture, this was then pressed into thin discs and fixed onto a sample holder using a small amount of conductive paint. The first inflection point in the XANES spectrum for a sulfur standard was taken as the calibration reference at 2472.0 eV[24]. Iodine L_{III} edge XAS spectra were obtained in fluorescence detection mode (beamline station 8.1) using a

Canberra solid-state multichannel detector. Rejection of beam harmonics was achieved by detuning the double Si(111) monochromators to 50% of maximum reflectivity. The resulting incident X-ray flux was monitored by an ion chamber (20% absorbance at L_{III} edge) containing a He / Ar mixture. In this case, ground samples were placed into a liquid nitrogen cooled aluminium sample holder. The liquid 2-iodothiophene monomer was loaded into a PTFE container and mounted onto a liquid nitrogen cryostat.

A FTIR Mattson Polaris instrument was used for transmission infrared analysis of 2-iodothiophene monomer and the plasma polymer layers deposited onto pressed potassium bromide discs. Typically, 100 scans were acquired at a resolution of 4 cm^{-1}.

6.3 RESULTS

6.3.1 Continuous Wave Plasma Polymers

6.3.1.1 X-ray Photoelectron Spectroscopy

Negligible variation was found in C(1s), $I(3d_{5/2})$, and $S(2p_{3/2,1/2})$ XPS peak shapes over the 2 - 20 W power range. The C(1s) region consists of a major component centred at 285.0 eV corresponding to most of the carbon atoms being located in a hydrocarbon/crosslinked environment ($\underline{C}_xH_y$), and a weak shoulder at slightly higher binding energy reflecting the incorporation of the more electronegative sulfur and iodine atoms into the plasma polymer structure[25], figure 6.1. The $S(2p_{3/2,1/2})$ region comprises an unresolved 2 : 1 doublet centred at 164.3 eV which is characteristic of covalently bound sulfur centres[26], figure 6.2 The $I(3d_{5/2})$ envelope could be fitted with two components centred at 619.1 eV and 620.8 eV corresponding to I_3^- and covalently bonded iodine environments respectively[25,27], figure

6.3; the two weaker peaks discernible at 622.5 eV and 624.0 eV can be attributed to shake-up satellites associated with the two major peaks[25] (having taken into account the $I(3d_{3/2})$ Mg $K\alpha_{3,4}$ X-ray satellite lines).

The monomer contains 66.7 % carbon, 16.7 % sulfur, and 16.7 % iodine (ignoring hydrogen because it can not be detected by core level XPS[28]). Iodine incorporation into the plasma polymer film was found to be lower than in the original monomer, whilst sulfur content was greater; however, both of these percentages were found to diminish with increasing glow discharge power, figure 6.4. A small amount of oxygen incorporation was observed at higher glow discharge powers; the most likely origin of this being reaction between trapped free radical centres at the surface and the laboratory atmosphere during transport of the substrate from the plasma reactor to the XP spectrometer[29].

6.3.1.2 X-ray Absorption Near Edge Structure

XANES spectroscopy provides detailed information about the molecular orbitals associated with a chemical structure by identifying dipole electronic transitions from low lying core levels to unoccupied molecular orbitals. Peak positions and assignments from some previous XAS studies on a variety of sulfur containing compounds are listed in table 6.1. In the present work 2,5-diiodothiophene which is a solid was used as a substitute standard for the 2-iodothiophene liquid monomer, since the latter is incompatible with a high-vacuum environment. The sulfur K-edge XANES spectrum of 2,5-diiodothiophene shows two prominent features, figure 6.5; peak **a** can be assigned to the overlap of a π^*_{ring} resonance with a σ^*_{C-S} shape resonance, whilst peak **b** is characteristic of a σ^*_{C-C} resonance[30]. The relatively intense appearance of peak **b** can be taken as being indicative of delocalisation of the σ^*_{C-C} orbitals throughout the aromatic thiophene ring system.

Figure 6.1

C(1s) XP spectra of 2-iodothiophene plasma polymer as a function of glow discharge power.

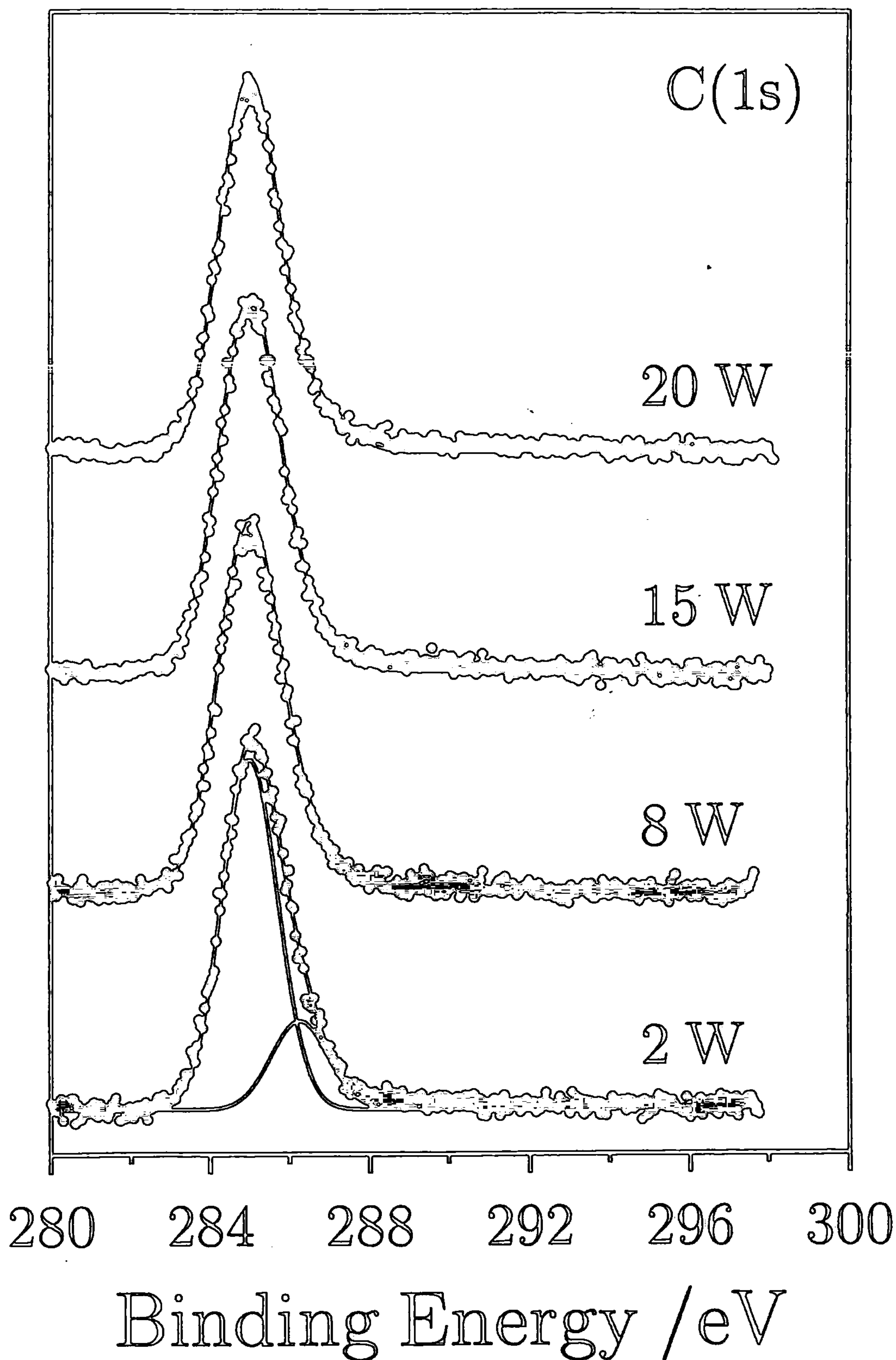

Figure 6.2

S(2p) XP spectra of 2-iodothiophene plasma polymer as a function of glow discharge power.

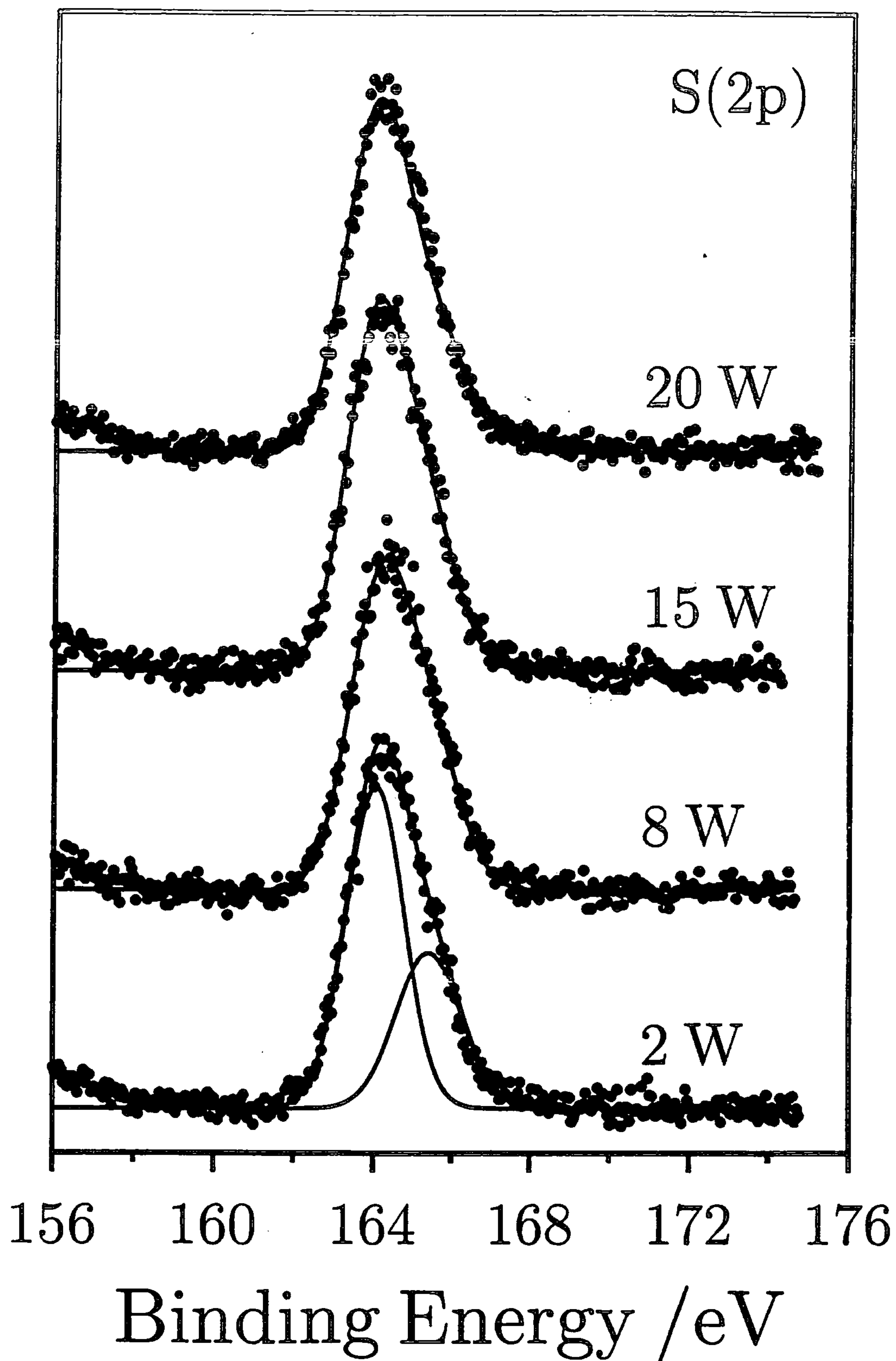

Figure 6.3

$I(3d_{5/2})$ XP spectra of 2-iodothiophene plasma polymer as a function of glow discharge power.

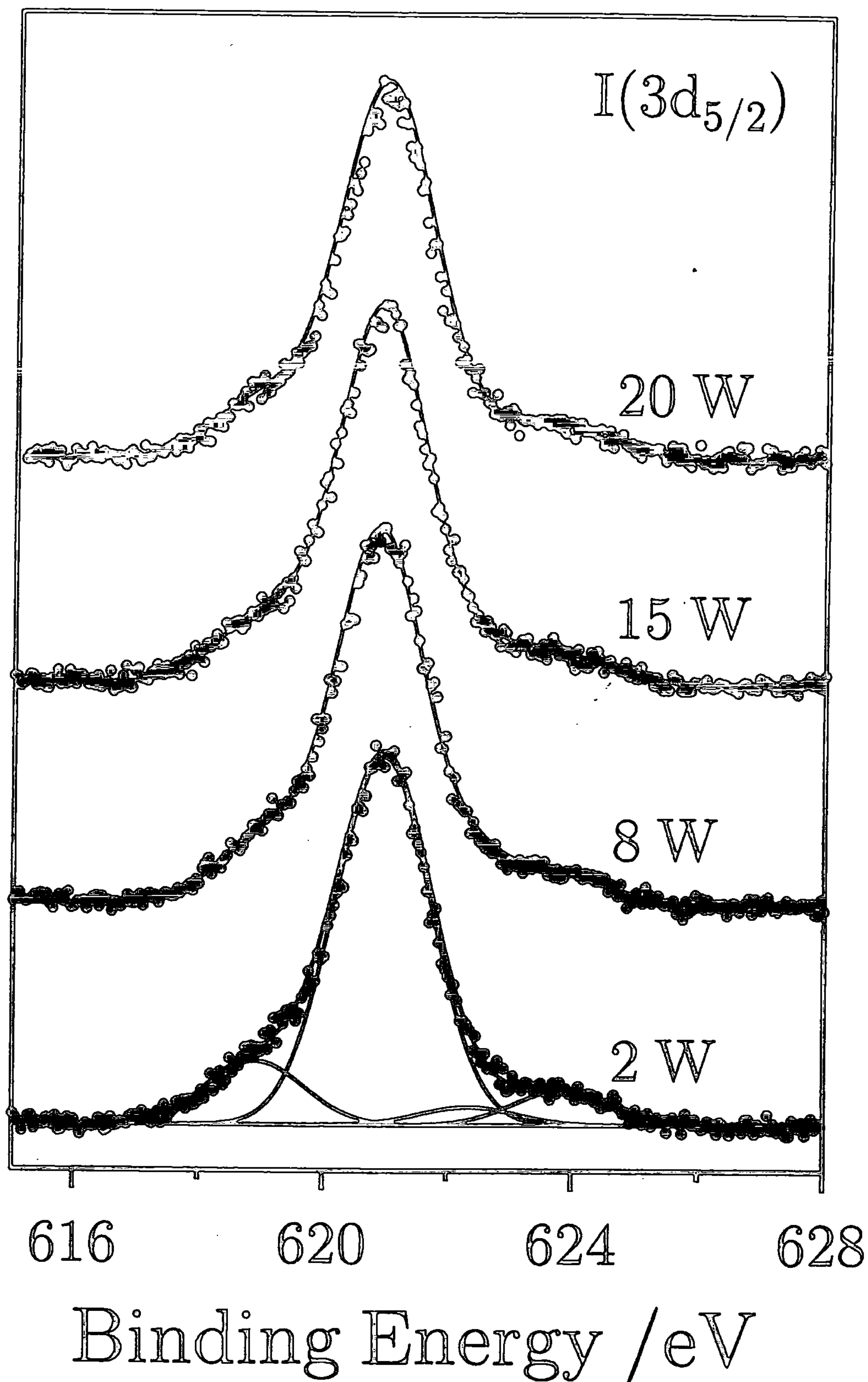

Figure 6.4

Variation in elemental composition of 2-iodothiophene plasma polymers with power (0 W corresponds to the monomer composition).

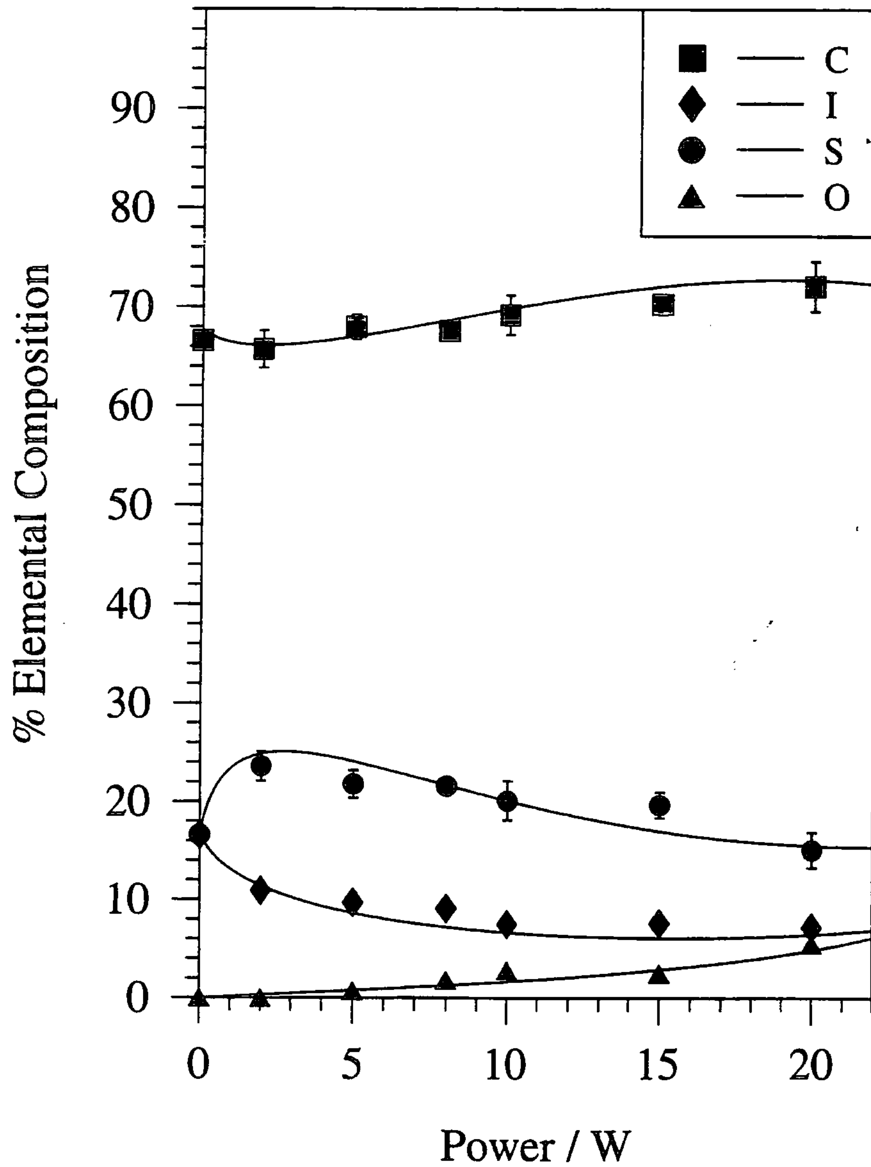

Figure 6.5

S K edge XANES spectra of 2,5-diiodothiophene with 5 W, 8 W and 20 W 2-iodothiophene plasma polymers.

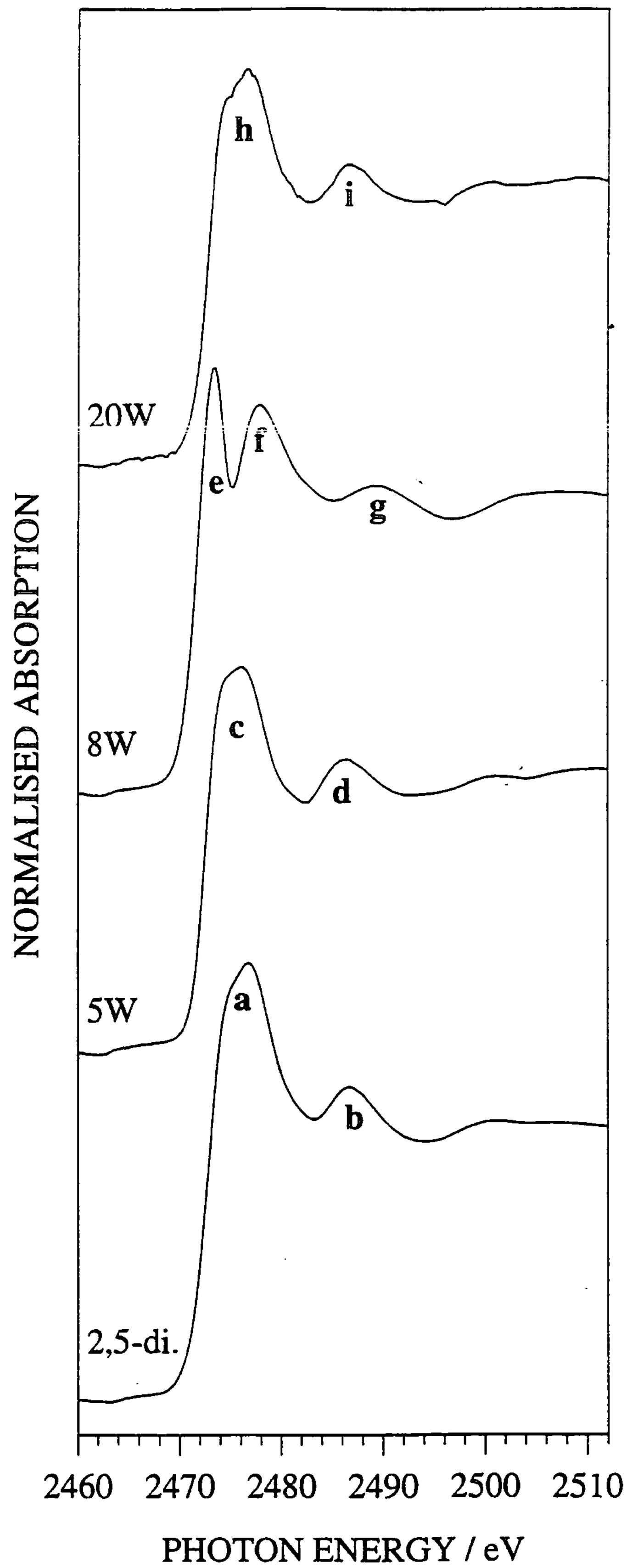

Table 6.1

S K-edge XANES assignments from previous studies.

Photon Energy / eV	Assignment	System Studied	Reference
2473 2478	π* σ*	SO_2 on Ni (111)	31
2473.4 2475.1 2475.6 2476.3 2478.4 2480.8 2482.5 2487	π*, σ* (C-S) 4s 4p 5p IP σ* (C-C) σ* (C-C) Shakeup	Thiophene gas	30
2473.2 2481.8 2479	π* (C-S) π* (S-O) π* ($C_4H_8SO_3$)	Thermal ageing of (poly-3,4-ethylenedioxy-thiophene)	32
2473.4 2475.7	Unassigned Unassigned	Bis(4-hydroxyphenyl)-disulphide	33
2473.5 2475.5 2476.8	Unassigned Unassigned Unassigned	Thionin	33
2474.6	Unassigned	Thiosalicylic acid	33
2475.0	Unassigned	Benzothiophene	33
2472.3 2479	σ* (C-S) σ* (C-C)	Thiolane	30

Table 6.2

Peak assignments from figure 6.5.

Peak	Energy / eV	Proposed Assignment
a	2476.8	π^*, σ^* (C-S)
b	2486.7	σ^* (C-C)
c	2476.0	π^*, σ^* (C-S)
d	2486.3	σ^* (C-C)
e	2473.5	π^*
f	2477.8	σ^* (C-S)
g	2489.2	σ^* (C-C)
h	2476.5	π^*, σ^* (C-S)
i	2486.6	σ^* (C-C)

Plasma polymerization of 2-iodothiophene at 5 W yields very similar near edge features (c and d) to those observed for the 2,5-diiodothiophene reference compound. This suggests that a significant proportion of the sulfur atoms are retained in a monomer-like environment at low glow discharge energies. These features become perturbed with increasing glow discharge power. The low photon energy peak c observed at 5 W splits into two components (e and f) at 8 W. A greater extent of aromatic ring rupture is to be expected with increasing glow discharge energy; this loss of aromaticity will result in a lowering of the π^* energy levels[34], which will in turn shift the π^* resonance towards smaller XANES photon energies (peak e). The observed shift in the σ^*_{C-S} resonance towards higher photon energy at 8 W (peak f) suggests a shorter C-S bond[35] relative to the 5 W case (peak c). This shift in the σ^*_{C-S} resonance together with the intense π^* resonance would indicate the incorporation of some C=S double bond environments within the 8 W plasma polymer network. It has been previously reported

that on comparing the sulfur K edge XANES spectra of the aromatic thiophene molecule to its saturated analogue, thiolane, the σ^*_{C-C} resonance appears at higher photon energy in the aromatic system[30]. The difference between the positions of peaks <u>**d**</u> and <u>**g**</u> along with the broadening of the latter suggests a mixture of C-C environments, some of which must at least be C=C double bonds. The loss in intensity of the σ^*_{C-C} resonance is consistent with a diminishing delocalisation of the σ^*_{C-C} orbitals onto the sulfur atoms as would be expected upon loss of aromaticity. At even higher glow discharge powers (20 W), the sulfur K edge XANES spectrum is reminiscent of the spectra observed for the 2,5-diiodothiophene model compound and the 5 W 2-iodothiophene plasma polymer. This can be attributed to the complete fragmentation and rearrangement of the 2-iodothiophene precursor molecule to form a plasma polymer containing a conjugated network of unsaturated centres, such a bonding arrangement will raise the π^* energy levels and cause delocalisation of the C-S bonds, thereby causing the π^* and σ^*_{C-S} resonances to shift towards each other and coincide (peak <u>**h**</u>). The rise in intensity of peak <u>**i**</u>, the σ^*_{C-C} resonance is consistent with a return to a greater delocalisation of the σ^*_{C-C} orbitals onto the sulphur atom. Following the line of argument mentioned above for the σ^*_{C-C} resonance based upon thiophene versus thiolane, there must be increased conjugation at 20 W relative to the 8 W case.

In comparison to the sulphur data, the iodine L_{III} edge XANES spectra for the 2-iodothiophene plasma polymers are relatively featureless and do not show much change with glow discharge power, figures 6.6 and 6.7. Comparison with inorganic (KIO_3 and KI) and organic (2-iodothiophene, IBr and I_2) standards suggests that most of the iodine centres contained in the plasma polymer deposits are located in a covalent environment.

Figure 6.6

I L_{III} edge XANES spectra of reference compounds; iodine, iodine bromide, potassium iodide and potassium iodate.

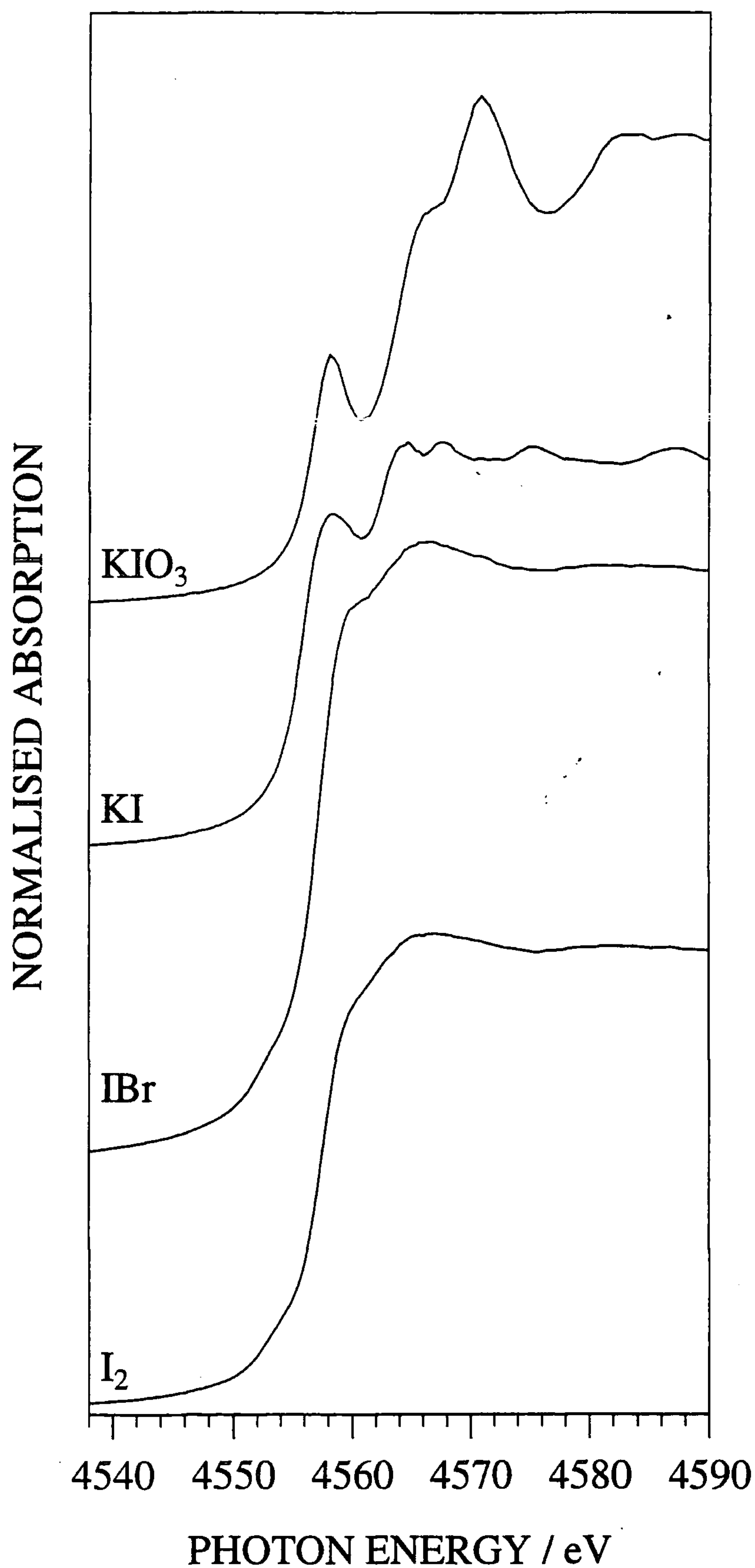

Figure 6.7

I L_{III} edge XANES spectra of 2-iodothiophene with 5 W, 8 W and 20 W plasma polymers.

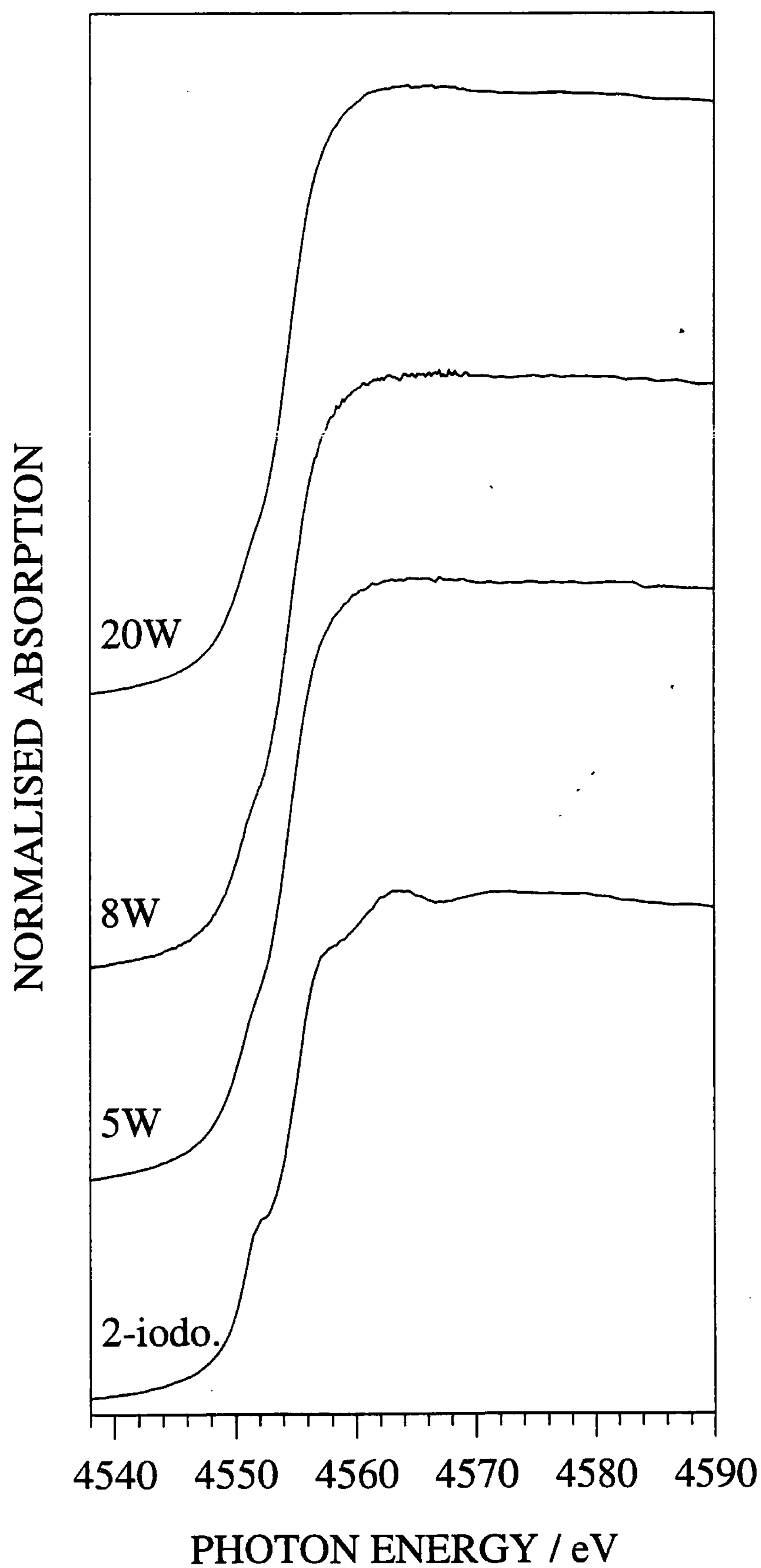

6.3.1.3 Infrared Spectroscopy

The following absorbances were assigned in the transmission infrared spectrum of the 2-iodothiophene monomer, figure 6.8: 450 cm^{-1} (C-I stretch[36]); 700 cm^{-1} (C-H out of plane vibration of a 2-substituted thiophene[37]); 821 cm^{-1} (ring skeletal breathing vibration[38,39]); 842 cm^{-1} and 947 cm^{-1} (C-H out of plane deformations[39]); 1043 cm^{-1} and 1085 cm^{-1} (C-H in plane deformation vibrations of 2-substituted thiophenes[38,39]); 1222 cm^{-1}, 1338 cm^{-1}, 1396 cm^{-1}, and 1506 cm^{-1} (characteristic aromatic ring stretches of 2-substituted thiophenes[39]); and 3100 cm^{-1} (aromatic C-H stretch[38]).

Most of the infrared absorption features characteristic of the 2-iodothiophene monomer are retained during plasma polymerization, figure 6.8; although the peaks become broader which is consistent with the highly disordered nature of plasma polymers in general. The C-I absorbance shifts to 500 cm^{-1} during plasma polymerization, this increase in stretching frequency suggests that the iodine substitution of the aromatic rings changes from exclusively 2-substituted thiophene. With increasing glow discharge powers, both the C-I band at 500 cm^{-1} and the C-H out of plane vibration at 700 cm^{-1} (characteristic of 2-substituted thiophenes) lose signal intensity with respect to the C-H out of plane deformation (842 cm^{-1}) and the aromatic ring skeletal breathing (821 cm^{-1}) modes, this is consistent with the loss of iodine as previously observed by XPS analysis. The 1222 cm^{-1} absorbance (aromatic C=C stretching) widens in line width at higher powers which reflects the disruption of the aromatic thiophene rings. The C-H stretch at 3100 cm^{-1} remains unperturbed throughout the range of plasma polymerizations conditions investigated. The weak features in the 2250 - 2350 cm^{-1} range are associated with a small amount of background CO_2 in the FTIR spectrometer.

Figure 6.8

Infrared spectra of 2-iodothiophene monomer and plasma polymers as a function of glow discharge power.

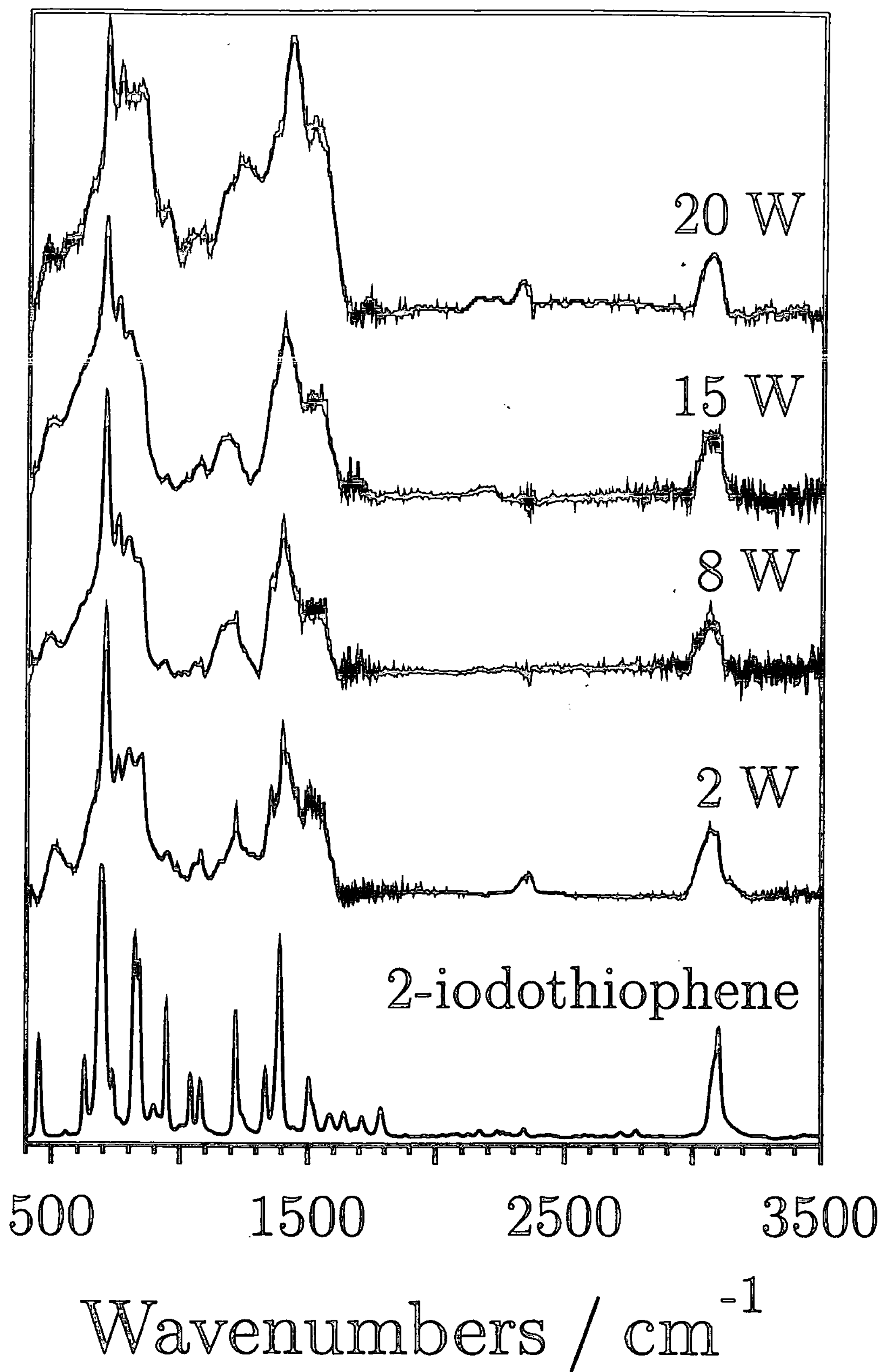

6.3.2 Pulsed Plasma Polymers

Similar studies were performed with 2-iodothiophene to those used in the last chapter with maleic anhydride. A fixed duty cycle off-period of 1000 μs, and peak power of 5 W produced very little compositional changes in the resultant polymer with decreasing on-times down to 50 μs, beyond which incomplete coverage of the glass substrate was observed, table 6.3. Similarly, for a constant duty cycle on-time (50 μs) and peak power (5 W) no variation in polymer stoichiometry is seen with increasing off-times, table 6.4. A final study was undertaken in which the on- and off-times were kept fixed whilst the peak power was varied, table 6.5. The polymer was again unaffected by the changing pulse parameters. The iodine content of all pulsed plasma polymers is much lower than for the low power (2 W) continuous wave polymer, but the sulfur content in both cases is comparable.

The IR spectra of two pulsed plasma polymers along with that of the 2 W CW plasma polymer and the monomer are shown in figure 6.9. The peaks appear sharper than those produced under CW conditions.

Table 6.3

Elemental composition of 2-iodothiophene pulsed plasma polymer (peak power = 5 W, off-time = 1000μs, and on-time varied).

On-Time	Av. Power	% I	% C	% S	% O
1000 μs	2.50 W	8.0 ± 0.4	66.8 ± 0.1	23.1 ± 0.5	2.2 ± 0.8
500 μs	1.67 W	7.9 ± 0.2	67.7 ± 2.3	22.4 ± 3.3	2.0 ± 1.2
350 μs	1.30 W	8.0 ± 0.3	67.6 ± 0.4	22.6 ± 2.1	1.5 ± 1.0
250 μs	1.00 W	6.2 ± 0.8	68.3 ± 3.0	22.1 ± 1.8	3.5 ± 0.4
50 μs	0.24 W	5.7 ± 0.4	69.6 ± 0.1	23.2 ± 0.2	1.7 ± 0.2

Table 6.4

Elemental composition of 2-iodothiophene pulsed plasma polymer (peak power = 5 W, on-time = 50μs, and off-time varied).

Off-Time	Av. Power	% I	% C	% S	% O
50 μs	2.5 W	6.6 ± 0.2	69.4 ± 1.1	22.9 ± 2.6	1.3 ± 1.8
250 μs	0.83 W	6.1 ± 0.4	68.2 ± 0.2	24.3 ± 1.0	1.5 ± 0.4
500 μs	0.45 W	6.2 ± 0.7	68.8 ± 2.5	23.9 ± 2.1	1.2 ± 0.4
750 μs	0.31 W	6.0 ± 0.4	69.4 ± 0.8	23.3 ± 1.6	1.4 ± 0.4
1000 μs	0.24 W	5.7 ± 0.4	69.6 ± 0.1	23.2 ± 0.2	1.7 ± 0.2

Table 6.5

Elemental composition of 2-iodothiophene pulsed plasma polymer (on-time = 50μs, off-time = 1000μs, and peak power varied.)

Peak Power	Av. Power	% I	% C	% S	% O
5 W	0.24 W	5.7 ± 0.4	69.6 ± 0.1	23.2 ± 0.2	1.7 ± 0.2
20 W	0.95 W	6.3 ± 0.1	68.6 ± 0.4	22.6 ± 1.5	2.6 ± 1.7
40 W	1.90 W	5.9 ± 0.1	68.8 ± 0.1	22.1 ± 0.3	5.4 ± 0.5

Figure 6.9

Infrared spectra of; (a) 2-iodothiophene monomer, (b) pulsed plasma polymer t_{on} = 50 μs, t_{off} = 1000 μs at P_p = 5 W, (c) pulsed plasma polymer t_{on} = 50 μs, t_{off} = 50 μs at P_p = 5 W, (d) 2 W CWplasma polymer.

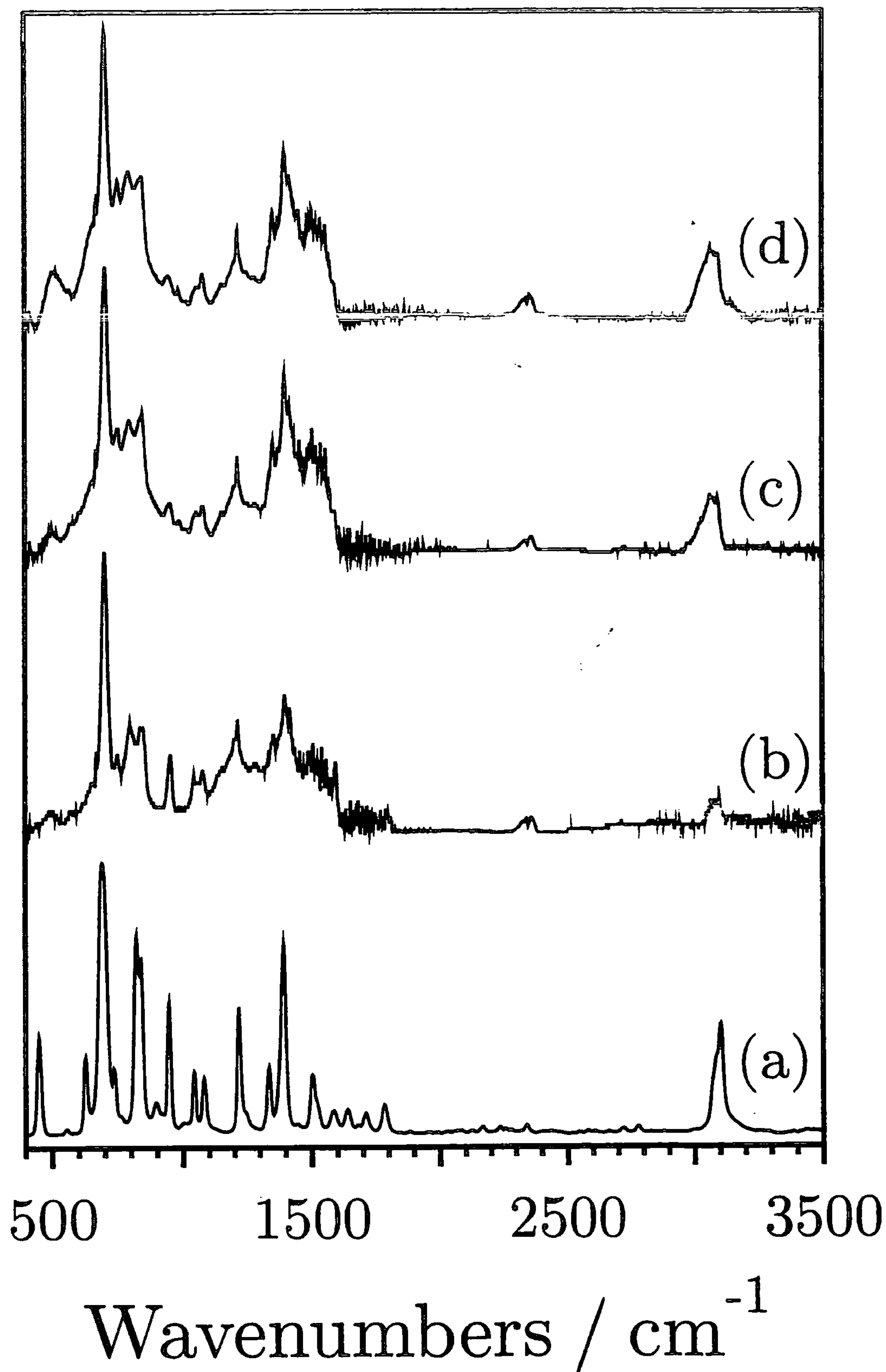

6.4 DISCUSSION

XPS, XANES, and FTIR analysis of continuous wave plasma polymerized 2-iodothiophene films show that there is a drop in iodine and sulfur content with increasing power. This is consistent with C-I (D°_{298} = 209 kJ mol^{-1})[24] and C-S (D°_{298} = 698 kJ mol^{-1})[24] bonds being weaker than the C=C bond (D°_{298} = 720 kJ mol^{-1})[24] in the 2-iodothiophene precursor molecule. The preferential retention of sulfur into the plasma polymer layers with respect to iodine incorporation can be accounted for on the basis of the C-I bond being weaker than the C-S bond. The observed loss in aromaticity with increasing glow discharge power is consistent with previous studies carried out using other aromatic heterocyclic monomers (e.g. 1-benzothiophene[15]). Higher powers lead to a shift in population of energetic electrons in the tail of the Maxwellian electron energy distribution[40], thereby providing a more energetic plasma environment. It is also interesting to note that there appears to be more sulfur and iodine incorporation during RF plasma polymerization compared to corresponding microwave studies[10,11,18]; this can again be explained in terms of the higher population of energetic electrons in the tail of the Maxwellian electron energy distribution[40,41] in conjunction with increased electron / ion densities[42] for the microwave discharges. Clearly this will lead to a greater fragmentation of any precursor molecule during plasma polymerization.

All pulsed plasma polymerization experiments yielded very similar results. XPS showed the pulsed plasma polymer to have similar sulfur content but much lower iodine retention than that of the low power (2 W) CW plasma polymer. Infrared analysis indicated the structure of the 2 W CW and pulsed plasma polymers to be very similar. Pulsed plasmas were shown in chapter 5 to increase the possibility of radical chain growth polymerization. Conventionally polythiophene polymerizes through the 2-

and 5- positions of the ring, with removal of hydrogen, structure 6.2. If this mechanism occurred during the off-cycle of the pulsed plasma polymerization, HI would be eliminated from this monomer so reducing the level of iodine incorporation in the polymer.

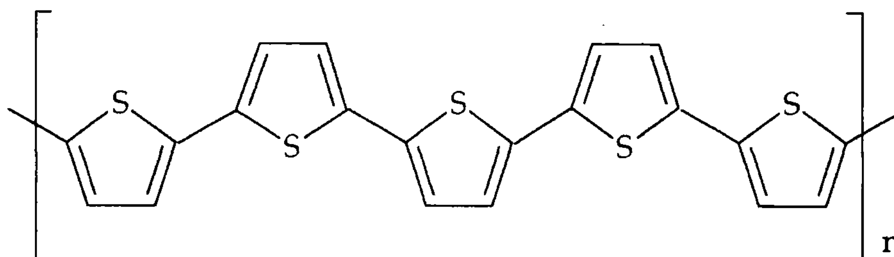

Structure 6.2

6.5 CONCLUSIONS

Continuous wave RF plasma polymerization of 2-iodothiophene produces a polymeric network which retains many of the structural characteristics associated with the original precursor molecule. Sulfur and iodine incorporation into the growing plasma polymer layer drops with increasing glow discharge power due to the weaker C-S and C-I bond linkages contained in the monomer. Pulsed plasma polymerization leads to a reduction in the iodine content without effecting the sulphur incorporation in the polymer.

6.6 REFERENCES

1. Wang, C. G.; Benz, M. E.; Legoff, E.; Schinder, J. K.; Allbrittonthomas, J.; Kannewurf, C. R.; Kanatzidis, M. G. *Chem. Mat.* **1994**, *6*, 401.
2. Wang, C.; Schindler, J. L.; Kannewurf, C. R.; Kanatzidis, M. G. *Chem. Mat.* **1995**, *7*, 58.
3. Van Dyke, L. S.; Brumlik, C. J.; Liang, W.; Lei, J.; Martin, C. R.; Yu, Z.; Li, L.; Collins, G. J. *Synth. Met.* **1994**, *62*, 75.
4. Bazzaoui, E. A.; Marsault, J. P.; Aeiyach, S.; Lacaze, P. C. *Synth. Met.* **1994**, *66*, 217.
5. Visy, C.; Lukkari, J.; Kankare, J. *Synth. Met.* **1994**, *66*, 61.
6. Randazzo, M. E.; Toppare, L.; Fernandez, J. E. *Macromolecules* **1994**, *27*, 5102.
7. Sadhir, R. K.; Schoch, K. F. *Thin Solid Films* **1993**, *223*, 154.
8. Tanaka, K.; Yoshizawa, K.; Takeuchi, T.; Tamabe, T. *Synth. Met.* **1990**, *38*, 107.
9. Kruse, A.; Baalmann, A.; Budden, W.; Schlett, V.; Hennecke, M. *Surf. Coatings Technol.* **1993**, *59*, 359.
10. Kruse, A.; Schlett, V.; Baalmann, A.; Hennecke, M. *Fresenius J. Anal. Chem.* **1993**, *346*, 284.
11. Thomas, B.; Pillai, M. G. K.; Jayalekshmi, S. *J. Phys. D Appl. Phys.* **1988**, *21*, 503.
12. Horvath, Z. J. *J. Appl. Phys.* **1990**, *68*, 5899.
13. Yasuda, H. *Plasma Polymerization*; Academic: London, 1985.
14. Suleimanov, B. A.; Akhmedov, M. M.; Suleimanova, Y. I.; Kerimov, M. K. *Thin Solid Films* **1991**, *197*, 319.
15. Tanaka, K.; Tamabe, T.; Takeuchi, T.; Yoshizawa, K. *J. Appl. Phys.* **1991**, *70*, 5653.
16. Grunwald, H.; Munro, H. S.; Wilhelm, T. *Synth. Met.* **1991**, *42*, 1465.

17. Takai, Y.; Hayase, Y.; Mizutani, T.; Ieda, M. *J. Phys. D Appl. Phys.* **1984**, *17*, 399.

18. Kruse, A.; Baalmann, A.; Hennecke, M. *Proc. 11th Internat. Symp. Plasma Chem.* Loughborough, England, 1993, 1077.

19. Tourillon, G. In *Handbook of Conducting Polymers Vol. 1*; Skotheim, T. A. Ed.; Dekker: New York, 1986, chapter 9.

20. Kossmehl, G.; Chatzitheodorou, G. *Makromol. Chem. Rap. Comm.* **1981**, *2*, 551.

21. Tourillon, G.; Garnier, F. *J. Electroanal. Chem.* **1982**, *135*, 173.

22. Kaneto, K.; Yoshino, K.; Inuishi, *Jap. J. Appl. Phys.* **1982**, *21*, L567.

23. Hotta, S.; Hoshaka, T.; Shimotsuma, W. *Sythn. Met.* **1983**, *6*, 317.

24. Weast, R. C.; Astle, M. J. CRC *Handbook of Chemistry and Physics 63rd Edition*; CRC Press: Florida, 1982.

25. Chilkoti, A.; Ratner, B. D. *Chem. Mat.* **1993**, *5*, 786.

26. Clark, D. T.; Lilley, D. M. *J. Chem Phys. Letts.* **1971**, *9*, 234.

27. Salaneck, W. R.; Thomas, H. R.; Bigelow, R. W.; Duke, C. B.; Plummer, E. W.; Heger, A. J.; MacDiarmid, A. G. *J. Chem. Phys.* **1980**, *72*, 3674.

28. Briggs, D.; Seah, M. P.; *Practical Surface Analysis 2nd Ed*; Wiley: Chichester,1990.

29. Yasuda, H.; Marsh, H. C.; Brandt, S.; Reilley, C. N. *J. Polym. Sci. Polym. Chem. Ed.* **1977**, *15*, 991.

30. Hitchcock, A.P.; Hosley, J.A.; Stohr, J. *J. Chem. Phys.* **1986**, *85*, 4835.

31. Muryn, C.A.; Purdie, D.; Hardma, P.; Johnson, A.L.; Prakash, N.S.; Raiker, G.N.; Thornton, G.; Law, D. S-L. *Faraday Discuss. Chem. Soc.* **1989**, *89*, 77.

32. Winter, I.; Reese, C.; Hormes, J.; Heywang, G.; Jonas, F. *Chem. Phys.* **1995**, *194*, 207.

33. Wong, J.; Spiro, C.L.; Maylotte, D.H. In *EXAFS and Near-Edge Structure III*; ed. Hodgson, K.O.; Hedman, B.; Penner-Hahn, J.E., Springer-Verlag: Berlin, 1984.

34. Fleming, I. *Frontier Orbitals and Organic Chemical Reactions*; Wiley: London, 1982.

35. Stohr, J.; Sette, F.; Johnson, A.L. *Phys. Rev Lett.* **1984**, *53*, 1684.

36. Silverstein, R. M.; Bassler, G. C.; Morrill, T. C. *Spectrometric Identification of Organic Compounds* ; Wiley: New York, 1981.

37. Furukawa, Y.; Akimoto, M.; Harada, I. *Synth. Met.* **1987**, *18*, 151.

38. Rao, C. N. R. *Chemical Applications of Infrared Spectroscopy*; Academic: New York, 1963.

39. Kellogg, R. M. In *Comprehensive Heterocyclic Chemistry Vol 4*; Katritzky, A. R.; Rees, C. W. Eds.; Pergamon; Oxford, 1984; p 768.

40. Ferreira, C. M.; Loureiro, J. *J. Phys. D* **1984**, *17*, 1175.

41. Lucovsky, G.; Tsu, D. V.; Rudder, R. A.; Markunas, R. J. In *Thin Film Processes II*; Vossen, J. L.; Kern, W. Eds.; Academic: London, 1991, chapter IV-2.

42. Moisan, M.; Barbeau, C.; Claude, R.; Ferreira, C. M.; Margot, J.; Paraszczak, J.; Sa, A. B.; Sauve, G.; Wertheimer, M. R. *J. Vac. Sci. Technol.* **1991**, *B9*, 8.

CHAPTER 7

CONCLUSIONS

7.1 CONCLUSIONS

This thesis has examined the processes occurring in non-isothermal glow discharges and the mechanism of polymer formation within such discharges. Plasma polymerization and surface modification are found to be a function of both the nature of the discharge and the type of excitation used.

Interactions between a polymer (PTFE) and the plasma were studied using various feed gases. Chemical modification at the surface was greatest for a hydrogen plasma due to its reducing nature. AFM studies illustrated the physical effects that plasmas have on polymers. Oxygen treatment gave the highest level of surface roughening.

There is a wide range of excited species present in glow discharges. The types and proportions of these species obviously varies with the nature of the discharge. The importance of the ion component with respect to polymer modification has been studied. The extent of chemical modification was found to be approximately the same for both argon plasma and low energy argon ions. In future individual components within the discharge environment should be studied. For example, the VUV radiation could be filtered out in order to asses its impact on surface modification. Selecting certain components of the plasma whilst blocking out others may lead to more specific surface modification of polymers, therefore enabling them to be tailored for particular requirements.

The physical effect of ions within a plasma were used for sputter plasma polymerization. Changing the carrier gas led to differences in the polymerizable species available. The nature of these gas phase species was correlated to the composition of the resulting deposit. Thus, different mechanisms of polymerizaton were able to occur and films containing different amounts of fluorine were obtained. Polymers that were more 'PTFE like' or more 'carbonaceous' in nature may be synthesized by choosing different plasma conditions.

Manipulating the outcome of a plasma polymerization process is usually difficult. The materials manufactured are normally crosslinked, branched and different in nature to their parent monomer. In order to make a polymeric material more specific the species present in the plasma phase must be controlled. Using different feed gases in the sputtering of solid substrates appear to be one way of achieving this. Another method is to modify the type of RF excitation used.

Pulsing the power supply allows control over how much energy the system receives. As the on-time is shortened and the off-time lengthened the degree of monomer fragmentation is reduced. There is a concomitant decrease in the number of excited species, therefore, the surface of the growing polymer receives less damage. In the off-phase of the pulse, excited species that exist from the on-phase may react with conventionally polymerizable functionalites within the monomer

For maleic anhydride this leads to radically initiated opening of the double bond, during the off phase, leading to the anhydride functionality remaining intact in the polymer. These processes become particularly important when the pulse on-time is of the order of the lifetime (i.e. microseconds) of the heterogeneous excited species present.

In complicated molecular systems more elaborate analytical techniques may be required to elucidate polymerization mechanisms. In continuous wave plasmas the effect of power on the fragmentation of 2-iodothiophene was found to be critical. The technique of XANES, which is only just beginning to be explored for plasma polymer systems, revealed large structural changes in the polymer which were not fully appreciated using XPS or IR.

In summary, this thesis has shown that with careful choice of reaction conditions (i.e. carrier gas and discharge excitation) selective chemistry can be achieved in plasmas. Control of reaction pathways during plasma polymerization can lead to more regular polymer structures.

Finally, new techniques of analyzing plasma polymers can be used to gain further information on their structure and chemical composition.

APPENDIX

SEMINARS, CONFERENCES AND COURSES ATTENDED

UNIVERSITY OF DURHAM - BOARD OF STUDIES IN CHEMISTRY

COLLOQUIA, LECTURES AND SEMINARS FROM INVITED SPEAKERS

1992

October 20	Dr. H. E. Bryndza, Du Pont Central Research Synthesis, Reactions and Thermochemistry of Metal (Alkyl) Cyanide Complexes and Their Impact on Olefin Hydrocyanation Catalysis.
October 22	*The Ingold-Albert Lecture* Prof. A. Davies, University College London The Behaviour of Hydrogen as a Pseudometal.
October 28	Dr. J. K . Cockcroft, University of Durham Recent Developments in Powder Diffraction.
November 5	Dr. C. J. Ludman, University of Durham Explosions, A Demonstration Lecture.
November 18	Dr. R. Nix, Queen Mary College, London Characterisation of Heterogeneous Catalysts.
December 9	Dr. A. N. Burgess, ICI Runcorn The Structure of Perfluorinated Ionomer Membranes.

1993

January 20	Dr. D. C. Clary, University of Cambridge Energy Flow in Chemical Reactions.
March 3	Dr. K. J. P. Williams, B.P. Raman Spectroscopy for Industrial Analysis.
May 13	*The Boys-Rahman Lecture* Prof. J. A. Pople, Carnegie-Mellon University, Pittsburgh, USA Applications of Molecular Orbital Theory.
October 4	Prof. F.J. Feher, University of California, Irvine, USA Chemistry in Solution versus Catalysis on Surfaces - How Do We Bridge the Gap.
October 27	Dr. R.A.L. Jones, Cavendish Laboratory, Cambridge Perambulating Polymers.
November 10	Prof. M.N.R. Ashfold, University of Bristol High Resolution Photofragment Translational Spectroscopy : A New Way to Watch Photodissociation.
November 17	Dr. A. Parker, Rutherford Appleton Laboratory, Didcot Applications of Time Resolved Resonance Raman Spectroscopy to Chemical and Biochemical Problems.

1994

January 26	Prof. J. Evans, University of Southampton Shining Light on Catalysts.
February 2	Dr. A. Masters, University of Manchester Modelling Water Without Using Pair Potentials.
February 16	Prof. K.H. Theopold, University of Delaware, USA Paramagnetic Chromium Alkyls : Synthesis and Reactivity.
February 23	Prof. P.M. Maitlis, University of Sheffield Across the Border : From Homogeneous to Heterogeneous Catalysis.
October 19	Prof. N. Bartlett, University of California Some Aspects of Ag(II) and Ag(III) Chemistry.
November 16	Prof. M. I. Page, University of Huddersfield Four Membered Rings and β-Lactamase.
November 23	Dr. J. Williams, University of Loughborough New Approaches to Asymmetric Catalysis.
December 7	Prof. D. Briggs, ICI Wilton and University of Durham Surface Mass Spectrometry.

1995

January 18	Dr. G. Rumbles, Imperial College, London Real or Imaginary 3rd Order Non-Linear Optical Materials.
February 1	Dr. T. Cosgrove, Bristol University Polymers do it at Interfaces.
March 1	Dr. M. Rosseinsky, Oxford University Fullerene Intercalation Chemistry.
April 26	Dr. M. Schroder, University of Edinburgh Redox Active Macrocyclic Complexes: Rings, Stacks and Liquid Crystals.
May 3	Prof. E. W. Randall, Queen Mary and Westfield College New Perspectives in NMR imaging.

CONFERENCES

August 22 - 27 1993	11th International Symposium on Plasma Chemistry, Loughborough University, England.
August 20 - 25 1995	12th International Symposium on Plasma Chemistry, University of Minnesota, USA.

EXAMINED LECTURE COURSES

October to December 1992	General Laboratory Techniques (Dr. Hampshire) Spectroscopies (Dr. Halliday) Electron Microscopy (Dr. Durose)
November to December 1992	Structure and Bonding in Solids (Prof. Howard)